4-29-2022

Bis(Tryptophan) Amphiphiles: Design, Synthesis and Efficacy as Antimicrobial Agents

Michael McKeever
University of Missouri-St. Louis, mpm.mckeever@gmail.com

Bis(Tryptophan) Amphiphiles: Design, Synthesis and Efficacy as Antimicrobial Agents

Michael McKeever

M.S. Organic Chemistry, University of Missouri-St. Louis, 2020
B.S. Medicinal Chemistry, Queen's University Belfast, 2017

A Dissertation Submitted to The Graduate School at the University of Missouri-St. Louis
in partial fulfillment of the requirements for the degree
Doctor of Philosophy in **Chemistry** with an emphasis in Biochemistry

May
2022

Advisory Committee

George W. Gokel, Ph.D.
Chairperson

Eike B. Bauer, Ph.D.

Chung F. Wong, Ph.D.

Bruce C. Hamper, Ph.D.

ABSTRACT OF THE DISSERTATION

Bis(Tryptophan) Amphiphiles: Design, Synthesis and Efficacy as Antimicrobial Agents

by

Michael McKeever

Doctor of Philosophy in Chemistry

University of Missouri – St. Louis, 2022

Dr. George W. Gokel, Advisor

Amphiphiles play important roles in nature. These molecules contain both hydrophilic and hydrophobic regions, leading to some astonishing properties. The lipid bilayer of the cell membrane is a fascinating organization of amphiphilic phospholipids. Natural and synthetic amphiphiles, such as antimicrobial peptides, are known to interact with the cell membrane. Such interactions can impact transport of molecules across the cell membrane, disrupting cell functions. In this work, a library of tryptophan-containing amphiphiles was synthesized and their antimicrobial properties were explored.

First, a library of *bis*(tryptophan) amphiphiles was synthesized. Preparation included a coupling reaction of a diamine with tryptophan residues, via the carboxy-termini of the amino acids, at either end. The carbon chain length of the diamine was varied to yield *bis*(tryptophan) amphiphiles of varying lengths. Traditional methods of characterization, including NMR, mass-spectrometry, and melting-point determination, were used to confirm identification of the compounds

synthesized. The alkylene linker chains varied from 3-14 carbons in length.

Second, the antimicrobial activity of the *bis*(tryptophan) amphiphiles was explored. Minimum inhibitory concentrations (MICS) were determined for each of the amphiphiles against three bacterial strains. *E. coli* (K-12) was used for the initial screening, followed by a methicillin-resistant *S. aureus* (MRSA) strain and then a multi-drug resistant (MDR) strain of *E. coli*. Biological activity was observed for four of the amphiphiles in the micromolar range. The C_{14}BT [$(CH_2)_{14}$(L-Trp)$_2$·2HCl] was the most potent of the amphiphiles against both *E. coli* and *S. aureus*.

Third, characterization of the properties of the *bis*(tryptophan) amphiphiles was conducted. Dynamic light scattering studies showed that some of the amphiphiles formed aggregates in phosphate buffered saline solution. The amphiphiles that did not form aggregates were also not biologically active against any of the three bacterial strains. Scanning electron microscopy confirmed the presence of spherical aggregates > 1000 nm in diameter.

This work has allowed for the development of more potent *bis*(tryptophan) amphiphiles. It has shown their ability to form aggregates in saline solution and demonstrated a link between antimicrobial activity and aggregate formation.

Summary and Contributions

The majority of the work reported herein was completed by the author. This section details contributions to the experimental work undertaken as part of this dissertation.

Chapter 2. I performed all the chemical syntheses and collected NMR and melting point data. The mass spectrometry data was collected with the assistance of Dr Rensheng Luo in the mass spectrometry facility at UMSL. I made the attempts at forming crystals in the Gokel laboratory.

Chapter 3. Mike Gokel, a coworker from the Gokel Laboratory, and I both performed the bacterial cell work.

Chapter 4. I performed the dynamic light scattering studies using samples I had prepared. The scanning electron microscopy was completed with the assistance of Dr Bishal Nepal in the MIST laboratory at UMSL.

Acknowledgements

I am grateful and thankful for a great number of people who have helped me along this journey. There is not enough space to convey the full extent of my gratitude to everyone in this section.

Firstly, I would like to thank Dr George W. Gokel, my research advisor. Dr Gokel has not only helped shape the direction of this project and develop my research skills, but he has also aided my intellectual and professional development. He taught me that being PhD-worthy is about a lot more than a successful research project. I will forever be grateful for the trajectory he has helped set me on in life.

My dissertation committee, Dr Eike Bauer, Dr Bruce Hamper and Dr Chung Wong, have been instrumental in my success. There have been several stimulating conversations over the last four years that have helped push my intellectual boundaries and helped shape the course of this work. I must also thank Dr Bishal Nepal for his hard work and assistance with the microscopy studies and Dr Rensheng Luo for his assistance with mass spectroscopy.

Over the past four years at UMSL I developed several important relationships with friends and colleagues, including my coworkers in the Gokel laboratory. Dr Mohit Patel, Dr Saeedeh Negin, Mike Gokel, Shanheng (Andrew) Yin and Helena Spikes have all been a pleasure to work alongside.

Finally, I would like to thank my extensive network of friends and family, spanning across continents. They have endured all the struggles I faced alongside me. A special mention must be given to my sister Gemma Dowie. In the absence of parents who have passed, my sister has been the one constant in my life who has shown unwavering support and is wise beyond her years.

Table of Contents

List of Figures and Tables

Chapter 1

Chapter 2

Chapter 1

Introduction and Background

1.1 Amphiphiles and Membranes

1.1.1 Cell Membranes. Cellular membranes are complex and varied structures seen throughout nature in living organisms. The *fluid-mosaic model* of the cell membrane structure was developed by Singer and Nicolson in 1972. [1]

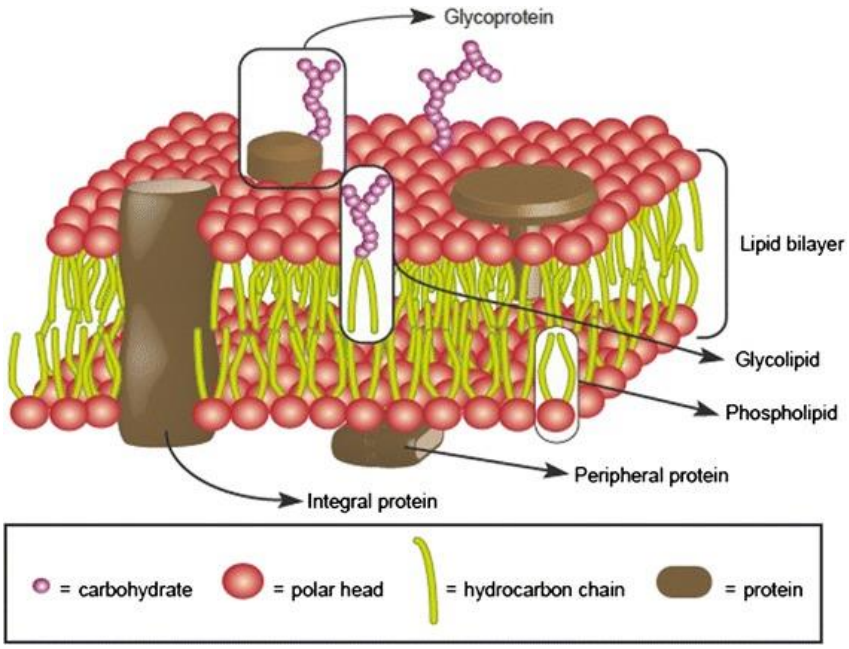

Figure 1.1 Schematic representation of the *fluid-mosaic model* of a cell membrane as depicted by J. Lombard. [2]

In his work in 2014, Lombard describes the *fluid mosaic model* as the agreed upon model for cell membranes in modern day science. [2] As seen in **Fig. 1.1**, the membrane consists primarily of a lipid bilayer with many carbohydrates and proteins protruding into or through the fatty layers. The main components of the lipid bilayer are phospholipids. These molecules are

described as being amphipathic or amphiphilic molecules. They are composed of a polar “head” group (hydrophilic) and an apolar tail (hydrophobic). The molecule is arranged such that the “water-loving” head groups are interacting with the water molecules and the hydrophobic tails are facing each other. [1] [2]

Cell membranes have a vast array of functions including exerting control over which substances enter and leave the cell. This allows the cell to maintain ion homeostasis, which is essential for cell survival. Low molecular weight hydrophobic molecules along with small uncharged molecules, such as O_2 and CO_2 can pass through the membrane unaided, as can some small molecule drugs and waste products, such as urea. [3] Larger molecules and ions are transported across the cell membrane via specialized proteins, such as aquaporins, a type of integral protein which facilitates the transport of water molecules across the cell membrane. [4]

The ability of cell membranes to control substances entering and leaving the cell also serves as a defense mechanism. If substances that are toxic to the cell cannot cross the cell membrane, either with or without the use of membrane proteins, then the toxin cannot impact the cell functions. If the toxin is capable of passing into the cell, but the cell is very efficient at removing the toxin from the cell, perhaps by the use of specialized proteins, then the cell can protect itself from the toxin having a high enough concentration within the cell, or enough time, to impact the cell functions. Compartmentalized cell types (cells with a cell membrane) are diverse and many have developed self-defense mechanisms that are much more complex and beyond the scope of this research, however all start

with the presence of a cell membrane. [5]

As this research will be concerned with the cell membranes of bacterial cells specifically, it is important to note two of the main bacteria cell types and to look at their cell membranes comparatively and contrastively.

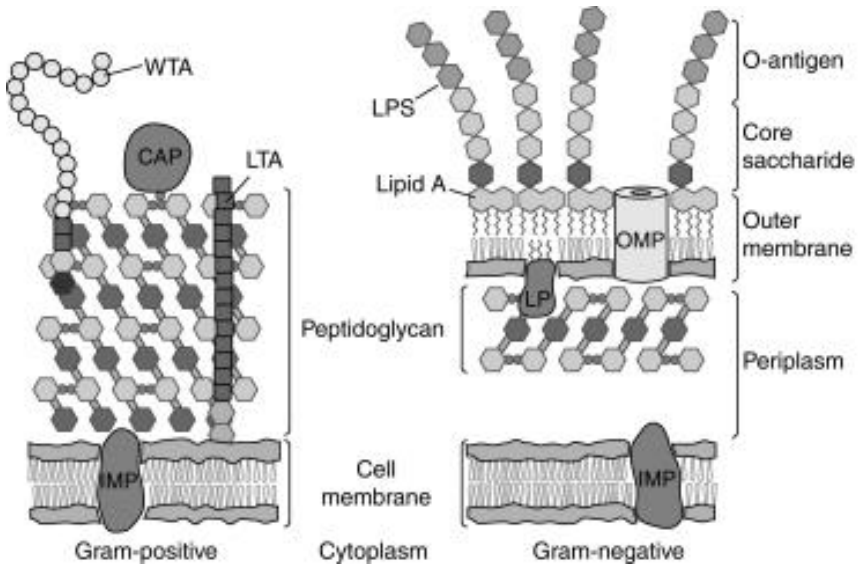

Figure 1.2 Schematic representation of Gram-positive and Gram-negative cell envelopes: CAP = covalently attached protein; IMP, integral membrane protein; LP, lipoprotein; LPS, lipopolysaccharide; LTA, lipoteichoic acid; OMP, outer membrane protein; WTA, wall teichoic acid [6]

The two major groups of bacterial cell types are Gram-positive and Gram-negative bacteria, the cell envelopes of which are depicted in **Fig. 1.2**. [6] As can be seen in the diagram, the Gram-negative cell envelope has three distinct components: the outer membrane, the periplasmic space, which also contains the peptidoglycan layer, and the inner cell membrane. Contrastively to this, the Gram-positive bacteria lack an outer membrane in their cell structure. The outer

membrane is a significant defense mechanism for the Gram-negative bacteria and also, indirectly, helps stabilize the inner membrane of the Gram-negative cell envelope. This added stabilization decreases the need for a thicker peptidoglycan layer within the Gram-negative bacterial envelope and so a much thinner peptidoglycan layer is observed than in the Gram-positive structure. The thicker peptidoglycan layer in Gram-positive bacteria provides extra protection to the bacteria since they lack an outer membrane. Turgor pressure experienced from many of the environments where bacteria exist can also be tolerated due to the presence of an outer membrane (Gram-negative) or much thicker peptidoglycan layers (Gram-positive). The other components of the cell envelopes, such as the proteins and carbohydrates anchored in the membrane or peptidoglycan layer, vary greatly and can be influenced by specific cell type, function and the environment in which they exist. [6]

1.1.2 Amphiphiles in Nature. The word amphiphile became the popular term to describe a molecule having both a hydrophilic and hydrophobic region, around the middle of the 20th century. [1] These molecules are important throughout nature having the ability to form thermodynamically stable aggregates of varying shapes and orientations. The shape and size of the aggregates formed vary significantly as can be seen in **Fig. 1.3**. [7]

The conditions of the solution in which the amphiphile is present will influence the shape and size of the aggregates. The pH, temperature and ionic strength of the solution can all have an impact on the formation of the aggregates. The

overall determining factor, however, is the geometry of the component amphiphilic molecules. The morphology of the resulting aggregate most commonly will be a spherical or cylindrical micelle, a bilayer vesicle, lamellar (such as a bilayer membrane) or an inverted micelle. [7]

Israelachvili determined that the morphology of the aggregates could be predicted using the *critical-packing factor* (C_{pp}). [7] [8]

$$C_{pp} = V_0 / A_{mic} l_c$$

In this equation, V_0 is the volume taken up by the hydrophobic chains in the core of the aggregate, A_{mic} is the effective surface area of the hydrophilic headgroup at the aggregate-solution interface, and l_c is the critical chain length (maximum effective length of the chain). The aggregates with the smallest C_{pp} value ($C_{pp} < 1/3$) are spherical aggregates. With an increase in C_{pp} value, cylindrical aggregates are formed ($1/3 < C_{pp} < ½$). Vesicles with an internal cavity will be formed when the C_{pp} value is larger than ½ but less than 1 ($½ < C_{pp} < 1$). When the C_{pp} value is 1, lamellar aggregates are observed. When the *critical packing parameter* is greater than one, inverted micelles are formed. In this type of aggregate, the hydrophilic head groups are clustered around an aqueous solvent with the hydrophobic tails radiating outwards, in the opposite direction. [8]

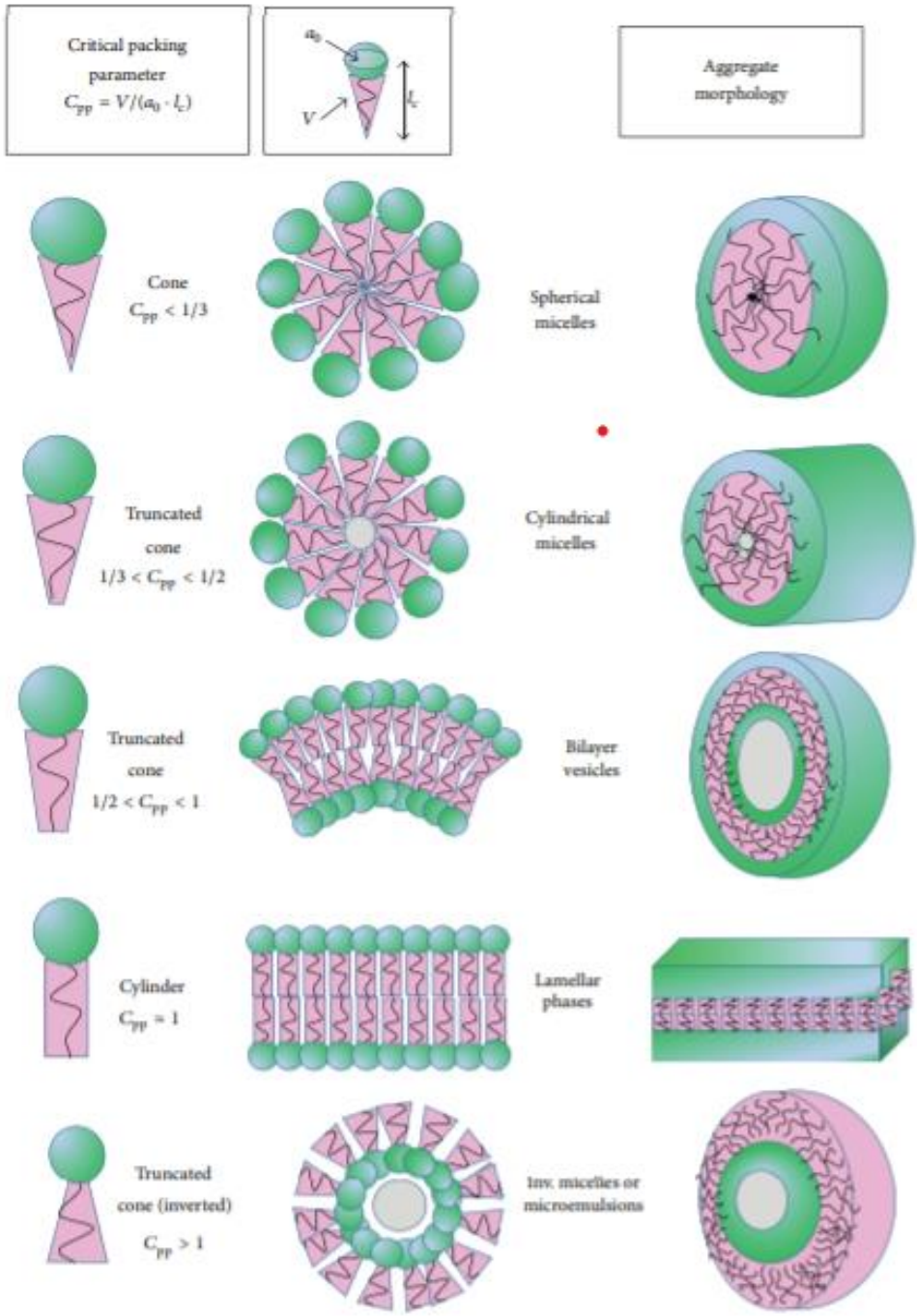

Figure 1.3 Diagram showing the impact of C_{pp} values and shape of component amphiphilic molecule on the overall shape of the aggregates formed. Reproduced from reference [7]

Undoubtedly, one of the most common and well-known amphiphilic aggregates occurring in nature is the bilayer membrane. There are many other amphiphilic aggregations seen throughout nature, some of which can be problematic for human survival, such as ß-amyloid (Aß) proteins that are linked to Alzheimer's Disease (AD). It is known that amyloid protein deposits in tissues can cause cell death and they are linked to numerous other diseases in addition to AD. [9] The various disease-causing amyloids may contain different proteins, however they all have the characteristic ß-sheet conformation. It was believed that the shared secondary structure was responsible for the mechanism causing cellular toxicity. No obvious connection between the sequence of amino acids forming the secondary structure was observed in the toxic amyloid proteins. It is understood that the Aß causes over-accumulation of H_2O_2, leading to lipid peroxidation and finally, cell death. Until recently, it was unknown that the presence of ß-sheets alone was not responsible. It has been shown that it is the amphiphilic nature of the peptides produced by the ß sheets and not merely the presence of ß sheets, that causes the amyloid toxicity. [9] [10]

Amphiphiles often perform functions that are advantageous to the cells and organism. Antimicrobial peptides (AMPs) are short chain peptides produced by most living organisms. In single cell organisms they assist the cell in competing for essential nutrients, whereas in multicellular organisms, they form an important component of the innate immune system. [11] AMPs have been around for a very long time and are very effective at killing bacteria, including antibiotic-resistant bacteria. Their non-specific mechanisms of action have allowed for very little

resistance to be developed against these compounds. The design of synthetic amphiphiles mimicking these compounds could provide an effective solution to the antibiotic-resistance issue that is becoming more concerning each day. [11]

1.1.3 *Synthetic Amphiphiles.* As seen in nature, amphiphiles are essential for life (*e.g.* cellular membranes) [2] and can be advantageous in numerous other ways, perhaps most importantly as antimicrobial agents. [11]

One well-known class of synthetic amphiphiles is pepducins. These lipopeptide compounds have shown the ability to modulate the transference of signal from receptors to G proteins, inside the cell. G protein-coupled receptors are essential for a number of cell functions including cell growth and metabolism, blood coagulation, and neuronal signaling. [12] For example, the peptide palmitoyl-LysLysSerArgAlaLeuPhe, which is known to inhibit platelet aggregation. Several other biological properties have also been confirmed for this compound.

In the 1990's, there was considerable development and utilization of various types of liposomes. Drug loading and delivery methods were optimized by utilizing ion gradients with polymorphic liposomes. Chemotherapy also benefited from the development of "stealth" liposomes, so called because of their reduced recognition by the immune system. [13] In the mid-20th century, the formation of vesicles was achieved using the phospholipid, dipalmitoyl lecithin, however, during the 1970's, Kunitake and Okahata developed a method to produce a fully synthetic bilayer membrane using didodecyldimethylammonium

bromide [$(C_{12}H_{25})_2N^+(CH_3)_2$ Br^-], a double-chained surfactant. [14] This new method made synthesis of liposomes much easier and so the interest in, development of and application of synthetic amphiphiles grew exponentially over the following decades. [15]

During the next few decades, the exploration of synthetic amphiphiles and their potential within healthcare was explored extensively, and this exploration still continues. There has been much success in the areas of gene therapy, drug targeting, drug development, and antibacterial treatment. [16]

1.1.4 *Amphiphiles in the Gokel Lab.* At the beginning of the 21st century, considerable attention in the wider community was being given to the development and characterization of synthetic anion transporters (SATs) and synthetic ion channels. [17] [18] At this time, the Gokel lab was also making significant progress and discoveries in this area. In the late 2000's, the Gokel group used their work with SATs to explore the aggregation behavior and molecular organization of amphiphiles at the membrane / aqueous interface of cells. The molecular dynamics surrounding membrane insertion and, more generally, the organization and aggregation of amphiphiles, had not been explored until this point. [19] As part of this work involving the SATs, eleven different amphiphilic compounds, comprising amino acids, were studied. The structures of these amphiphiles are shown in **Fig. 1.4.**

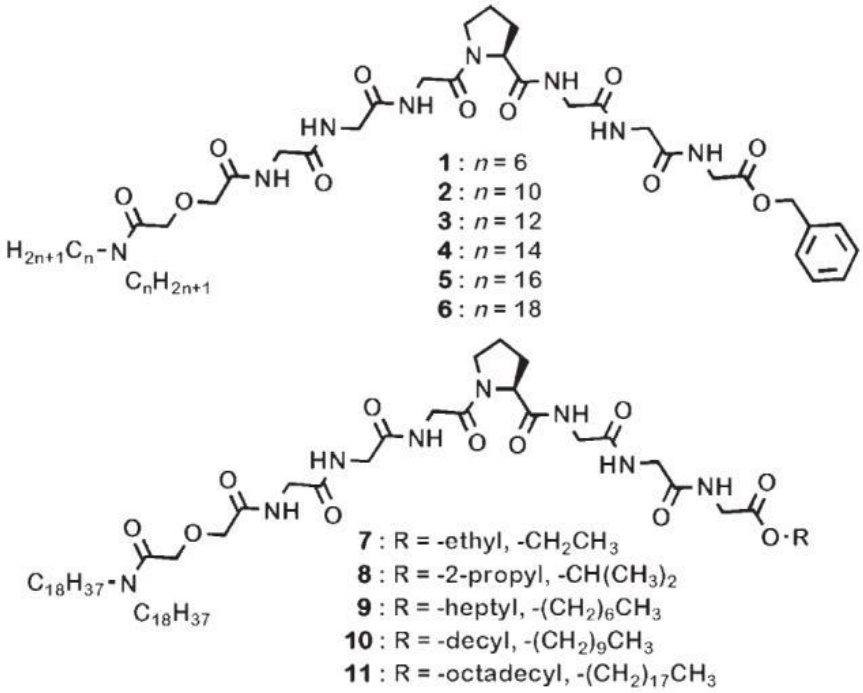

Figure 1.4 Structures of 11 amphiphiles explored in the SAT series of compounds. [19]

A range of techniques was used during this study, including Langmuir trough studies and Brewster angle microscopy (BAM) to determine the organization and stability of aggregates at the air-water interface. Dynamic light scattering (DLS) studies and transmission electron microscopy confirmed the results of the Langmuir trough and BAM studies and also defined how SATs aggregated and behaved in solution. Overall, the study found that when compounds formed stable monolayers at the air-water interface, they also formed spherical aggregates in solution. This study also found that transport of anions was more effective by amphiphiles that formed less-stable monolayers. Less stable amphiphiles are able to join with other amphiphiles in the membrane layer

and form a pore for the anions to pass through. If the amphiphiles are too stable, they may not readily form pores and so are less effective at anion transport. [19]

The work on synthetic amphiphiles in the Gokel lab also included the creation and development of a class of compounds known as “hydraphiles.” These molecules are comprised of three crown ether macrocycles connected together by spacer chains of varying length. One of the hydraphiles synthesized by the lab is shown in **Fig. 1.5**. [20]

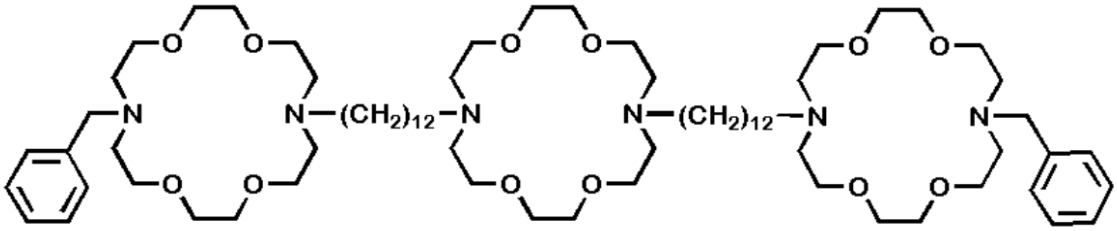

Figure 1.5 Structure of a hydraphile molecule, created by the Gokel lab [20]

The hydraphiles were designed to function as ion channels in bilayer membranes. This ability was extensively documented. These compounds also have shown much success as antimicrobial agents. They are capable of inserting into bilayer membranes and conducting the transport of ions. This allows for a disruption of ion homeostasis. This, of course, is inimical to the cellular function of bacteria, but also shows activity against yeast and even mammalian cells. Planar bilayer conductance studies have shown that these molecules mimic protein channels and exhibit open-close behavior once inserted into the bilayer membrane. The non-rectifying mechanism of action engenders toxicity to

bacteria and yeast. Lower levels of toxicity were observed towards mammalian cells, probably because the hydraphile's nitrogen atoms are protonated at physiological pH and are thus attracted to negative bacterial surfaces. Even so, an option is to co-administer hydraphiles at concentrations below their toxic threshold with an antimicrobial drug. Studies have shown that the hydraphiles can enhance antibiotic potency at such concentrations, presumably by enhancing membrane permeability, and therefore show potential as adjuvants. [20] [21]

Before the development of the hydraphiles, the Gokel lab also developed lariat ether amphiphiles and identified various applications for them. The general structure of the lariat ethers is similar to that of hydraphiles in that a crown ether macrocycle is employed. Initially, the lariat ethers were developed having donor group-containing side arms attached to the macrocycle. Recently developed lariat ethers had an *n*-alkyl side chain attached to either side of the crown ether macrocycle. The general structure of the lariat ether amphiphiles can be seen in **Fig. 1.6**. [22] [23]

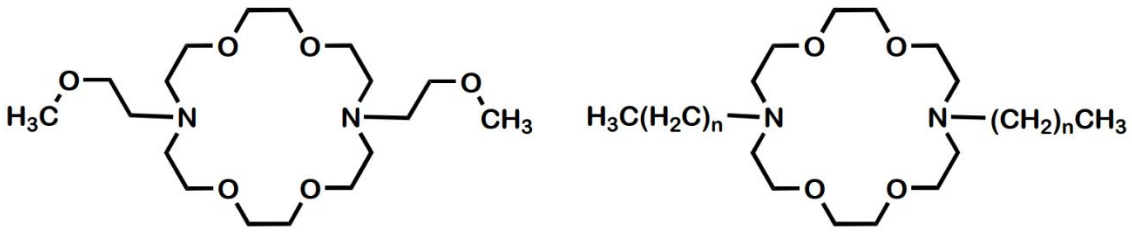

Figure 1.6 Structures of a lariat ether molecule having side arm donors (left) and a general structure of dialkyl lariat ether molecules [22]

The lariat ethers were initially designed as ion carrier molecules. The side arms wrapped around a ring-bound cation and provided solvation so the cation could be transported across bilayer membranes. In more recent times, the removal of the donor group coincided with the discovery of the ability of *n*-alkyl lariat ethers to form pores through which ions could be transported. At this time, it was also discovered by the Gokel lab that lariat ethers could enhance the potency of antibiotics, when they were co-administered to bacteria. In 2016, the Gokel lab showed that the administration of non-toxic levels of dialkyl lariat ethers could improve the potency of both rifampicin and tetracycline against two strains of *E. coli.* [22] [23]

Following the success of the Gokel lab in developing amphiphiles with antimicrobial activity, the group explored another family of compounds, the *bis*(amino acid) amphiphiles. [23] Firstly, the group focused on *bis*(tryptophan) amphiphiles (BTs), noting that indole groups may behave as anchors in the membrane [24] and that tryptophan residues appear only near the membrane boundaries in most peptides and proteins, such as the KcsA voltage-gated ion channel. [23] [25] The Gokel group designed a series of BTs with the general formula H_2N-Trp-Y-Trp-NH_2 (H_2N-W-Y-W-NH_2) in which Y is an aryl or alkyl linker residue. The expectation of these molecules is that the tryptophan indole group would behave as a membrane anchor and the molecular amphiphile would enhance membrane permeability. [23] The anticipated effect of the increased cell membrane permeability was a disruption to ion homeostasis and mechanisms of antibiotic resistance of the bacterial cell. It was predicted that the BTs might be

able to display antimicrobial activity through this mechanism of action. [23]

In 2016, the Gokel group screened nine of their tryptophan containing compounds against a strain of Gram-positive bacteria (*S. aureus*) and two strains of the Gram-negative bacteria *E. coli*. [26] One of the strains tested (*E. coli.* Tet^R), is a bacterial strain developed in the Gokel lab that displays resistance to tetracycline as it has been engineered to include a tetracycline selective TetA efflux pump. As expected, the activity of the compounds varied based on the spacer linker. Five of the BTs were found to be biologically active against both the Gram-positive and Gram-negative bacteria. All four of the BTs with phenylene linkers were active, however only one of the BTs with an alkyl chain linker was active. The active alkyl-linked BT had twelve carbons in the spacer chain so the formula was H_2N-Trp-$(CH_2)_{12}$-Trp-NH_2. The results from the minimum inhibitory concentration (MIC) study can be found in **Table 1.1**. [26]

Table 1.1 Minimal Inhibitory Concentrations (MICs) of the various BTs against the three bacterial strains. [26]

cpd	link (AA)[b]	*E. coli* K12 (μM)	*E. coli* Tet^R (μM)	*S. aureus* (μM)
1	*meta*-Ph (Gly)	>128	>128	>128
2	*meta*-Ph (L-Trp)	64	48 ± 8	32
3	*meta*-Ph (D-Trp)	64	28 ± 4	32
4	*meta*-Ph (IPA)[c]	>128	>128	>128
5	*ortho*-Ph (L-Trp)	64	56 ± 8	32
6	*para*-Ph (L-Trp)	128	120 ± 14	128
7	$(CH_2)_3$ (L-Trp)	>128	>128	>128
8	$(CH_2)_4$ (L-Trp)	>128	>128	>128
9	$(CH_2)_6$ (L-Trp)	>128	128	>128
10	$(CH_2)_{12}$ (L-Trp)	8	10 ± 2	4
11	C_6H_5-L-Trp-NH_2	>128	>128	>128

[a]MIC resolution is in powers of 2 unless otherwise indicated by a range with ±. [b]Structure of both amino acids. [c]3-(3-Indolyl)propanoic acid.

Two controls (*meta*-Ph (Gly) and *meta*-Ph (IPA)) were also included. [b]Structure of both amino acids. [c] 3-(3-Indolyl)propanoic acid.

Interestingly, while the phenylene-linked BTs all showed some level of potency against all three bacterial strains, the orientation of substitution on the arene made a significant difference to the activity of the molecule. The C_{12}BT (H_2N-Trp-$(CH_2)_{12}$-Trp-NH_2) was the only active alkyl-linked BT and was the most active compound overall. This suggests that the length of the spacer chain, and perhaps the hydrophobicity of the linker also, are important for the activity of the amphiphile. [26]

At the same time, these compounds were studied for their efficacy to reverse tetracycline resistance in *E. coli.* It was revealed that at subinhibitory concentrations, a number of the BTs were able to recover the antibacterial

activity of tetracycline against the Tet^R *E. coli.* [26] The *meta*-Ph (L-Trp), *meta*-Ph (D-Trp), *ortho*-Ph (L-Trp), *para*-Ph (L-Trp), C_3BT (H_2N-Trp-$(CH_2)_3$-Trp-NH_2) and the C_{12}BT (H_2N-Trp-$(CH_2)_{12}$-Trp-NH_2) all recovered tetracycline potency at ½ MIC or lower.

Whilst the scope of the antimicrobial activity studies at this time were limited, they did show that BTs could be toxic to bacterial cells at concentrations at which there was limited cytotoxicity to mammalian cells. The potential of this class of amphiphiles was significant, particularly against efflux-pump mediated resistance in bacteria and the group sought to expand their family of BTs and explore the potential mechanisms of action and scope of activity further. [26]

Following on from this work, the Gokel lab explored developing other amino acid derivatives of the BT amphiphiles. The general formula H_2N-Aaa-Y-Aaa-NH_2 would be used to develop the series further. The group decided to use the *meta*- phenylene model (W-*m*C_6H_4-W) as their “first pass” screening for active compounds. This model was chosen for a variety of reasons including the less complicated isolation of compound during synthesis and the surprising differences in activity between the D,D- and L,L-isomers of the *meta*-phenyl BT (**Table 1.1**). This difference in activity of isomers would offer potential for further exploration of the amino acids if any active compounds were developed. [26] The structures of the compounds synthesized and analyzed can be seen in **Fig. 1.7**. [23]

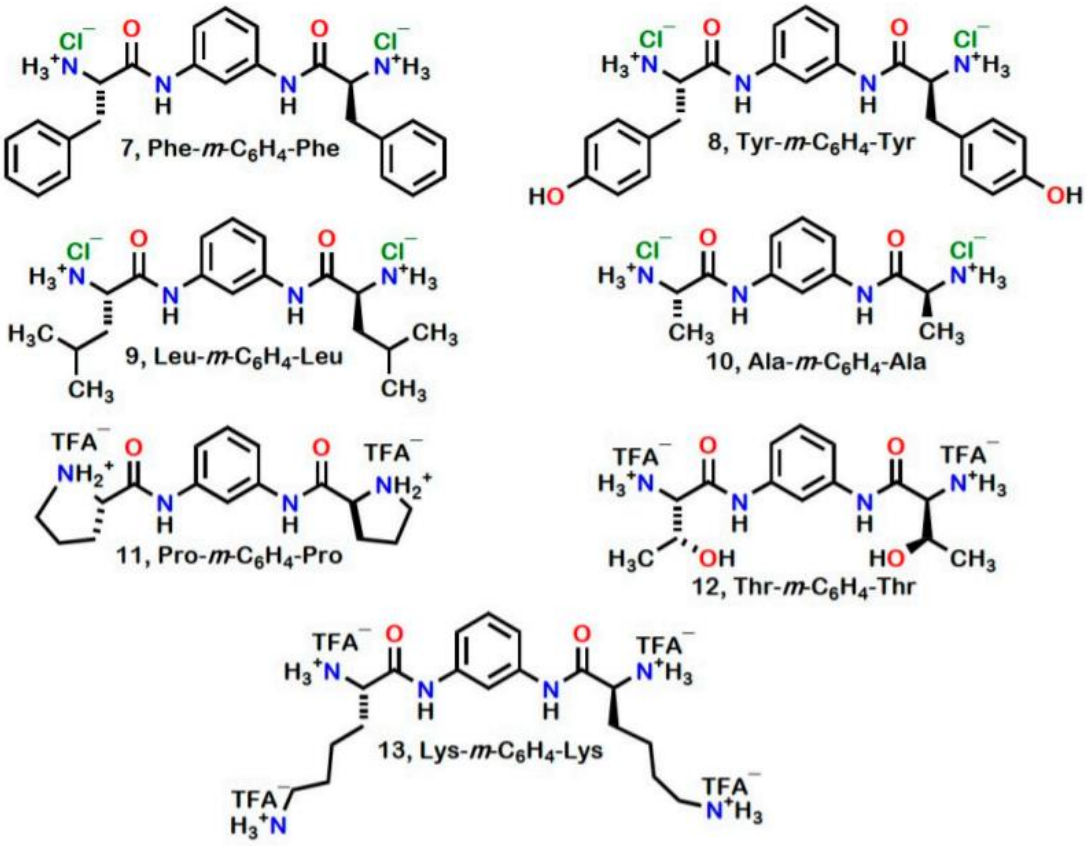

Figure 1.7 Structures of the *bis*(amino acid) compounds having arene spacers that were synthesized and analyzed. [23]

Compounds **7** and **8** are phenylalanine and tyrosine derivatives, respectively. They, like tryptophan, have electron-rich aromatic groups and so may behave similarly. Compounds **9** and **10** are the leucine and alanine derivatives. They contain simple alkyl groups and so were prepared to investigate the absence of more electron-rich terminal groups. Compound **11** is a proline derivative, providing assessment of a compound with a smaller cyclic terminal group. Threonine is used as the amino acid group in compound **12**. Both compound **12** and compound **8** have hydroxyl groups, and both can accept and

donate hydrogen bonds. Compound **13** is a lysine derivative and has double the number of positive charges present compared with the other derivatives. The variety of the compounds in **Fig. 1.7** encompassed a significant range of the variation observed among the 20 common amino acids. [23]

Table 1.2 Minimum Inhibitory Concentrations (μM) of the amino acid derivatives and the previously explored BTs against *S. aureus* and Tet^R *E. coli* [23]

Cmpd	Spacer (Aaa)	*S. aureus* 1199B	Tet^R *E. coli*
1	*meta*-C_6H_4(L-Trp)$_2$	128	48
2	*meta*-C_6H_4(D-Trp)$_2$	16	28
3	*ortho*-C_6H_4(L-Trp)$_2$	64	56
4	*para*-C_6H_4(L-Trp)$_2$	64	120
5	$(CH_2)_4$(L-Trp)$_2$	128	>128
6	$(CH_2)_{12}$(L-Trp)$_2$	4	10
7	*meta*-C_6H_4(L-Phe)$_2$	>128	>128
8	*meta*-C_6H_4(L-Tyr)$_2$	>128	>128
9	*meta*-C_6H_4(L-Leu)$_2$	>128	>128
10	*meta*-C_6H_4(L-Ala)$_2$	>128	>128
11	*meta*-C_6H_4(L-Pro)$_2$	>128	>128
12	*meta*-C_6H_4(L-Thr)$_2$	>128	>128
13	*meta*-C_6H_4(L-Lys)$_2$	>128	>128
(control)	Tetracycline	<1	~900
(control)	Norfloxacin	64	N/D [b]
(control)	Ethidium bromide	16	128
(control)	CCCP [a]	8	64
(control)	Reserpine	>128	>128

Notes. [a] Carbonyl cyanide *m*-chlorophenyl hydrazine. [b] Not determined.

Table 1.2 shows the results of the bacterial studies for the amino acid derivatives, along with data for the previously successful BTs (compounds (**1**-**6**)) and five control compounds. None of the amino acid derivatives showed any activity below 128 μM against either the Gram-positive bacterial strain (*S. aureus*) or the tetracycline resistant Gram-negative strain (Tet^R *E. coli*). The absence in activity for this selection of amino acid containing compounds reinforced the hypothesis that the indole group of the tryptophan is important for

cell membrane activity of these compounds. [23]

Further work was also carried out with the BTs previously found to be active against bacteria. Bilayer Lipid Membrane (BLM) studies were conducted, and traces indicating pore formation obtained for some of the BTs. The D,D-isomer of the *m*-phenyl BT provided the traces (not shown) with greatest reproducibility. Open-close behavior was observed, and the traces evinced clear channel activity. The traces alluded to the presence of either two open channels or aggregation of an unknown number of monomers. Molecular models of the *m*-phenyl BT suggests that the distance between the amino groups is ~ 12Å, whereas the hydrocarbon section of a bilayer membrane is estimated to be around 30-35Å. This suggests that a single molecule would be too short to span a bilayer and so a barrel-stave or toroidal pore may be formed by the amphiphile. [23]

To investigate the ability of the BTs to penetrate the bacterial membrane and enhance membrane permeability, the Gokel group conducted bacterial permeability analysis using fluorescence. Propidium iodide is a popular red-fluorescent counterstain for the cell nucleus and other DNA-containing organelles. It does not pass through the cell membrane of healthy cells under normal conditions so the presence of propidium iodide inside cells suggests increased cell membrane permeability. Both L,L- (W) and D,D-isomers (w) of the *m*-phenyl BT (W-*m*Ph-W and w-*m*Ph-w) and the L,L-isomer of the C_{12}BT (W-C_{12}-W) were investigated against Gram-positive *S. aureus* cells. [23]

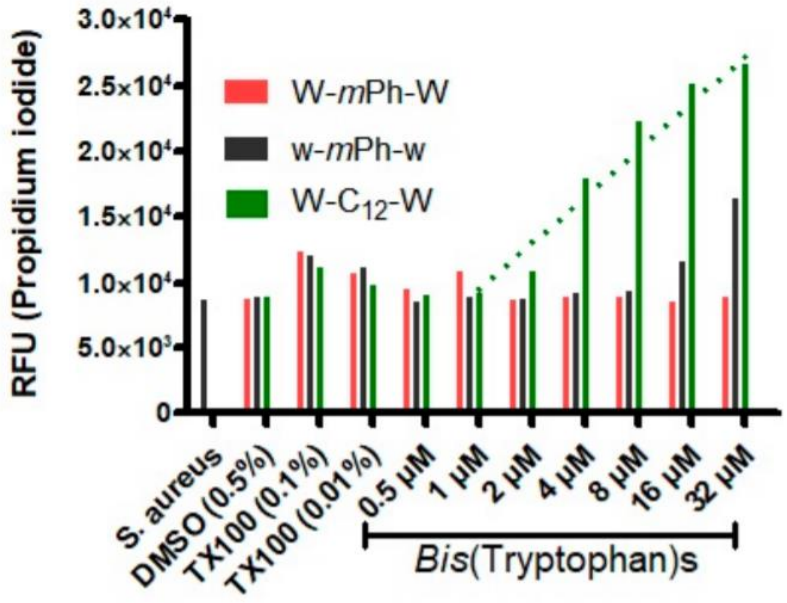

Figure 1.8 Results of the fluorescence-based cell permeability assay using propidium iodide for BTs against *S. aureus* cells. TX100 = Triton X-100 (detergent). RFU = relative fluorescence units. Each bar represents an average of three independent trials. [23]

As seen in **Fig. 1.8**, there is no increase in propidium iodide fluorescence in concentrations of BTs up to and including 2 µM. The L,L-isomer of *meta*-phenylene BT (W-*m*Ph-W) did not appear to have any impact on the measured fluorescence up to 32 µM, which coincided with the lack of activity of the compound against *S. aureus* below 128 µM (**Table 1.2**). The D,D-isomer (w-*m*Ph-w) almost doubled the measured fluorescence at 32 µM, this also matched the biological data, which showed that the compound was active against *S. aureus* at concentrations as low as 16 µM. The alkyl BT W-C_{12}-W increased fluorescence the most, however, with a 3-fold increase from 4 µM to 32 µM. Furthermore, it is evident that an increase in fluorescence can be seen from a concentration as low as 4 µM, again coinciding with the bacterial activity seen above. [23]

At this point, the Gokel lab had developed a small library of BT compounds and established potency against both Gram-positive and Gram-negative bacteria, along with a tetracycline resistant strain of *E. coli*. There was evidence of cell membrane activity through both the BLM studies and fluorescence assays that coincided with the biological activity. Significant work had also been done on cytotoxicity to mammalian cells that framed the range within which compounds showed activity against bacterial cells. At this time, the Gokel lab had also established activity for BTs as adjuvants, which will be discussed later in this chapter. Further development of the library of BTs and further exploration of the potential mechanism of action will be the primary focus of this doctoral thesis.

1.2 Antimicrobial Resistance

1.2.1 Mechanisms of Resistance. Antimicrobial resistance (AMR) is a serious international concern. Bacteria, yeast, fungi, and viruses have a remarkable capability of adapting to their environments and overcoming antimicrobial medications through a variety of mechanisms. The World Health Organization (WHO) has labeled AMR as one of the top ten leading health crises facing the human race. [27] As resistance to current medications continues to develop, the primary concern is the inability to treat emerging “superbugs” which are so resistant as to be untreatable, with mortal consequences, especially to those most vulnerable in society. There are also many other concerns about the continued increase in resistance including, disability, long term illness, complications to surgery, and cancer treatments. The impact will also be felt financially from a variety of viewpoints. It is estimated that AMR will be responsible for around 300 million premature deaths by 2050, costing the global economy around $100 trillion. [28] Longer hospital stays and expensive medications will be a financial strain on all those acquiring infections. The cost of research and development of new medications is also a crucial burden to society. It is unsurprising that the WHO considers this problem one to be addressed urgently and one that transcends multiple sectors of medicine and scientific research. [27]

While the problem of resistance includes various microbials, it would be beyond the scope of this introduction to discuss each of those in detail. Antibiotic resistance and the mechanisms which allow bacteria to be resistant are the focus

of this discussion.

One of the first major breakthroughs in targeting bacterial infections occurred in 1909. Paul Ehrlich developed a “magic bullet” capable of attacking *Treponema pallidum*, the bacterium responsible for causing syphilis infections. Arsphenamine (Salvarsan) is an arsenic containing compound that proved effective against *T. pallidum* (**Fig 1.9**). Ehrlich’s work helped revolutionize the fight against bacteria. [29] [30]

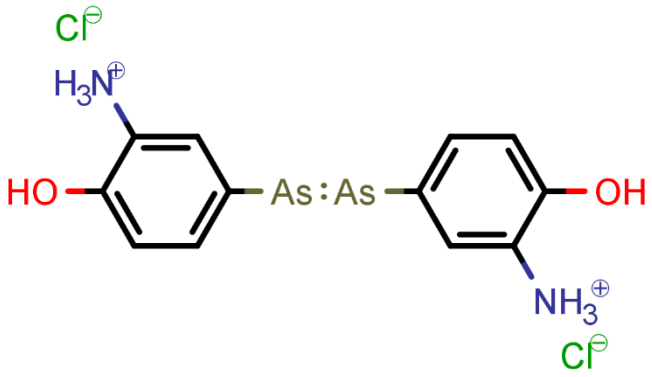

Figure 1.9 Structure of arsphenamine, also called Salvarsan

Since the 1940’s, the name Alexander Fleming has become synonymous with the term “antibiotic.” Fleming is often considered the father of antibiotic compounds due to his accidental discovery of the antibiotic ability of a *Penicillium* fungus in 1928. Penicillin was then developed for use as an antibiotic in the late1930s. [31] Other drugs, such as sulfa drugs and quinolones soon followed as antibiotic agents.

Although penicillin is thought of as the first successful antimicrobial drug, the first effective antibiotic drug was the azo dye called prontosil (**Fig 1.10**). It was discovered by Gerhand Domagk working in Germany. Prontosil is actually a prodrug; the active component is sulfanilamide. Domagk won the 1939 Nobel Prize for this work. Alexander Fleming would not share the Nobel Prize until 1945.

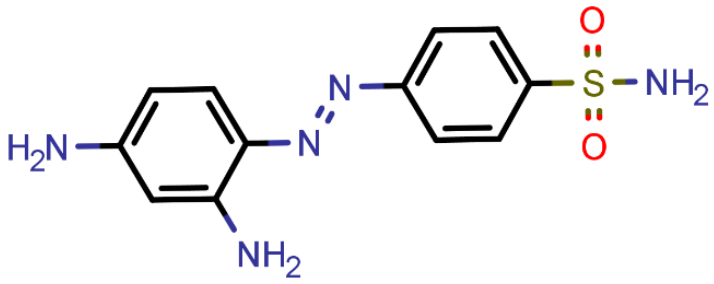

Figure 1.10 Structure of Prontosil

By the end of the 19th century, actinomycetes had already been discovered. These bacteria naturally produce antibiotic compounds to help them compete for food and survival in the soil. Although they were used to treat some bacterial infections at the time, interest was limited, until the discovery of streptomycin in 1943. Streptomycin, which came from the genus *Streptomyces*, was the first effective treatment for tuberculosis (TB). [31] During the 20th century, the development and use of antibiotics accelerated exponentially. Many of the antibiotics employed were natural compounds, although synthetic analogues and novel compounds did emerge. With this rapid increase in the use of antibiotics, resistance seemed to emerge almost as quickly. Several reasons account for such rapid development of resistance. One is simply overuse and poor antibiotic

stewardship. The fact that many antibiotics are naturally occurring compounds is another issue. Bacteria have coexisted for millions of years with the antibiotics and other antibiotic producing organisms. Some strains are likely to have already developed resistance to the antibiotics during evolution. It is important, therefore, that while inspiration may be derived from nature, newly developed compounds should be novel and target bacterial cells via new mechanisms of action. [32]

To better understand how to overcome antibiotic resistance, it is important to acknowledge the different mechanisms of resistance. **Fig. 1.11** shows the most prevalent resistance mechanisms observed in bacteria. [33]

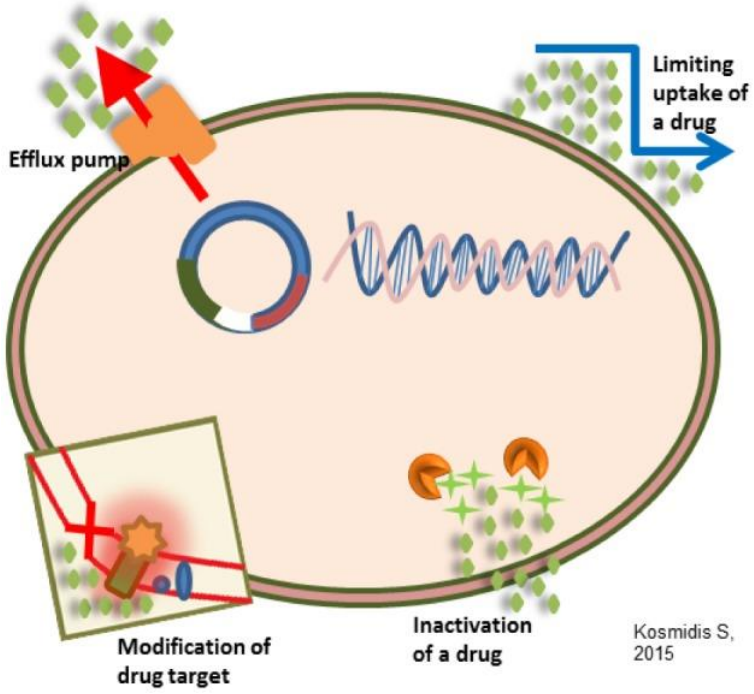

Figure 1.11 Representation of the general resistance mechanisms in bacteria cells, reproduced from AIMS Microbiology, Vol. 4 [33]

As mentioned earlier in this chapter, one of the main mechanisms of resistance is the cell membrane itself, which limits the initial uptake of the drug molecules. If the compound cannot penetrate the cell membrane, it is unlikely it will have any impact on the viability of the cell. The other mechanism that concerns the cell structure, is the modification of the drug target. Many bacterial cells have the ability to modify part of the cell the drug is targeting. Methylation and ribosomal mutations are among the most common ways for the cell to adapt in this manner. [33]

A well-known mechanism of resistance is the bacterial cell's ability to modify the drug. ß-Lactamases are efficient at hydrolytic cleavage of the peptide bond in the ß-lactam ring, which alters the drug structure. It is a common mechanism of resistance against the ß-lactam drugs, such as penicillins and cephalosporins. [33]

Another resistance mechanism shown in **Fig. 1.11** is the action of efflux pumps. Drug efflux is an effective and efficient form of resistance. Efflux pumps can transcend the bacterial cell membrane and expel a variety of molecules from the cell. Efflux pumps are often non-specific and so may expel various waste products and unwanted foreign materials, allowing the cell to become multi-drug resistant (MDR). [33] Efflux pumps are of potential importance in this research effort. Further discussion of their efficacy and the importance of ion homeostasis in bacterial cells follow in this chapter.

1.2.2 Efflux Pumps and Ion Homeostasis. The importance of metal ions for life on earth cannot be overemphasized. Photosynthesis, respiration, and metabolism are all dependent on metal ions. [34] Therefore, it is no surprise that maintaining the appropriate concentrations of metal ions within bacterial cells is integral to cell survival. Metabolism in bacterial cells primarily depends on adequate levels of iron, zinc and manganese ions. Without adequate levels of specific metal ions, the cells cannot survive. Similarly, an overabundance of metal ions is toxic to the cell. As a result, bacteria have developed complex systems to regulate ions within the cell, maintaining ion homeostasis. Metalloregulator enzymes, ion specific reservoirs, influx and efflux pumps, and the cell membrane, are all essential components of ion homeostasis and cell survival. [35]

The roles of both influx and efflux pumps are critical to survival for many cells, with efflux pumps often being developed as a form of antibiotic resistance. As the name suggests, influx pumps transport essential ions into the cell and therefore can increase the concentration of essential ions inside the cell when levels are depleted. This is a core component of the metalloregulatory process. [35]

The efflux pumps play a more significant role in terms of antibiotic resistance. There are five families of efflux pump with most bacteria possessing more than one type of pump. These five families have been categorized based upon their energy source and structure. Most of the pumps transport substrates across the cell membrane only, however, one family is capable of transporting substrates across the entire cell envelope (cell membrane and outer membrane). A

schematic representation of the five families of efflux pumps can be seen in **Fig. 1.12.** [33]

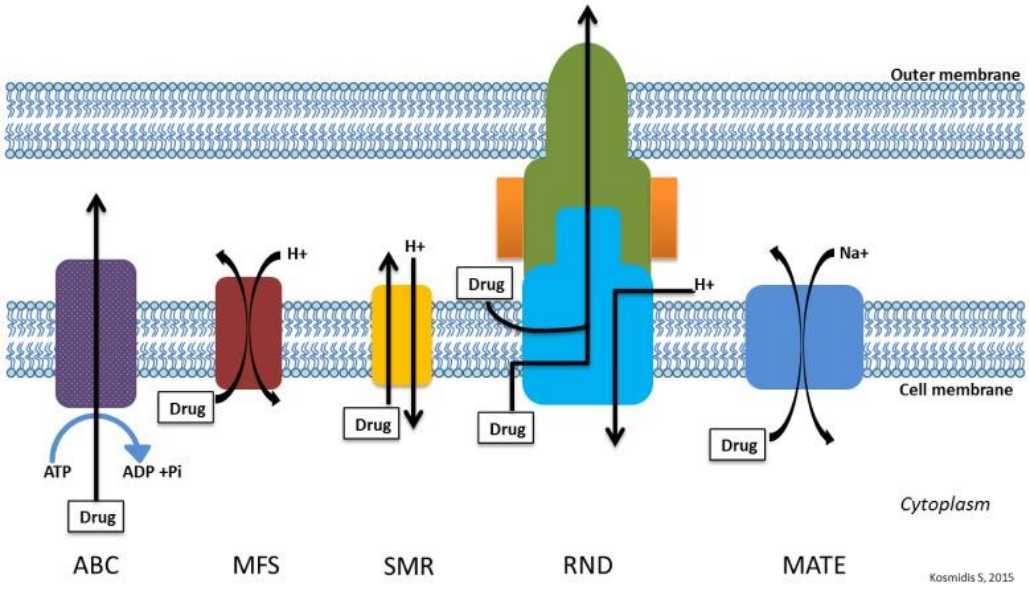

Figure 1.12 Schematic representation of the five families of efflux pumps found in cell membranes, reproduced from AIMS Microbiology. [33]

All of the efflux pump types are dependent upon a regulated ion gradient for energy, with the exception of the ABC family. The ATP binding cassette (ABC) efflux pumps use the hydrolysis of ATP to ADP as their energy source. [33] Of course, the ATP – ADP cycle relies on proton transport in the bacterial cell [36] so each of these efflux pumps can be affected by disruption of ion homeostasis in the cell.

The major facilitator superfamily (MFS), small multidrug resistance (SMR) family, multidrug and toxic compound extrusion (MATE) family, along with the ABC family are all single-component pumps. The resistance-nodulation division

(RND) family are multi-component pumps and comprise the one family of pumps which are able to span the entire bacterial cell envelope. The RND efflux pumps are found almost exclusively in Gram-negative bacteria. [33]

It is important to note that the ABC efflux pumps have very specific substrates and are rarely found in any clinically significant bacteria. The SMR, MFS and RND efflux pumps are much more effective at extruding antibiotic drugs. They are all capable of removing fluoroquinolones, macrolides, aminoglycosides, tetracyclines, and ß-lactam antibiotics, all five classes of antibiotics. Around 50% of the efflux pumps found in *E. coli* are MFS pumps and they are the most diverse pumps, in terms of substrate specificity. [33] It is unsurprising that multi-drug resistance (MDR) is becoming more prevalent among bacteria with efflux pumps active against all classes of antibiotics. The emergence of methicillin-resistant *Staphylococcus aureus* (MRSA) and the devastation it has caused, especially in hospital settings, is one example of this. [23]

It is evident that the development of efflux pumps has provided bacteria an efficient form of antibiotic resistance. By extruding the drug molecules before they have an opportunity to work in the cell, the bacterial cells can avoid any toxic effects. This may allow the bacterial cells time to develop other forms of resistance to the drug molecule, therefore adding to the antibiotic resistance problem currently facing humanity. [37] Furthermore, the number of different efflux pumps and the diversity of their substrates, makes targeting individual efflux pumps a particularly difficult and costly task. The common essential

component across all families of efflux pump for effective extrusion of substrates is an ion gradient. Disruption of ion homeostasis in the cell can remove the energy source(s) required for efflux pump action and hold potential for overcoming antibiotic resistance. To date, no efflux pump inhibitor has reached the market to be co-administered with antibiotics in the treatment of bacterial infections. Pharmacokinetic issues along with toxicity are among the issues that have hindered promising compounds so far. The design and development of new compounds in this area are critical and urgently needed. [37]

1.3 Synthetic Amphiphiles for Overcoming Antimicrobial Resistance

1.3.1 Successes of Amphiphiles as Antimicrobials. Antimicrobial peptides (AMPs), mentioned earlier in section 1.1, are short chain peptides that form part of the immune system in multicellular organisms. [11] AMPs are often comprised of two hydrophilic or charged residues connected, but separated and connected by a hydrophobic region. It is this amphipathic nature of the molecules to which their antimicrobial capabilities are attributed. [38] There are close to 1000 different AMPs identified so far. They are commonly divided into four families: (i) anionic peptides, (ii) helical cationic peptides, (iii) anionic / cationic peptides forming disulfide binds, and (iv) cationic peptides enriched in a specific amino acid (such as proline, arginine, phenylalanine, glycine, or tryptophan). Their size along with other factors, such as amphiphilicity and amino acid composition, allow AMPs to be attracted towards and insert into the negatively charged bacterial bilayer membranes and form pores. The “barrel-stave”, “toroidal pore” and “carpet” models are the mechanisms by which AMPs are predicted to work as antimicrobials. Considerable biochemical and biophysical work is currently focused on the mechanisms of efflux pump function. [39]

One particularly interesting AMP is indolicidin, a tridecapeptide amide and a cationic peptide (**Fig. 1.13**). The peptide contains only 13 amino acid residues: H-Ile-Leu-Pro-Trp-Lys-Trp-Pro-Trp-Trp-Pro-Trp-Arg-Arg-NH_2. The high proportion of tryptophan and proline residues makes this peptide indole-rich, hence the inspiration for the name upon discovery. The presence of five tryptophan residues is extremely rare for such a short peptide, in fact, this peptide had the

highest mole percentage of tryptophan residues upon its discovery at the end of the last century. The short chain length, and consequently small overall size and atomic mass (1906 g/mol), were not the only surprising attributes upon isolation of this peptide. It was found that concentrations of 10 µg/mL (10 mg/L) were sufficient to kill suspensions of *S. aureus* and *E. coli*, thus showing efficacy against both Gram-positive and Gram-negative bacteria. [40]

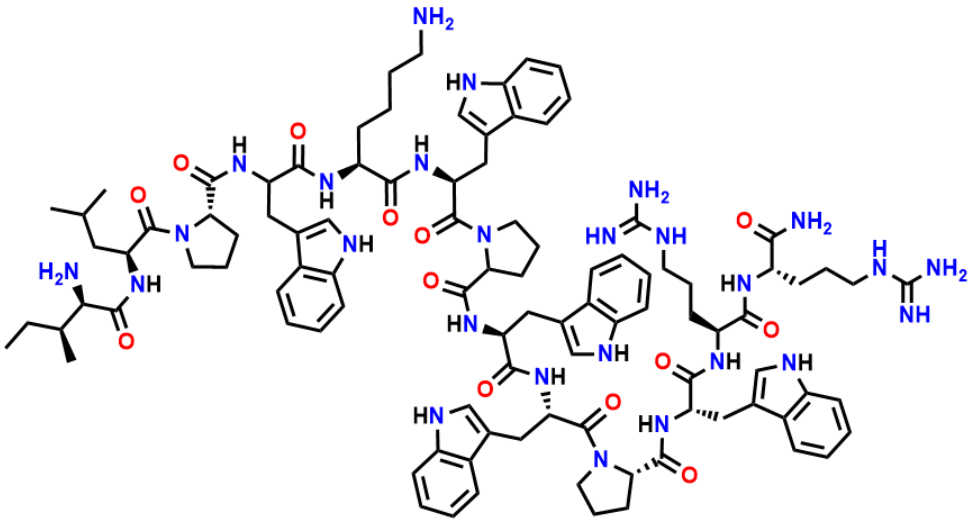

Figure 1.13 Structure of indolicidin

The use of AMPs to treat bacterial infections in clinical practice has been employed for a considerable amount of time. Colistin, (**Fig 1.14),** which appears on the World Health Organization's (WHO) list of essential medicines, [41] was approved for medical use in 1970. Due to toxicity concerns, the use of colistin was very limited until the 2000's when the prevalence of MDR bacteria surged. [42] [43] In addition to the toxicity issues with colistin and despite the success at

treating MDR infections, bacterial resistance has recently been observed against colistin. [44] It is expected that any antibiotic molecule may only have a window of 10-15 years from when it is first used to treat bacterial infections, before resistance is developed. It is perhaps surprising that resistance to the colistin amphiphile molecule was not observed until recently. The success of colistin, along with other amphiphiles, such as daptomycin [23] and polymyxin B, [43] invokes hope that other amphiphilic molecules can be designed, developed, and utilized in the fight against antimicrobial resistance.

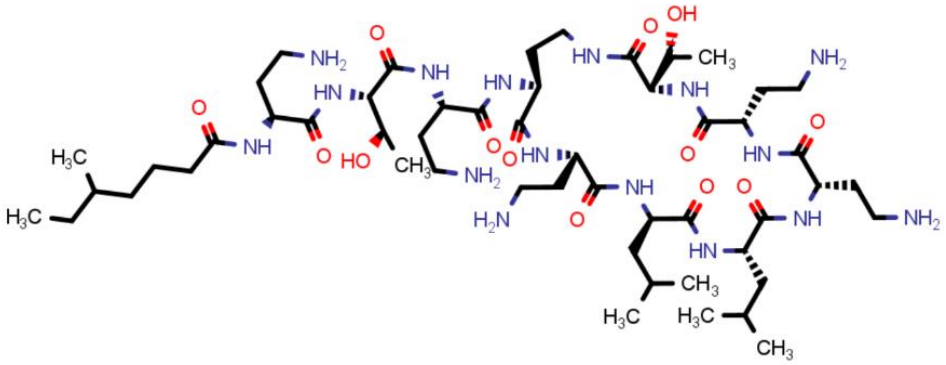

Figure 1.14 Structure of colistin

Some of the successes of the Gokel lab in designing and developing amphiphiles with antimicrobial activity, have already been highlighted in this chapter. The hydraphiles, lariat ethers, and *bis*(tryptophan)s have all shown antimicrobial activity against an array of organisms including yeast and bacteria. The antibiotic resistance of bacteria is a huge concern and so forms the main focus of much of the Gokel lab research. Minimum inhibitory concentrations (MICs) of various hydraphiles, lariat ethers and BTs against the K12 strain of *E. coli* have been established. [26] [45] [46] While activity can vary considerably

from one molecule to the next, MICs were established in the micromolar range for all three families of amphiphiles.

1.3.2 Successes of Amphiphiles as Adjuvants. The use of adjuvants in the fight against antibiotic resistance is an established plan of attack. Augmentin is a well-established and highly successful drug cocktail, comprising amoxicillin and clavulanate potassium as the active ingredients. The clavulanate potassium inactivates ß-lactamases, which would otherwise provide resistance to penicillin antibiotics, such as amoxicillin. Interestingly, many of the Gokel group amphiphiles show adjuvant activity, in addition to being antibiotic compounds in their own right. In recent work involving the hydraphiles, the Gokel group investigated the mechanism of antimicrobial action of these amphiphiles. [46] It was discovered that administration of particular hydraphiles, even at concentrations lower than ½ MIC, along with administration of known antimicrobials, could increase potency of these drugs by up to 30-fold against *E. coli* and *P. aeruginosa.* In previous work, the Gokel group explained that hydraphiles not only insert into membranes and form channels, but they also exhibit open-close behavior (monitored using the planar bilayer lipid membrane voltage clamp apparatus). Furthermore, a preference for cations was observed over anions and transport of Na^+ ions was preferred to K^+ ions, by a ratio of 4:1. [47] It is expected that the disruption of ion homeostasis is the foundation of the antimicrobial activity seen, including adjuvant activity. It is logical that disruption of a cell membrane may increase permeability of other antibiotic compounds and

the disabling of efflux pumps will add to the accumulation of those drug molecules inside the bacterial cells. This will, of course, lead to increased toxicity to the cell.

Similarly, there has been interesting work into the efficacy of lariat ethers as adjuvants, by the Gokel group. The dialkyl lariat ethers are proposed to work in a fashion similar to hydraphiles, disrupting the cell membrane and therefore disrupting ion homeostasis, along with the integrity of the membrane. Ion balance is essential for many cell functions, including enzymatic functions and efflux pumps. The Gokel lab has conducted a plethora of combination studies involving lariat ethers and antibiotic drugs already on the market. Some of the exciting results showing the potential of lariat ethers can be seen in **Table 1.3**. [45]

Table 1.3 The Effect of Lariat Ethers on the Fold Recovery of Tetracycline Potency against the Tetracycline Resistant Strain Tet^R *E. coli* [45]

Cpd.[a]	*MIC (μM)*	*Used (μM)*	*Tetracycline*[b] *MIC used (μM)*	*Fold Enhance-ment*
C_6LE	>512	192	413	2
C_8LE	120	80	87	10
C_8LE	120	60	175	5
C_8LE	120	40	233	4
C_{10}LE	16	6	225	4
C_{10}LE	16	9	56	16
C_{11}LE	24	18	87	10
C_{11}LE	24	16	87	10
C_{11}LE	24	12	87	10
C_{11}LE	24	8	175	5
C_{12}LE	>512	192	450	2

a. C_6LE refers to C_6<N18N>C_6, etc. b. *E. coli* used is tet^R, a transformed bacterium incorporating the Tet A efflux pump, MIC = 900 μM against tetracycline.

In the first column, the lariat ether being investigated is listed. The second column shows the MIC of the lariat ether as a drug *per se* against tet^R *E. coli,* the third column shows the concentration of the lariat ether being used. The fourth column in the table shows the concentration of tetracycline being used (the MIC of tetracycline against tet^R is 900 μM). In the column on the right-hand side, the fold enhancement is listed. Of the compounds listed in this study, the greatest fold enhancement can be seen when 9 μM C_{10}LE is used with 56 μM tetracycline. A 16-fold enhancement was observed meaning $^1/_{16}{}^{th}$ of the MIC of tetracycline (when used without an adjuvant) is needed to stop growth of the bacterial strain. [45] These data also shows that changing the chain length has an impact on the bacterial activity of these compounds. It is unsurprising that changes in the chain length of the lariat ethers, or indeed any amphiphile would have an impact on their activity. In the case of these lariat ethers, increasing the chain length not only leads to an increase in the size of the molecule, but also causes an increase in hydrophobicity. It is understood that these lariat ethers, like other amphiphiles, are active due to their ability to insert into cell membranes. Cell membranes have polar and non-polar regions and so the polar/non-polar character of amphiphiles would presumably have an impact on their efficacy as membrane disruptors. The impact of changing chain lengths is more complex than these two factors alone and so it is impossible to predict exactly how changing chain length will influence antibacterial activity.

The *bis*(tryptophan) amphiphiles (BTs) are a third class of amphiphiles

that have shown antibacterial activity both when used alone or as adjuvants with other clinical antibiotics. In 2016, the Gokel lab highlighted some of the adjuvant activity displayed by the BTs. [26] They discovered that compounds containing arene or aliphatic linkers both showed adjuvant activity. **Table 1.4** shows the impact of co-administration of BTs to recover the potency of tetracycline against tet^R *E. coli.* [26]

Table 1.4 Impact of BTs on the Fold Recovery of Tetracycline Potency against Tet^R *E. coli* [26]

compounds used	[compound] μM	MIC [Tet] μM[a]	fold recovery	FIC[c]
none	0	900	n.a.[b]	n.a.
meta-Ph (L-Trp) (2)	24 [1/2 MIC]	56.25	16-fold	0.56
meta-Ph (L-Trp) (2)	12 [1/4 MIC]	112.5	8-fold	0.38
meta-Ph (L-Trp) (2)	14	112.5	8-fold	0.42
meta-Ph (D-Trp) (3)	14 [1/2 MIC]	112.5	8-fold	0.63
meta-Ph (D-Trp) (3)	7 [1/4 MIC]	225	4-fold	0.50
ortho-Ph (L-Trp) (5)	28 [1/2 MIC]	112.5	8-fold	0.63
ortho-Ph (L-Trp) (5)	14 [1/4 MIC]	225	4-fold	0.50
para-Ph (L-Trp) (6)	60 [1/2 MIC]	112.5	8-fold	0.63
para-Ph (L-Trp) (6)	30 [1/4 MIC]	225	4-fold	0.50
para-Ph (L-Trp) (6)	14	450	2-fold	0.62
n-C_3 (L-Trp) (7)	60 [1/2 MIC]	112.5	8-fold	0.63
n-C_3 (L-Trp) (7)	30 [1/4 MIC]	112.5	8-fold	0.38
n-C_3 (L-Trp) (7)	5	450	2-fold	0.54
n-C_{12} (L-Trp) (10)	5 [1/2 MIC]	225	4-fold	0.75
n-C_{12} (L-Trp) (10)	2.5 [1/4 MIC]	450	2-fold	0.75

[a]MIC is the observed inhibitory concentration of tetracycline in the presence of the indicated compound. MIC values represent two trials of two replicates each. MIC resolution is in powers of 2. [b]"n.a." means not applicable. [c]FIC is the fractional inhibitory concentration.

The BTs in **Table 1.4** are all being used at ½ MIC or lower (second column). It was shown that the cytotoxicity of each of these compounds to mammalian cells was minimal at the MIC at which it was administered. Therefore, by using concentrations at ½ MIC or lower, there would be little or no cytotoxicity to mammalian cells. [26] The third column of the table shows the MIC of tetracycline against the tetracycline resistant *E. coli* strain when the specified concentration of amphiphile had been co-administered. The fourth column shows the calculated fold-recovery by using the amphiphile with tetracycline. The column on the right shows the fractional inhibitory concentration (FIC). This index is calculated by dividing the MIC of each compound when used in combination by the MIC of the compound when used alone. The FIC index was developed around the Loewe additivity zero-interaction theory. This is based on the hypothesis that a drug molecule cannot interact with itself and so a self-drug combination will always be additive. As such, an FIC index of 1 is considered additive, lower than 1 implies synergy and a value higher than 1 suggests antagonism. [48] [49] Based on this understanding of the FIC index, it can be said that all of the BTs have synergy with tetracycline against tet^R *E. coli.* [26]

The compound that showed the greatest enhancement in potency was the *meta*-Ph (L-Trp), with a 16-fold enhancement at ½ MIC. Of the aliphatic BTs, the shortest compound, C_3BT, showed the greatest fold enhancement of 8-fold. Interestingly, when the C_3BT was co-administered at ½ MIC or ¼ MIC, the fold enhancement for the tetracycline was the same. It was noted earlier in this chapter and in **Table 1.2**, that the C_{12}BT was the most potent against tet^R *E. coli*,

among the BTs, even more so than *meta*-Ph (L-Trp). [23] It is therefore surprising that the adjuvant activity does not follow the same trend. It can only be concluded at this time that more investigation would be necessary before any trends can be noted or successfully predicted.

1.3.3 *The Potential for Amphiphiles for the Future.* While amphiphiles were first used clinically for their antimicrobial properties more than half a century ago, exploration of their potential and approval for use in clinical settings both seem to be in their infant stages. Amphiphiles may indeed prove effective as antibiotic drugs in their own right, achieving FDA approval for new drug molecules is an expensive and rigorous process. [50] Gaining approval for a novel amphiphile as an adjuvant to be delivered with an existing antibiotic drug already on the market, may be a more efficient pathway. Adjuvants are exploited constantly in medicine, whether it is the addition of aluminum to help with vaccines such as Infanrix (administered to children for prevention of diphtheria, tetanus and pertussis) [51] or the use of clavulanate potassium in Augmentin.® All three families of amphiphiles from the Gokel lab discussed in this chapter, have shown activity as adjuvants and activity as drug molecules without being co-administered. [23] [45] [46]

With the constant emergence of additional antibiotic resistance, it seems that any of the classes of bacteria could be the right target. Multidrug resistance is the most worrying and urgent threat from bacteria. Gram-positive, Gram-negative and other bacterial types outside these classes, such as *Mycobacterium*

tuberculosis are all displaying multidrug resistance. [27] The Gokel lab compounds have significant potential to be effective against Gram-positive, Gram-negative and MDR bacterial strains. This thesis describes additional work to validate and expend the previous findings.

1.4 References

[1] S. J. Singer and G. L. Nicolson, "The fluid mosaic model of the structure of cell membranes," *Science,* vol. 175, pp. 720-731, 1972.

[2] J. Lombard, "Once upon a time the cell membranes: 175 years of cell boundary research," *Biology Direct,* vol. 9, no. 32, pp. 1-35, 2014.

[3] N. S. Yang and M. J. Hinner, "Getting Across the Cell Membrane: An Overview for Small Molecules, Peptides and Proteins," *Methods of Molecular Biology,* no. 1266, pp. 29-53, 2015.

[4] K. Takata, T. Matsuzaki and Y. Tajika, "Aquaporins: water channel proteins of the cell membrane," *Progress in Histochemistry and Cytochemistry,* vol. 39, no. 1, pp. 1-83, 2004.

[5] F. Ranow, J. D. MacMicking and L. C. James, "Cellular Self-Defense: How Cell-Autonomous Immunity Protects Against Pathogens," *Science,* vol. 10, no. 340, pp. 701-706, 2013.

[6] T. J. Silhavy, D. Kahne and S. Walker, "The Bacterial Cell Envelope," *Cold Spring Harbor Perspectives in Biology,* vol. 2, no. 5, pp. 1-16, 2010.

[7] D. Lombardo, M. A. Kiselev, S. Magazu and P. Calandra, "Amphiphiles Self-Assembly: Basic Concepts and Future Perspectives of Supramolecular Approaches," *Advances in Condensed Matter Physics,* vol. 2015, pp. 1-22, 2015.

[8] J. Israelachvili, Intermolecular and Surface Forces, 2nd ed., Academic Press Ltd, 1992, pp. 366-382.

[9] D. Shubert, C. Behl, R. Lesley, A. Brack, R. Dargusch, Y. Sagara and H. Kimura, "Amyloid Peptides are Toxic via a Common Oxidative Mechanism," *Neurology,* vol. 92, pp. 1989-1993, 1995.

[10] J. C. Phillips, "Thermodynamic Description of Beta Amyloid Formation Using Physciochemical Scales and Fractal Bioinformatic Scales," *Neuroscience,* no. 6, pp. 745-750, 2015.

[11] J. M. Ageitos, A. Sanchez-Perez, P. Carlo-Mata and T. G. Villa, "Antimicrobial Peptides (AMPs): Ancient Compounds that Represent Novel Weapons in the Fight Against Bacteria," *Biochemical Pharmacology,* vol. 133, pp. 117-138, 2017.

[12] L. Covic, A. L. Gresser, J. Talavera, S. Swift and A. Kuliopulos, "Activation and Inhibition of G Protein-coupled Receptors by Cell-penetrating Membrane-tethered Peptides," *Proceedings of the National Academy of Sciences,* vol. 99, no. 2, pp. 643-648, 2002.

[13] D. D. Lasic and D. Papahadjopoulos, "Liposomes Revisited," *Science,* vol. 267, pp. 1275-1276, 1995.

[14] T. Kunitake and Y. Okahata, "A Totally Synthetic Bilayer Membrane," *Journal of the American Chemical Society,* vol. 99, p. 3860, 1977.

[15] J. T. Kunjappu and P. Somasundaran, "Recent Trends in Bilayer Formatiion of Synthetic Amphiphiles," *Colloids and Surfaces A: Physiochemical and Engineering Aspects,* vol. 117, pp. 1-5, 1996.

[16] C. Bombelli, L. Giansanti, P. Luciani and G. Mancini, "Gemini Surfactant Based Carriers in Gene and Drug Delivery," *Current Medicinal Chemistry,* vol. 16, no. 2, pp. 171-183, 2009.

[17] B. A. McNally, W. M. Leevy and B. D. Smith, "Recent Advances in Synthetic Membrane Transporters," *Supramolecular Chemistry,* vol. 19, pp. 29-37, 2007.

[18] P. H. Schlesinger, R. Ferdani, J. Liu, J. Pajewska, P. R, M. Saito, H. Shabany and G. W. Gokel, "SCMTR: A Chloride-Selective, Memrane-Anchored Peptide Channel that Exhibits Voltage Gating," *Journal of the American Chemical Society,* vol. 124, no. 9, pp. 1848-1849, 2002.

[19] E. K. Elliott, M. Daschbach and G. W. Gokel, "Aggregation Behavior and Dynamics of Synthetic Amphiphiles that Self-Assemble to Anion Transporters," *Chemistry A European Journal,* vol. 14, pp. 5871-5879, 2008.

[20] S. Negin, B. A. Smith, A. Unger, W. M. Leevy and G. W. Gokel, "Hydraphiles: A Rigorously Studied Class of Synthetic Channel Compounds with In Vivo Activity," *International Journal of Biomedical Imaging,* pp. 1-11, 2013.

[21] J. L. Atkins, M. B. Patel, Z. Cusumano and G. W. Gokel, "Enhancement of Antimicrobial Activity by Synthetic Ion Channel Synergy," *Chemical Communications,* vol. 46, pp. 8166-8167, 2010.

[22] S. Negin, M. B. Patel, M. R. Gokel, J. W. Meisel and G. W. Gokel, "Antibiotic Potency against E. coliis Enhanced by Channel-Forming Alkyl Lariat Ethers," *ChemBioChem,* vol. 17, pp. 2153-2161, 2016.

[23] M. Patel, S. Negin, J. Meisel, S. Yin, M. Gokel, H. Gill and G. Gokel, "Bis(Tryptophan) Amphiphiles Form Ion Conducting Pores and Enhance Antimicrobial Activity against Resistant Bacteria," *Antibiotics,* vol. 10, no. 1391, pp. 1-18, 2021.

[24] M. R. R. de Planque, B. B. B, J. A. A. Demmers, D. V. Greathouse, R. E. Koeppe, F. Separovic, A. Watts and J. A. Killian, "Interfacial Anchor Properties of Tryptophan Residues in Transmembrane Peptides Can Dominate over Hydrophobic Matching Effects in Peptide-Lipid Interactions," *Biochemistry,* vol. 42, pp. 5341-5348, 2003.

[25] D. D. A, J. M. Cabral, R. A. Pfuetzner, A. Kuo, J. M. Gulbis, S. L. Cohen, B. T. Chait and R. MacKinnon, "The Structure of the Potassium Channel: Molecular basis of K+ conduction and selectivity," *Science,* vol. 280, pp. 69-77, 1998.

[26] J. W. Meisel, M. B. Patel, E. Garrad, R. A. Stanton and G. W. Gokel, "Reversal of Teracycline Resistance in Escherichia coli by Noncytotoxic bis(Tryptophan)s," *Journal of the American Chemical Society,* vol. 138, pp. 10571-10577, 2016.

[27] "World Health Organization Antimicrobial Resistance," 17 November 2021. [Online]. Available: https://www.who.int/news-room/fact-sheets/detail/antimicrobial-resistance.

[28] "Antimicrobial Resistance Review," [Online]. Available: https://amr-review.org/. [Accessed 23rd January 2022].

[29] Britannica, "Paul Ehrlich Biography," [Online]. Available: https://www.britannica.com/biography/Paul-Ehrlich. [Accessed 22 03 2022].

[30] Center of Disease Control (CDC), "Sexually Transmitted Diseases - Syphilis," [Online]. Available: https://www.cdc.gov/std/syphilis/default.htm. [Accessed 22 03 2022].

[31] D. A. Hopwood, "Streptomyces in Nature and Medicine: The Antibiotic Makers," New York, Oxford Universty Press, 2007.

[32] E. Peterson and P. Kaur, "Antibiotic Resistance Mechanisms in Bacteria: Relationships Between Resistance Determinants of Antibiotic Producers, Environmental Bacteria, and Clinical Pathogens," *Frontiers in Microbiology,* vol. 9, pp. 1-21, 2018.

[33] W. C. Reygaert, "An Overview of the Antimicrobial Resistance Mechanisms of Bacteria," *AIMS Microbiology,* vol. 4, no. 3, pp. 482-501, 2018.

[34] M. Moustakas, "The Role of Metal Ions in Biology, Biochemistry and Medicine," *Materials,* vol. 14, no. 549, pp. 1-4, 2021.

[35] P. Chandrangsu, C. Rensing and J. Helmann, "Metal Homostasis and Resistance in Bacteria," *Nature Reviews Microbiology,* vol. 15, pp. 338-350, 2017.

[36] H. Guo, T. Suzuki and J. L. Rubinstein, "Structure of a Bacterial ATP Synthase," *eLife,* pp. 1-17, 2019.

[37] A. Dashtbani-Roozbehani and M. H. Brown, "Efflux Pump Mediated Anitmicrobial Resistance by Staphylococci in Health-Related Environments: Challenges and the Quest for Inhibition," *Antibiotics,* vol. 10, no. 1502, pp. 4-33, 2021.

[38] R. E. W. Hancock and A. Rozek, "Role of Membranes in the Activities of Antimicrobial Cationic Peptides," *FEMS Microbiology Letters,* vol. 206, no. 2, pp. 143-149, 2006.

[39] K. A. Brogden, "Antimicrobial Peptides: Pore Formers or Metabolic Inhibitors in Bacteria?," *Nature Reviews,* vol. 3, pp. 238-250, 2005.

[40] M. E. Selsted, M. J. Novotny, W. L. Morris, Y. Q. Tang, W. Smith and J. S. Cullor, "Indolicidin, a Novel Bactericidal Tridecapeptide Amide from Neutrophils," *The Journal of Biological Chemistry,* vol. 26, no. 7, pp. 4292-4295, 1992.

[41] W. H. Organization, "World Health Organization Model List of Essential Medicines," vol. 22, 2021.

[42] I. Karaiskos, M. Souli, I. Galani and H. Giamarellou, "Colistin: Still a Lifesaver for the 21st Century?," *Expert Opinion on Drug Metabolism & Toxicology,* vol. 13, no. 1, pp. 59-71, 2016.

[43] S. E. Cheah, J. Li, B. T. Tsuji, A. Forrest, J. B. Bulitta and R. L. Nation, "Colistin and Polymyxin B Dosage Regimens against Acinetobacter baumannii: Differences in Activity and the Emergence of Resistance," *Antimicrobial Agents and Chemotherapy,* vol. 60, no. 7, pp. 3921-3933, 2016.

[44] R. Jasim, M. A. Baker, Y. Zhu, M. Han, E. K. Schneider-Futschik, M. Hussein, D. Hoyer, J. Li and T. Velkov, "A Comparative Study of Outer Membrane Proteome between Paired Colistin-Susceptible and Extremely-Resistant Klebsiella pneumoniae Strains," *ACS Infectious Diseases,* vol. 4, pp. 1692-1704, 2018.

[45] M. R. Gokel, M. McKeever, J. W. Meisel, S. Negin, M. B. Patel, S. Yin and G. W. Gokel, "Crown Ethers having Side Arms: A Diverse and Versatile Supramolecular Chemistry," *Journal of Coordination Chemistry,* vol. 74, no. 1-3, pp. 14-39, 2021.

[46] M. B. Patel, J. W. Meisel, S. Negin, M. R. Gokel and G. W. Gokel, "Resensitization of Resistant Bacteria to Antimicrobials," *Annals of Pharmacology and Pharmaceutics,* vol. 2, no. 10, pp. 1-5, 2017.

[47] W. M. Leevy, S. T. Gammon, T. Levchenko, D. D. Daranciang, O. T. V. Murillo, D. Piwnica-Worms, J. E. Huettner and G. W. Gokel, "Structure-activity Relationships Kinetics, Selectivity, and Mechanistic Studies of Synthetic Hydraphile Channels in Bacterial and Mammalian Cells," *Organic Biomolecular Chemistry,* vol. 3, pp. 3544-3550, 2005.

[48] M. C. Berenbaum, "What is Synergy?," *Pharmacological Reviews,* vol. 41, no. 2, pp. 93-141, 1989.

[49] J. Meletiadis, S. Pournaras, E. Roilides and T. J. Walsh, "Defining Fractional Inhibitory Concentration Index Cutoffs for Additive Interactions Based on Self-Drug Additive Combinations, Monte Carlo Simulation Analysis, and In Vitro - In Vivo Correlation Data for Antifungal Drug Combinations against A. fumigatus," *Antimicrobial Agents and Chemotherapy,* vol. 54, no. 2, pp. 602-609, 2010.

[50] The U.S. Food and Drug Administration, "Drug Development and Approval Process," 28 10 2019. [Online]. Available: https://www.fda.gov/drugs/development-approval-process-drugs. [Accessed 31 January 2022].

[51] C. f. D. Control, "Adjuvants and Vaccines," CDC, 2020. [Online]. Available: https://www.cdc.gov/vaccinesafety/concerns/adjuvants.html. [Accessed 31 January 2022].

Chapter 2

Design, Synthesis and Characterization of *Bis*(Tryptophan) Amphiphiles

1.2 Introduction

There are hundreds of naturally occurring amino acids, however, the 21 common amino acids make all the proteins found in the human body and most other forms of life. An amino acid contains an amino group ($-NH_2$) and a carboxylic acid group (-COOH). The common amino acids are all α-amino acids (Aaa) meaning the α-carbon connects both the amino and carboxylic acids groups. Furthermore, all 21 common amino acids are the L-isomer of the molecule. The general structure of these amino acids can be seen in **Fig. 2.1**. [1]

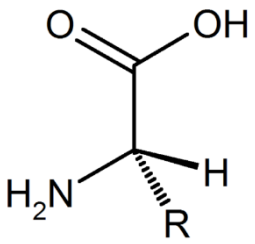

Figure 2.1 General structure of amino acids [1]

The R-group varies for each of the amino acids. Side chains can be aliphatic, aromatic, polar-neutral, amide containing, sulfur-containing, basic or acidic. As such, the physiochemical properties of amino acids can be quite diverse. Hydrophilicity and hydrophobicity, pKa, charges, flexibility and steric effects of the molecules will vary depending on the R-group attached. In some

cases, this leads to special properties, such as cysteine's ability to form disulfide bonds with other cysteine residues. [2]

With such variety present among the AAAs, they are most often categorized based on whether the side chain is acidic, basic, polar, or hydrophobic, **Fig. 2.2**. There is also a fifth group, "other important amino acids with special cases" which includes amino acids such as cysteine, mentioned previously and selenocysteine which is an analogue of cysteine containing selenium instead of sulfur. This group also encompasses glycine, which is a special case due to its lack of chirality of the central carbon and is more flexible than other AAAs. Proline is also a special case as the α-carbon is part of a pyrrolidine ring, which leads to the inclusion of a heterocycle into the polypeptide backbone when it forms part of a polypeptide chain. [2] [3]

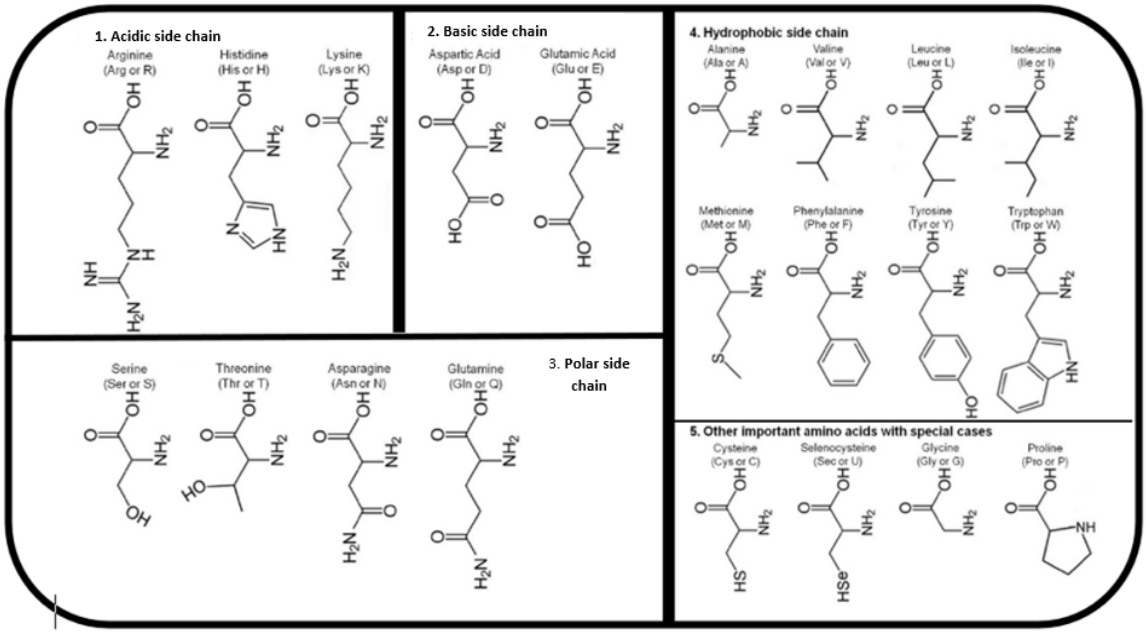

Figure 2.2 Diagram categorizing the 21 common amino acids

The most interesting characteristic of the amino acid side chains for the purposes of this research is hydrophobicity. The focus of this research is to explore membrane-active amphiphiles for a potential antimicrobial effect. It is known that cell membranes, including bacterial cell membranes, are comprised of a bilayer of lipids. The phospholipids of the membrane have a hydrophilic and a hydrophobic regime. [4] Antimicrobial peptides (AMPs) such as colistin (**Fig. 2.3**) [5], work by inserting into the cell membrane, disrupting ion homeostasis, and ultimately preventing essential metabolic processes from continuing. The structure of colistin has three clearly defined regions, including a hydrophobic tail and hydrophilic head. Amphiphilicity is an important characteristic of AMPs, therefore the hydrophobicity of any amino acids used in the development of antimicrobial molecules is a primary consideration. [56] [7]

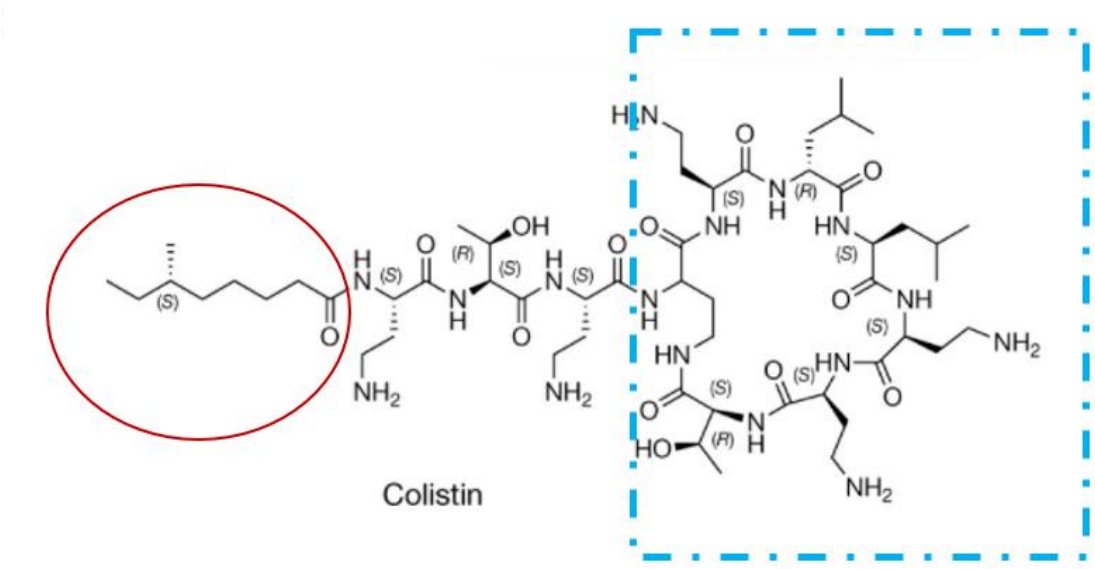

Figure 2.3 Structure of colistin. The molecule is comprised of three main segments. Hydrophobic tail (red circle), Hydrophilic heptapeptide ring (blue square) and a tripeptide linear region in the middle. [5]

Another consideration is the charges of the residues. The overall surface charge of a cell membrane can vary considerably from cell to cell. While bacterial cells generally have a negatively charged cell wall, owing to the excess of ionized phosphate and carboxyl groups, [8] the overall charge of a cell membrane is influenced by the presence of charged proteins embedded in the membrane. [9] It is often found that the inner layer of the membrane is more negatively charged than the outer layer, which can also be problematic when trying to develop membrane-active molecules based upon charges. [10] Furthermore, many mammalian cells are negatively charged. Mitochondrial membranes can contain up to 20% cardiolipin, which each have two negative charges. [11] With the unpredictability of which cells are truly being targeted on the basis of charges, designing membrane-active compounds based around the charges of the amino acids, may be a futile methodology.

Tryptophan is the least abundant of the common 21 amino acids, but is found frequently in membrane proteins. Tryptophan is most commonly observed at the lipid-water interface and is commonly thought to play a role as a membrane anchor. [12] Tryptophan has polar and non-polar regions and has more hydrophobic character, due to the indole moiety, than many of the other amino acids. All these factors make tryptophan an interesting choice when designing antimicrobial amphiphiles.

2.2 Rational Design

2.2.1 *The Design Criteria.* One of the most successful methods for targeting bacteria is to target their cell walls and membranes. [13] As antibacterial resistance has increased against current antibiotics, including the efficacy of efflux pumps, [14] novel methods of targeting the bacteria cell membranes are needed urgently. [15] Natural antimicrobial peptides (AMPs) in nature have shown us how effective amphiphilic molecules can be as part of the immune system. [56] [16]

Earlier work in the Gokel lab also demonstrated how effective synthetic amphiphiles could be with the design, synthesis, and applications of hydraphiles [17] and lariat ethers. [18] Both of these classes of compounds involved hydrophobic cyclic systems attached to alkyl or aryl side arms or linkers. The hydraphiles and lariat ethers have both shown antibiotic activity in the μM concentration range. [19] [20] The success of both of these classes of compounds heightened interest in the development of a third class of amphiphiles, the *bis*(amino acid)s.

2.2.2 *Successes of Bis(amino acid) Amphiphiles.* In continued work into amphiphiles, the Gokel group developed a series of *bis*(amino acid)s that had varying antimicrobial potencies. While the aliphatically-linked C_{12}BT molecule (tryptophan residues linked by an aliphatic carbon chain containing 12 carbon atoms) was most potent against a strain of *S. aureus* and a tetracycline-resistant

strain of *E. coli* (tet^R *E. coli*), it was the only active compound with an aliphatic linker. The general structure of the *bis*(tryptophan)s (BTs) is shown in **Fig 2.4**.

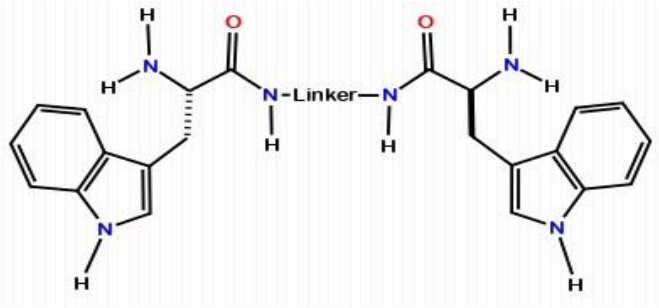

Figure 2.4 General Structure of *bis*(tryptophan) amphiphile

The *ortho-, meta-* and *para*-phenylene BTs showed more consistent activity than the aliphatically linked BTs. Therefore, phenylene linked *bis*(amino acid) compounds were synthesized for the remaining 19 common amino acids (selenocysteine was not included). [21] [22]

The published results from this work, including **Table 1.2,** show that none of the *bis*(amino acid) compounds were active against Gram-positive or Gram-negative bacterial strains other than the BTs. [22] The Gokel group also synthesized the other *bis*(amino acid) derivatives that have not yet been published, none of these displayed antimicrobial activity either. This research suggested that attention should be directed towards the BTs.

The Gokel group discovered multiple BTs were active against Gram-negative and Gram-positive bacteria, including a strain of *E. coli* resistant to tetracycline, due to the presence of the tet (A) efflux pump (tet^R *E. coli*). The phenylene-linked BTs all showed some level of potency, with the *meta*-phenylene BT being the

most active of the three. The aliphatic-linked BTs were all essentially inactive, with the exception of C_{12}BT, which proved to be more potent against the *E. coli* (K-12), *E. coli* (tet^R) and *S. aureus* than any of the phenylene-linked compounds. [21]

The BTs were also investigated for their cytotoxic effects. It was found that at the MIC against tet^R *E. coli*, the phenylene-linked BTs and the C_{12}BT showed minimal cytotoxic effects against various mammalian cells. [21] Furthermore, the BTs were investigated for their adjuvant capabilities. It was found that when co-administered with tetracycline, the BTs were able to reverse antibiotic resistance up to 16-fold against the tet^R *E. coli* at when co-administered at sub-MIC levels. [21]

Limited work has been carried out to investigate the mechanism(s) of action of BTs. Ion transport studies using propidium iodide have confirmed increased membrane permeability of *S. aureus* upon treatment with *m*-phenylene BT. Bilayer lipid membrane (BLM) studies have indicated potential channel activity or aggregation of the amphiphile in the membrane, although these results only pertain to the *m*-phenylene BT molecule also. [22]

The results of all of the research into the three categories of amphiphiles in the Gokel lab, in particular the efficacy of the BT molecules, has been used to guide the direction of this research. The library of BT amphiphiles have been expanded and additional techniques, such as ion transport studies, scanning electron microscopy (SEM) and dynamic light scattering (DLS), were used to better understand the mechanism(s) of action of these amphiphiles.

2.2.3 *The Library of Bis(tryptophan)s.* The greatest potential yet to be discovered was thought to be within the aliphatic-linked BTs. The C_{12}BT showed the highest potency so far, however, there were gaps in a potential sequence of compounds. C_3BT, C_4BT and C_6BT were the other three aliphatic BTs that had been synthesized and their activities investigated, however, none were biologically active. [21] [22] The thickness of the insulator regime of the phospholipid membrane is estimated to be in the 30-35 Å range so it would seem logical that longer chain molecules might transverse the membrane and potentially be more active. This would however require a carbon chain of 20 carbons in length, or greater, and there may be solubility issues with such a molecule. Furthermore, the mechanism of action seems not to require the molecule to span the entire thickness of a membrane, based on the activity of the C_{12}BT and phenylene-linked BT molecules. The latter certainly would be much shorter. It would therefore be proposed that the "gaps" in the series of aliphatic BTs be addressed first and exploration to continue from that point.

The new compounds that were synthesized for the purposes of this research are C_8BT, C_{10}BT and C_{14}BT. Extra quantities of the other BTs were also synthesized as required for analytical and biological experimentation. The entire library of compounds being investigated, and their structures are shown in **Fig. 2.5.** All compounds were synthesized as HCl salts and using the L-isomer of tryptophan (e.g. $(CH_2)_{12}$(L-Trp)$_2$·2HCl = C_{12}BT).

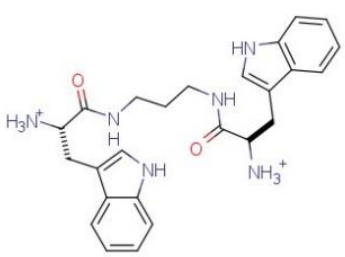

C_3BT
$(CH_2)_3$(L-Trp)$_2$·2HCl

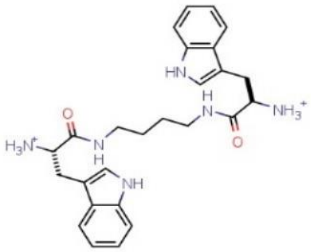

C_4BT
$(CH_2)_4$(L-Trp)$_2$·2HCl

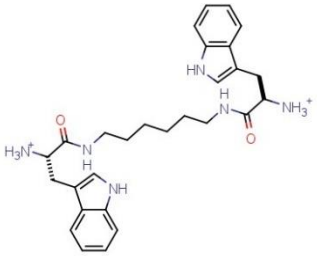

C_6BT
$(CH_2)_6$(L-Trp)$_2$·2HCl

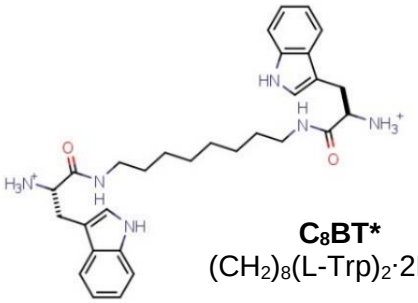

C_8BT*
$(CH_2)_8$(L-Trp)$_2$·2HCl

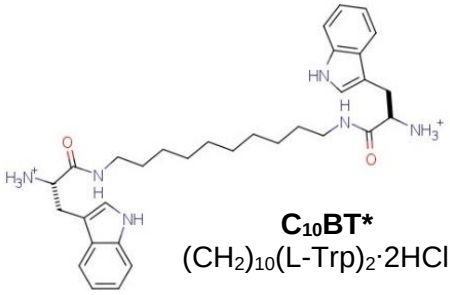

C_{10}BT*
$(CH_2)_{10}$(L-Trp)$_2$·2HCl

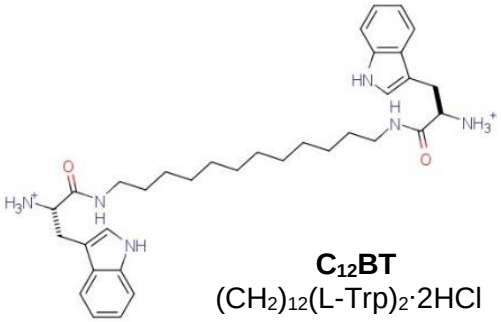

C_{12}BT
$(CH_2)_{12}$(L-Trp)$_2$·2HCl

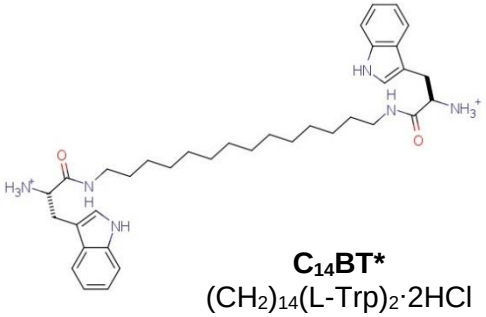

C_{14}BT*
$(CH_2)_{14}$(L-Trp)$_2$·2HCl

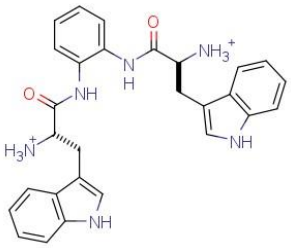

***o*-PhBT**
ortho-C_6H_4(L-Trp)$_2$·2HCl

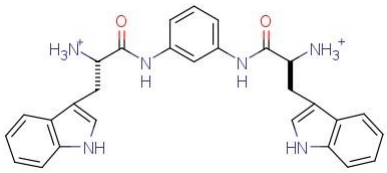

***m*-PhBT**
meta-C_6H_4(L-Trp)$_2$·2HCl

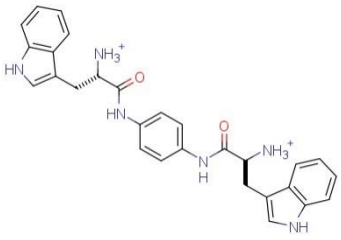

***p*-PhBT**
para-C_6H_4(L-Trp)$_2$·2HCl

Figure 2.5 Names and structures of the BTs investigated. The compounds that were first prepared as part of this research are marked with an asterisk (*)

2.3 Synthesis

The general procedure for the synthesis of BTs was available in the literature, [21] however some specific details were lacking. Thus considerable "trial and error" was required. Initially, it was assumed that the linker should be added at the beginning of the reaction at the same time as the tryptophan. As it turned out, this sequence failed to yield pure white solid product. The crude material would contain a little starting material, but mostly "contaminants." The NMR spectra were complex at this time. Eventually, it was decided that the tryptophan, DMF, HBTU and diisopropylethylamine may need to react for some time before the diamine could be coupled. The decision was also taken to try to isolate the crude product before attempting the deprotection and product-isolation steps. This led to the first breakthrough; the synthesis of a crude product that resembled the description in the literature. The NMR spectrum and melting point confirmed synthesis of the first BOC-protected BT of this research.

The isolated crude *m*-PhBT was dissolved in an appropriate solvent and then deprotected using HCl in dioxane. Choosing a suitable solvent was problematic. Methanol, the solvent suggested in the literature failed to afford product. Dioxane was eventually chosen and the deprotection was left overnight. In an attempt to ensure the reaction would have sufficient time, 24 hours was allowed for this step, initially. The crude product was a dark red/brown viscous liquid. The NMR showed remnants of the crude product; it was possible that HCl was degrading the compound.

Through trial and error, an inert environment was identified for the deprotection step, and a shorter reaction time of 16 hours was found to be sufficient. Thus, a yellow liquid resulted. Upon addition of cold hexane, a solid could be extracted. Trituration with cold DCM afforded the desired white solid / powder.

As the research progressed, it was discovered that the deprotection step could be achieved in high yield in less than an hour. It was also found that the overnight time frame for the initial coupling could be achieved in less than 3 hours with equivalent yields. The most time-consuming step was purification of the final product: a significant number of washes were required to achieve a pure product. The reaction scheme for the synthesis of *m*-PhBT [*meta*-C_6H_4(L-Trp)$_2$·2HCl] is shown in **Fig. 2.6**.

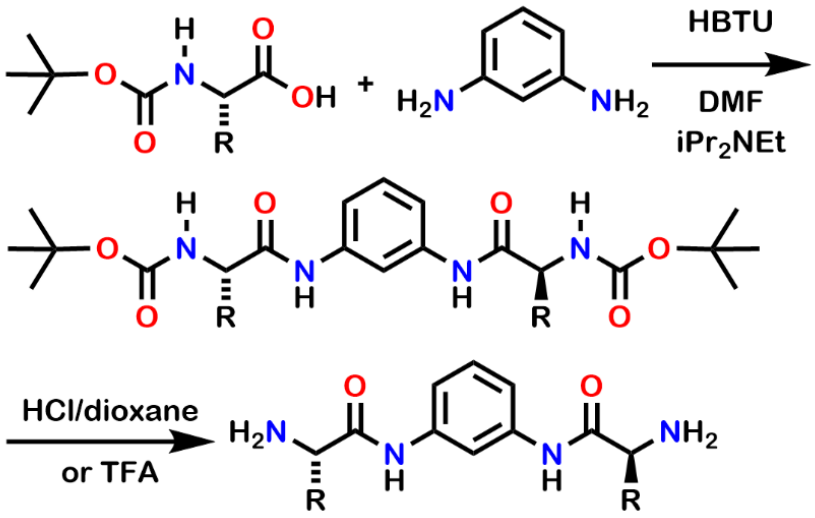

Figure 2.6 Synthetic scheme for *m*-PhBT (R = CH_2-Indole).

When an appropriate sequence was established, this synthetic pathway was chosen to form part of an advanced organic course for undergraduate students at the University of Missouri – St. Louis. The students would be tasked with developing a synthesis for the specified product (*m*-PhBT). The BOC-protected tryptophan and the *meta*-phenylenediamine were specified as starting reagents. The students were guided along the way with respect to solvent choices, purification techniques and the use of an inert environment. All of the students in the class were able to successfully synthesize the desired product. Purity and yields, of course, significantly varied, but the student feedback about how much they learned was very positive.

2.4 Analysis and Characterization

2.4.1 *Physical Characteristics*. The yields and physical characteristics of each of the compounds prepared is given in **Table 2.1.**

Table 2.1 Physical Characteristics of BTs. Data for non-novel compounds taken from literature [21]

Compound	Appearance	Yield (%)	Melting Point (°C)
C_3BT	White Powder	57	234
C_4BT	White Powder	89	204
C_6BT	White Powder	61	193
C_8BT	White Powder	70	182
C_{10}BT	White Powder	68	171
C_{12}BT	White Powder	93	158
C_{14}BT	Off-White Solid	61	156
o-PhBT	White Powder	34	201
m-PhBT	White Powder	80	223
p-PhBT	White Powder	83	237

The BTs were obtained as white powders, with the exception of the largest molecule, C_{14}BT. The longer alkyl chain made this compound more difficult to synthesize and to handle generally. The compound, after many washes remained a light-brown viscous oil. Upon drying a solid was formed, but the same white color could not be achieved.

The yields varied considerably from compound to compound. A low of 34% yield was observed for the *o*-PhBT. This is somewhat surprising as the

para-substituted BT had a high yield of 83%, similar to the 80% yield observed by the *m*-PhBT. In organic synthesis, activating groups tend to favor the *ortho* and *para*-substitution, while deactivating groups are *meta*-directing. Based on these electronic effects, it would be expected that the *ortho*- and *para*-substituted BTs would have similar yields. It may be that steric factors were blocking the effective coupling to both positions of the phenyl ring and that is why there is such a drop in the yield for the *o*-PhBT.

The melting points are listed in the final column of **Table 2.1.** For the aliphatic BTs, there is an obvious trend: as the chain lengths increase, the melting points decrease. A common trend exists for families of simple, unbranched, aliphatic, organic molecules: as the chain length of the molecule increases, the melting point increases. This is often explained by the fact longer chains will allow for more van der Waal's forces to be exerted. There are of course many other impacts to consider including hydrogen bonding, flexibility, and eccentricity and shape of the molecules. [23] Predicting the melting point of any new family of compounds may be considered a fool's errand. While many families of compounds follow the trend of increasing melting points with increased chain lengths, such as halogenated alkanes, alkanols, alkylamines and alkanoic amides, [23] there are also many that do not. Ionic liquids, for example, show an interesting trend in melting points. The ionic liquids with "short" alkyl chains, follow a trend of decreasing melting points as alkyl chain lengths increase. Ionic liquids that have "long" alkyl chains follow a trend of increasing melting points as the alkyl chain increases. [24] For these reasons**,** it is a

pleasant discovery that melting points of the aliphatic BTs in **Table 2.1** are inversely proportional to the chain lengths of the molecules.

The three phenylene-linked BTs also display a trend with regard to their melting points. In this case, the melting points seem to relate to the steric strain of the molecule. The less sterically restricted the molecule is, the more stable it appears to be and so a higher melting point is observed. Of course, there are many other factors involved, as previously mentioned, but the extent to which those are involved has not been estimated or quantitated.

2.4.2 *Nuclear Magnetic Resonance (NMR) Data.* All the ^{1}H-NMR spectra were determined at 300 MHz in CD_3OD. The spectrum for C_{14}BT, **Fig. 2.7**, shows the proton peaks expected for the compound, solvent peaks, and a reference peak (TMS) at 0.0 ppm, are present. For reference, the solvent peaks are: δ 3.304 (methanol), 3.653 (dioxane), 4.911 (H_2O), 5.491 (dichloromethane).

C_{14}BT proton peaks: δ 1.11-1.42 ppm (m, 24H, aliphatic CH_2), 2.96-3.40 ppm (m, 8H, -$CH_2\underline{CH_2}$NH-, CH_2ß), 4.02 ppm (ABX, 2H, CHα), 7.02-7.15 ppm (m, 4H, indole H5, indole H6) 7.18 ppm (s, 2H, indole H2), 7.36 ppm (d, 2H, indole H7), 7.60 ppm (d, 2H, indole H4).

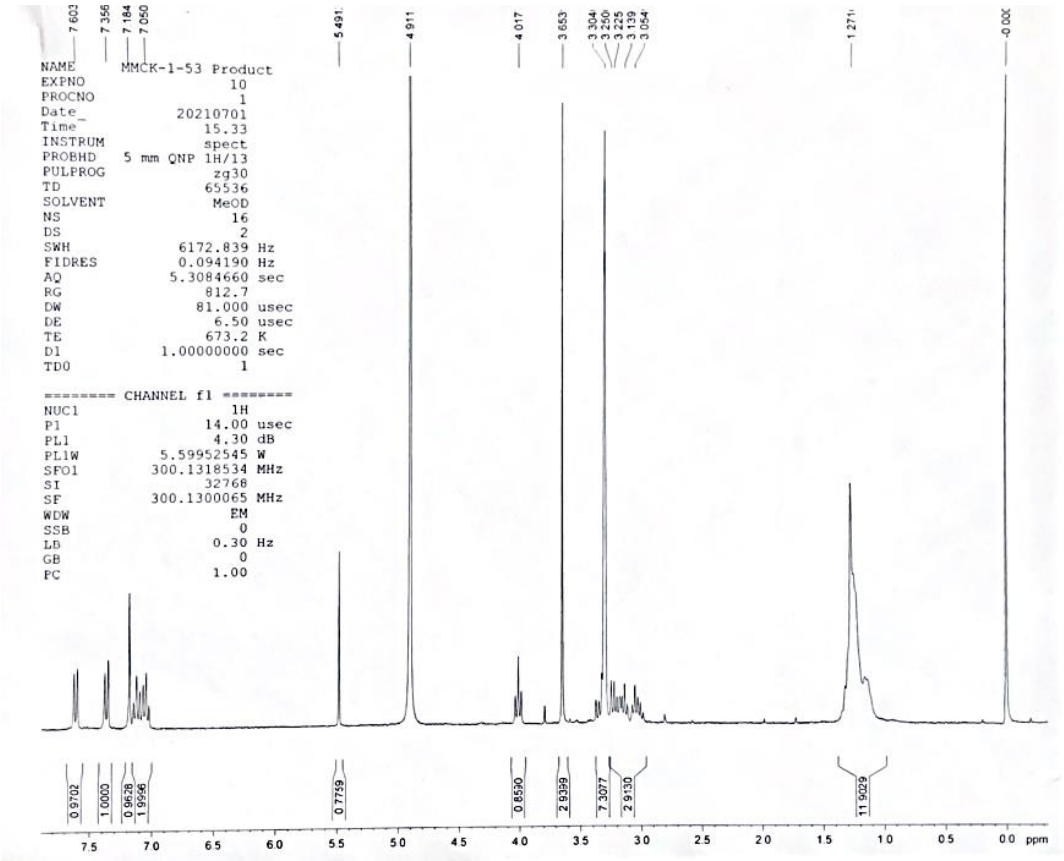

Figure 2.7 ^{1}H-NMR Spectrum for C_{14}BT in CD_3OD at 300 MHz

The proton peaks for each of the other BTs are given in **Table 2.2**. The data for the previously reported compounds have been taken from the literature. [21] All other ^{1}H-NMR was obtained experimentally, first-hand.

Table 2.2 ^{1}H-NMR peaks for all the BTs. Data for previously reported compounds taken from the literature [21]

Compound	^{1}H-NMR Peaks (ppm)
C_3BT	δ 1.40 (m, 2H, -$\underline{CH_2}CH_2$NH-), 2.98 (m, 4H, -$CH_2\underline{CH_2}$NH-), 3.22-3.65 (m, 4H, CH_2ß) 4.13 (ABX, 2H, CHα), 6.99-7.18 (m, 4H, indole H5, indole H6) 7.25 (s, 2H, indole H2), 7.39 (d, 2H, indole H7), 7.69 (d, 2H, indole H4).
C_4BT	δ 1.18 (m, 2H, -$\underline{CH_2}CH_2$NH-), 3.05 (m, 4H, -$CH_2\underline{CH_2}$NH-), 3.22-3.41 (ABX, 2H, CH_2ß) 4.09 (ABX, 2H, CHα), 7.05-7.17 (m, 4H, indole H5, indole H6) 7.23 (s, 2H, indole H2), 7.40 (d, 2H, indole H7), 7.66 (d, 2H, indole H4).
C_6BT	δ 1.05 (m, 2H, aliphatic CH_2),1.26 (m, 2H, aliphatic CH_2), 2.97-3.39 (m, 4H, -$CH_2\underline{CH_2}$NH-, CH_2ß), 4.06 (ABX, 2H, CHα), 7.02-7.15 (m, 4H, indole H5, indole H6) 7.20 (s, 2H, indole H2), 7.37 (d, 2H, indole H7), 7.63 (d, 2H, indole H4).
C_8BT	δ 1.02-1.38 (m, 12H, aliphatic CH_2), 2.97-3.42 (m, 8H, -$CH_2\underline{CH_2}$NH-, CH_2ß), 4.04 (ABX, 2H, CHα), 7.02-7.16 (m, 4H, indole H5, indole H6) 7.20 (s, 2H, indole H2), 7.36 (d, 2H, indole H7), 7.64 (d, 2H, indole H4).
C_{10}BT	δ 1.01-1.38 (m, 16H, aliphatic CH_2), 2.92-3.35 (m, 8H, -$CH_2\underline{CH_2}$NH-, CH_2ß), 3.99 (ABX, 2H, CHα), 7.00-7.14 (m, 4H, indole H5, indole H6) 7.15 (s, 2H, indole H2), 7.31 (d, 2H, indole H7), 7.59 (d, 2H, indole H4).
C_{12}BT	δ 1.08-1.34 (m, 20H, aliphatic CH_2), 2.96-3.40 (m, 8H, -

	$CH_2\underline{CH_2}$NH-, CH_2ß), 4.04 (ABX, 2H, CHα), 7.02-7.15 (m, 4H, indole H5, indole H6) 7.20 (s, 2H, indole H2), 7.37 (d, 2H, indole H7), 7.62 (d, 2H, indole H4).
C_{14}BT	δ 1.11-1.42 (m, 24H, aliphatic CH_2), 2.96-3.40 (m, 8H, -$CH_2\underline{CH_2}$NH-, CH_2ß), 4.02 (ABX, 2H, CHα), 7.02-7.15 (m, 4H, indole H5, indole H6) 7.18 (s, 2H, indole H2), 7.36 (d, 2H, indole H7), 7.60 (d, 2H, indole H4).
o-PhBT	δ 3.35-3.65 (ABX, 2H, ßCH_2), 4.58 (t, 1H, αCH), 7.00-7.73 (m, 7H, ArH, ArNH)
m-PhBT	δ 3.33-3.53 (ABX, 4H, 2CH_2ß), 4.26 (ABX, 2H, 2CHα), 7.01 (t, 2H, indole H5), 7.12 (t, 2H, indole H6) 7.22 (s, 2H, indole H2), 7.26 (m, 2H, phenylene H4), 7.27 (m, 1H, phenylene H5), 7.38 (d, 2H, indole H7), 7.67 (d, 2H, indole H4)., 7.93 (s, 2H, phenylene H2).
p-PhBT	δ 3.34-3.54 (ABX, 2H, CH_2ß), 4.27 (ABX, 1H, CHα), 6.97-7.14 (m, 2H, indole H5, indole H6), 7.24 (s, 1H, indole H7) 7.38 (d, 1H, indole H7), 7.67 (d, 1H, indole H4).

2.4.3 *Electrospray Ionization (ESI) Mass Spectroscopy Data.* Mass spectrometry data were obtained at the UMSL chemistry department facilities. Liquid chromatography and mass spectrometry are used so the purity of the product can be verified at this stage. **Fig. 2.8** shows the chromatograph and mass spectrum for C_{14}BT.

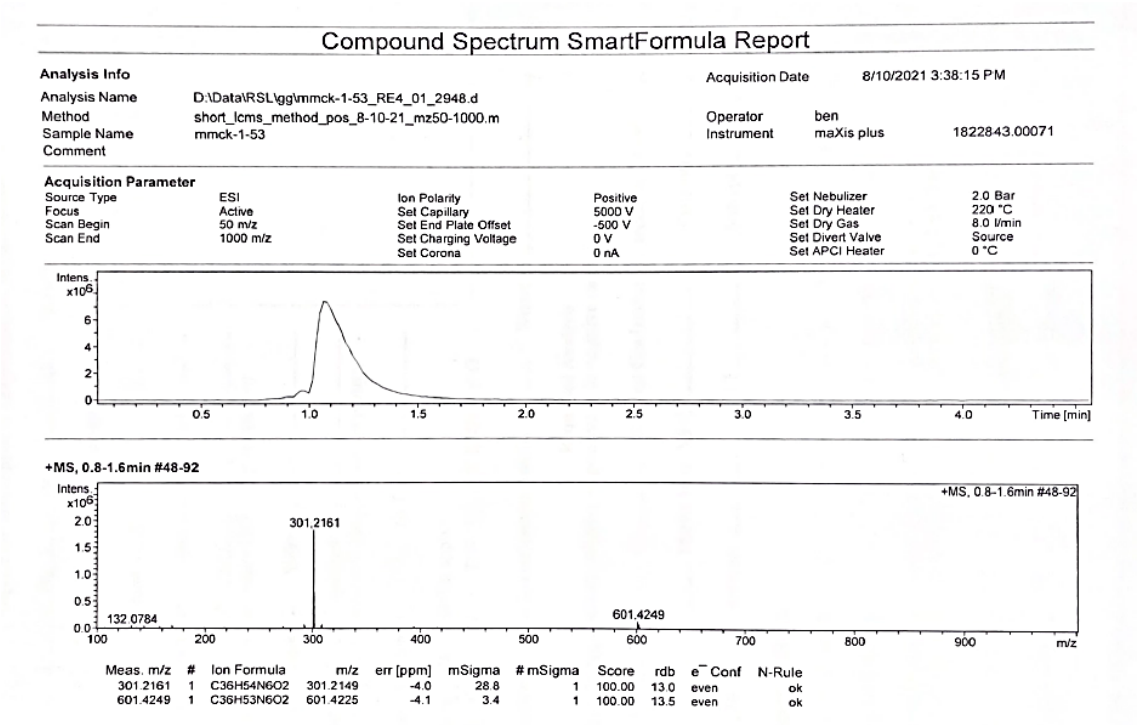

Figure 2.8 Chromatograph and mass spectrum of C_{14}BT dissolved in methanol.

The top panel of **Fig. 2.8** shows the chromatograph. It shows that the C_{14}BT sample is virtually pure given that only one major peak is detected during the liquid chromatography. The lower panel shows the mass spectrometry data. It shows the major ion peaks for C_{14}BT, which exists as $(CH_2)_{14}(L\text{-}Trp)_2{\cdot}2HCl$, the hydrochloride salt. The mass to charge ratio (m/z) of the base peak is observed

as 301.2161 ($C_{14}BT^{2+}$) while the second most abundant peak is 601.4249 ($C_{14}BT^{+}$). This represents the single and double charged species, which both exist in the sample. The mass spectrum confirms the identity of the $C_{14}BT$, which has a calculated mass of 601.4152 g/mol. Below the graphs, the error has been calculated. The error for each is within 5 ppm, well within the accepted margin of error. Mass spectrometry data, such as that shown in **Fig. 2.8**, was collected for all the BTs. The data from each of these has been summarized in **Table 2.3**.

Table 2.3 Mass Spectroscopy data for BTs. Data for non-novel compounds taken from the literature [21]

Compound	Calculated Mass (g/mol)	Experimental Mass (g/mol)	Error (ppm)
C_3BT	447.2503	447.2503	0
C_4BT	461.2660	461.2668	-1.7
C_6BT	489.2973	489.2972	+0.2
C_8BT	518.3358	518.3364	-1.2
$C_{10}BT$	546.3671	546.3677	-1.1
$C_{12}BT$	573.3912	573.3929	-3.0
$C_{14}BT$	601.4152	601.4125	+4.5
o-PhBT	481.2347	481.2359	-2.5
m-PhBT	481.2347	481.2356	-1.9
p-PhBT	481.2347	481.2346	0

The data in **Table 2.3** show that each synthesized BT compound had a mass close to the calculated mass, with the exception of the *p*-PhBT (+674.3 ppm). This compound was not synthesized as part of this work. The extremely small margin of error for the other BTs confirmed the identification of the BTs synthesized.

2.4.4 *Crystal Formation.* For decades, X-ray crystallography has been a preferred method to obtain structural information of small molecules, proteins, and biological macromolecules. A three-dimensional molecular structure can be obtained following the crystallization of a pure sample of the compound or specimen. Diffraction patterns of the X-ray beam are processed, and the repeating sub-units of the crystal can be determined. Diffraction spots can be used to determine structure factors which can in turn be used to create an electron density map. Further processing and refinement of the mapping allows for a three-dimensional molecular structure to be obtained. [25]

To date, no crystal structure has been obtained for any of the BTs included in this research. It was decided that crystal structures could be useful to help understand potential interactions within a membrane of the BTs and their potential going forward. There are many different methods used for crystal formation and growing, including slow cooling, vapor diffusion, seeding, convection, slow evaporation, and even more specialized methods, such as co-crystallization and diffusion of reagents. [26] Slow evaporation is one of the less complicated methods to perform. The downsides to this method are the larger

quantities of compound needed and significant volumes of solvents are required. A significant stock of *m*-PhBT was on hand and it has one of the higher melting points among the BTs. Thus, forming crystals may be more achievable by using this compound, compared to other BTs. The slow evaporation method is usually only avoided when the compounds are air-sensitive or when being performed in a dry box. It was decided that slow evaporation would be most useful in the attempt to produce crystals of the BTs. **Table 2.4** shows the solvent systems used, the conditions and the data gained so far.

For the slow evaporation method of crystal formation, it is imperative to first dissolve the compound in a minimal amount of solvent. The solution should be as concentrated as possible. A co-solvent is then added, if using a solvent system. This co-solvent should not dissolve the compound on its own and should have a similar, or slightly lower boiling point than the original solvent. The BTs are known to be soluble in methanol, ethanol, and water. These are the initial solvents used in each of the systems. The vials were covered with a dust guard and a small opening made in the lid to facilitate slow evaporation of the solvents. Most of the systems were tried at room temperature (RT). On some occasions, the temperature had been lowered to 5 °C to encourage slower evaporation. At room temperature, complete evaporation of solvents happened within 14 days. At 5 °C, it took almost twice as long (25+ days), depending on the opening size and solvent used. Crystals should form before complete evaporation.

Table 2.4 Compounds and solvent systems attempted for crystal growing.

Solvent Systems for Crystals - *m*- PhBT and C_{12}BT					
Code	**Compound**	**Solvent System**	**Ratio**	**Temp**	**Observations**
MMCK-001	m-PhBT	Methanol Alone	N/A	RT	Brown Solid
MMCK-002	m-PhBT	Methanol Alone	N/A	5 °C	Brown translucent solid
MMCK-003	m-PhBT	Ethanol Alone	N/A	RT	Brown Solid
MMCK-004	m-PhBT	Ethanol Alone	N/A	5 °C	Brown translucent solid
MMCK-005	m-PhBT	Water Alone	N/A	RT	Brown Solid
MMCK-006	m-PhBT	Methanol : Hexane	50/50	RT	Brown Solid
MMCK-007	m-PhBT	Methanol : Hexane	75/25	RT	Brown Solid
MMCK-008	m-PhBT	Methanol : Ethyl Aceta	50/50	RT	Brown Solid
MMCK-009	m-PhBT	Methanol : Ethyl Aceta	75/25	RT	Brown Solid
MMCK-010	m-PhBT	Methanol : Diethyl Eth	50/50	RT	Brown Solid
MMCK-011	m-PhBT	Methanol : Diethyl Eth	75/25	RT	Brown Solid
MMCK-012	m-PhBT	Ethanol : Acetonitrile	50/50	RT	Brown Goo / Solid
MMCK-013	m-PhBT	Ethanol : Acetonitrile	75/25	RT	Brown Goo / Solid
MMCK-015	m-PhBT	Ethanol : Toluene	75/25	RT	Brown Goo / Solid
MMCK-016	m-PhBT	Ethanol : Ethyl Acetate	50/50	RT	Brown Goo / Solid
MMCK-017	m-PhBT	Ethanol : Ethyl Acetate	75/25	RT	Brown Goo / Solid
MMCK-018	m-PhBT	Methanol : Acetonitrile	50/50	RT	Brown solid
MMCK-019	m-PhBT	Methanol : Acetonitrile	75/25	RT	Brown Solid
MMCK-020	m-PhBT	Methanol : Toluene	50/50	RT	Brown Solid
MMCK-021	m-PhBT	Methanol : Toluene	75/25	RT	Brown Solid
MMCK-022	m-PhBT	Ethanol : Hexane	50/50	RT	White solid
MMCK-023	m-PhBT	Ethanol : Hexane	75/25	RT	White solid
MMCK-024	m-PhBT	Ethanol : Diethyl Ether	50/50	RT	White solid
MMCK-025	m-PhBT	Ethanol : Diethyl Ether	75/25	RT	White Solid
MMCK-026	m-PhBT	Methanol : Chloroform	50/50	RT	Brown Solid
MMCK-027	m-PhBT	Methanol : Chloroform	75/25	RT	Brown Solid
MMCK-028	m-PhBT	Methanol : Acetone	50/50	RT	Brown Solid
MMCK-029	m-PhBT	Methanol : Acetone	75/25	RT	Brown Solid
MMCK-030	m-PhBT	Ethanol : Chloroform	50/50	RT	Brown Solid
MMCK-031	m-PhBT	Ethanol : Chloroform	75/25	RT	Brown Solid
MMCK-032	m-PhBT	Ethanol : Acetone	50/50	RT	Brown Solid
MMCK-033	m-PhBT	Ethanol : Acetone	75/25	RT	Brown Solid
MMCK-101	C12BT	Methanol Alone	N/A	5 °C	Brown transparent glacial solid
MMCK-102	C12BT	Ethanol Alone	N/A	5 °C	Brown transparent glacial solid
MMCK-103	C12BT	Methanol Alone*	N/A	5 °C	

Table 2.4 shows the 35 combinations that have been tried to date. No useful crystals have been obtained to date.

2.5 Conclusion

The aim of the work recorded in this chapter was to build upon the existing library of *bis*(tryptophan) amphiphiles (BTs). The library was expanded to include C_8BT, C_{10}BT and C_{14}BT, which had not been synthesized prior to this work. Analytical techniques, such as LC-MS and ^{1}H-NMR were used to confirm successful syntheses and attempts were made to resolve the first crystal structure for this family of compounds. A trend was observed for this group of compounds with regards to their melting points. As the length of the aliphatic linker, and thus the molecular weight of the molecule increased, the melting point decreased.

The synthetic procedure was also refined. Previous synthetic procedures were optimized to include reduced reaction times. The procedure was simplified and was successfully used to form a multi-step synthetic project for 3000 level undergraduate organic chemistry at UMSL.

Future work involving the synthesis of BTs might include synthesis of amphiphiles with linkers containing an odd number of carbons in the chain, for example, C_7BT,C_9BT, C_{11}BT and so on. It is worth noting that the characteristics may change significantly when the chain length is changed. Previous work in the Gokel lab showed that the dialkyl-substituted lariat ethers could be solids at room temperature when the alkyl side chains contained an even number of carbons, [27] but a liquid when the number of carbons was an odd number. [18] It was notable that the C_{10}LE and C_{12}LE both form solids at room temperature while the C_{11}LE is an oil. Considerations such as this should be made if planning future

synthetic work with the BTs.

Other work might include the synthesis of longer chains beyond C_{14}BT. Given the solubility issues experienced with the C_{14}BT during the synthesis, the procedure may need amended to include less-polar solvents, if this is attempted.

2.6 Experimental Details

All of the BTs were prepared according to the general procedure published by the Gokel group in 2016. [21] Adjustments and modifications were made as necessary depending on the specific properties of the reagents used and the intricacies of product isolation.

General Procedure

Dissolve *tert*-butyloxycarbonyl-protected (BOC-protected) tryptophan (2.0 equivalents, 2.5 mmol) and HBTU (2.1 equivalents, 2.7 mmol) in 10 mL anhydrous dimethylformamide (DMF). Place reaction mixture under argon and in an ice-bath. Add diisopropylethylamine (6.0 equivalents, 1.3 mL) and stir for 30 minutes. Dissolve diamine (1.25 mmol, 1.0 equivalent) in minimal amount of DMF and inject into amino acid mixture. Remove from ice bath and continue to stir at room temperature overnight (12-16 hours). The mixture is taken up in 75 mL ethyl acetate and washed with 1 M $NaHSO_4$ (2 x 75 mL), 5% $NaHCO_3$ (3 x 50 mL) and brine solution (2 x 75 mL). The organic layer is dried via filtration though a plug consisting of a 50:50 mixture of $MgSO_4$ and Celite©. The solvent is removed *in vacuo*. This yields the BOC-protected product. Deprotection was carried out using 4.0 M HCl in dioxane (10 equivalents, 3.5 mL), under argon. The product is isolated by precipitation using cold hexanes and trituration using cold dichloromethane. Structure and purity confirmed using ^{1}H-NMR and LC-MS. Melting point was determined using Fischer Scientific melting point apparatus.

C_3BT [$(CH_2)_3$(L-Trp)$_2$·2HCl] was prepared according to the general procedure using 1,3-diaminopropane dihydrochloride (200 mg, 1.36 mmol). The product was obtained as a white powder (346 mg, 57% yield), mp 234 °C. ^{1}H-NMR (CD_3OD): δ 1.40 (m, 2H, -$\underline{CH_2}CH_2NH$-), 2.98 (m, 4H, -$CH_2\underline{CH_2}NH$-), 3.22-3.65 (m, 4H, CH_2ß) 4.13 (ABX, 2H, CHα), 6.99-7.18 (m, 4H, indole H5, indole H6) 7.25 (s, 2H, indole H2), 7.39 (d, 2H, indole H7), 7.69 (d, 2H, indole H4). HRMS (FAB+) Calcd ($C_{25}H_{31}N_6O_2^+$): 447.2503 Found: 447.2503

C_4BT [$(CH_2)_4$(L-Trp)$_2$·2HCl] was prepared according to the general procedure using 1.4-diaminobutane dihydrochloride (210 mg, 1.30 mmol). The product was obtained as a white powder (534 mg, 89% yield), mp 204 °C. ^{1}H-NMR (CD_3OD): δ 1.18 (m, 2H, -$\underline{CH_2}CH_2NH$-), 3.05 (m, 4H, -$CH_2\underline{CH_2}NH$-), 3.22-3.41 (ABX, 2H, CH_2ß) 4.09 (ABX, 2H, CHα), 7.05-7.17 (m, 4H, indole H5, indole H6) 7.23 (s, 2H, indole H2), 7.40 (d, 2H, indole H7), 7.66 (d, 2H, indole H4). HRMS (FAB+) Calcd ($C_{26}H_{33}N_6O_2^+$): 461.2660 Found: 461.2668

C_6BT [$(CH_2)_6$(L-Trp)$_2$·2HCl] was prepared according to the general procedure using 1,6-diaminohexane dihydrochloride (250 mg, 1.32 mmol). The product was obtained as a white powder (394 mg, 61% yield), mp 193 °C. ^{1}H-NMR (CD_3OD): δ 1.05 (m, 2H, aliphatic CH_2),1.26 (m, 2H, aliphatic CH_2), 2.97-3.39 (m, 4H, -$CH_2\underline{CH_2}NH$-, CH_2ß), 4.06 (ABX, 2H, CHα), 7.02-7.15 (m, 4H, indole H5, indole H6) 7.20 (s, 2H, indole H2), 7.37 (d, 2H, indole H7), 7.63 (d, 2H, indole H4). HRMS (FAB+) Calcd ($C_{28}H_{37}N_6O_2^+$): 489.2973 Found: 489.2972

C_8BT [$(CH_2)_8$(L-Trp)$_2$·2HCl] was prepared according to the general procedure using 1,8-diaminooctane (180 mg, 1.25 mmol). The product was obtained as a white powder (453 mg, 70% yield), mp 182 °C. ^{1}H-NMR (CD_3OD): δ 1.02-1.38 (m, 12H, aliphatic CH_2), 2.97-3.42 (m, 8H, -$CH_2\underline{CH_2}$NH-, CH_2ß), 4.04 (ABX, 2H, CHα), 7.02-7.16 (m, 4H, indole H5, indole H6) 7.20 (s, 2H, indole H2), 7.36 (d, 2H, indole H7), 7.64 (d, 2H, indole H4). HRMS (ESI) Calcd ($C_{30}H_{41}N_6O_2^+$): 518.3358 Found: 518.3364

C_{10}BT [$(CH_2)_{10}$(L-Trp)$_2$·2HCl] was prepared according to the general procedure using 1,10-diaminodecane (215 mg, 1.25 mmol). The product was obtained as a white powder (464 mg, 68% yield), mp 171 °C. ^{1}H-NMR (CD_3OD): δ 1.01-1.38 (m, 16H, aliphatic CH_2), 2.92-3.35 (m, 8H, -$CH_2\underline{CH_2}$NH-, CH_2ß), 3.99 (ABX, 2H, CHα), 7.00-7.14 (m, 4H, indole H5, indole H6) 7.15 (s, 2H, indole H2), 7.31 (d, 2H, indole H7), 7.59 (d, 2H, indole H4). HRMS (ESI) Calcd ($C_{32}H_{45}N_6O_2^+$): 546.3671 Found: 546.3677

C_{12}BT [$(CH_2)_{12}$(L-Trp)$_2$·2HCl] was prepared according to the general procedure using 1,12-diaminododecane (250 mg, 1.25 mmol). The product was obtained as a white powder (667 mg, 93% yield), mp 158 °C. ^{1}H-NMR (CD_3OD): δ 1.08-1.34 (m, 20H, aliphatic CH_2), 2.96-3.40 (m, 8H, -$CH_2\underline{CH_2}$NH-, CH_2ß), 4.04 (ABX, 2H, CHα), 7.02-7.15 (m, 4H, indole H5, indole H6) 7.20 (s, 2H, indole H2), 7.37 (d, 2H, indole H7), 7.62 (d, 2H, indole H4). HRMS (ESI) Calcd ($C_{34}H_{49}N_6O_2^+$): 573.3912 Found: 573.3929

C_{14}BT [$(CH_2)_{14}$(L-Trp)$_2$·2HCl] was prepared according to the general procedure using 1,14-diaminotetradecane (285 mg, 1.25 mmol) . The product was obtained as a white powder (459 mg, 61% yield), mp 156 °C. ^{1}H-NMR (CD_3OD): δ 1.11-1.42 (m, 24H, aliphatic CH_2), 2.96-3.40 (m, 8H, -$CH_2\underline{CH_2}$NH-, CH_2ß), 4.02 (ABX, 2H, CHα), 7.02-7.15 (m, 4H, indole H5, indole H6) 7.18 (s, 2H, indole H2), 7.36 (d, 2H, indole H7), 7.60 (d, 2H, indole H4). HRMS (ESI) Calcd ($C_{36}H_{53}N_6O_2^+$): 601.4152 Found: 601.4125

***o*-PhBT [*ortho*-C_6H_4(L-Trp)$_2$·2HCl]** was prepared according to the general procedure using 1,2-phenylenediame (150 mg, 1.39 mmol). The product was obtained as a white powder (227 mg, 34% yield), mp 201 °C. ^{1}H-NMR (CD_3OD): δ 3.35-3.65 (ABX, 2H, ßCH_2), 4.58 (t, 1H, αCH), 7.00-7.73 (m, 7H, ArH, ArNH) HRMS (FAB+) Calcd ($C_{28}H_{28}N_6O_2^+$): 481.2347 Found: 481.2359

***m*-PhBT [*meta*-C_6H_4(L-Trp)$_2$·2HCl]** was prepared according to the general procedure using 1,3-phenylenediame (150 mg, 1.39 mmol). The product was obtained as a white powder (535 mg, 80% yield), mp 223 °C. ^{1}H-NMR (CD_3OD): δ 3.33-3.53 (ABX, 4H, 2CH_2ß), 4.26 (ABX, 2H, 2CHα), 7.01 (t, 2H, indole H5), 7.12 (t, 2H, indole H6) 7.22 (s, 2H, indole H2), 7.26 (m, 2H, phenylene H4), 7.27 (m, 1H, phenylene H5), 7.38 (d, 2H, indole H7), 7.67 (d, 2H, indole H4)., 7.93 (s, 2H, phenylene H2). HRMS (ESI) Calcd ($C_{28}H_{28}N_6O_2^+$): 481.2347 Found: 481.2356

***p*-PhBT [*para*-C_6H_4(L-Trp)$_2$·2HCl]** was prepared according to the general procedure using 1,4-phenylenediame (150 mg, 1.39 mmol). The product was obtained as a white powder (555mg, 83% yield), mp 237 °C. ^{1}H-NMR (CD_3OD): δ 3.34-3.54 (ABX, 2H, CH_2ß), 4.27 (ABX, 1H, CHα), 6.97-7.14 (m, 2H, indole H5, indole H6), 7.24 (s, 1H, indole H7) 7.38 (d, 1H, indole H7), 7.67 (d, 1H, indole H4). HRMS (FAB+) Calcd ($C_{28}H_{28}N_6O_2^+$): 481.2347 Found: 481.2346

2.7 References

[1] M. J. Lopez and S. S. Mohiuddin, "Biochemistry, Essential Amino Acids," 26 March 2021. [Online]. Available: https://www.ncbi.nlm.nih.gov/books/NBK557845/. [Accessed 04 February 2022].

[2] R. Bischoff and H. Schluter, "Amino Acids: Chemistry, Fucntionality and Selected Non-Enzymatic Post-Translational Modifications," *Journal of Proteomics,* vol. 75, pp. 2275-2296, 2012.

[3] J. Farrera-Sinfreu, E. Giralt, S. Castel, F. Albericio and M. Royo, "Cell-Penetrating cis-gamma-Amino-L-Proline-Derived Peptides," *Journal of the American Chemical Society,* vol. 127, pp. 9459-9468, 2005.

[4] J. Lombard, "Once upon a time the cell membranes: 175 years of cell boundary research," *Biology Direct,* vol. 9, no. 32, pp. 1-35, 2014.

[5] M. Rhouma, F. Beaudry, W. Theriault and A. Letellier, "Colistin in Pig Production: Chemistry, Mechanism of Antibacterial Action, Microbial Resistance Emergence, and One Health Perspectives," *Frontiers in Microbiology,* vol. 7, pp. 1-22, 2016.

[6] J. M. Ageitos, A. Sanchez-Perez, P. Carlo-Mata and T. G. Villa, "Antimicrobial Peptides (AMPs): Ancient Compounds that Represent Novel Weapoons in the Fight Against Bacteria," *Biohemical Pharmacology,* vol. 133, pp. 117-138, 2017.

[7] I. Karaiskos, M. Souli, I. Galani and H. Giamarellou, "Colistin: Still a Lifesaver for the 21st Century?," *Expert Opinion on Drug Metabolism & Toxicology,* vol. 13, no. 1, pp. 59-71, 2016.

[8] R. M. Goulter, I. R. Gentle and G. A. Dykes, "Issues in Determining Factors Influencing Bacterial Attachment: A Review using Attachment of E. coli to Abiotic Surfaces as an Example," *Letters in Applied Microbiology,* vol. 49, pp. 1-7, 2009.

[9] A. N. Gray, J. M. Henderson-Frost, D. Boyd, S. Shirafi, H. Niki and M. B. Goldberg, "Unbalanced Charge Distribution as a Determinant for Dependence of a Subset of E. coli Membrane Proteins on the Membrane Insertase YidC," *mBio,* vol. 2, no. 6, pp. 1-10, 2011.

[10] J. E. Rothman and E. P. Kennedy, "Rapid Transmembrane Movement of Newly Synthesized Phospholipids during Membrane Assembly," *PNAS,* vol. 74, no. 5, pp. 1821-1825, 1977.

[11] T. Heimburg, "Physical Properties of Biological Membranes," 16 February 2009. [Online]. Available: https://www.nbi.ku.dk/membranes/pdf/2009_Heimburg_arXiv. [Accessed 04 February 2022].

[12] A. J. de Jesus and T. W. Allen, "The Role of Tryptophan Side Chains in Membrane Protein Anchoring and Hydrophobic Mismatch," *Biochmica et Biophysica Acta,* vol. 1828, pp. 864-876, 2013.

[13] D. A. Hopwood, "Streptomyces in Nature and Medicine: The Antibiotic Makers," New York, Oxford Universty Press, 2007.

[14] W. C. Reygaert, "An Overview of the Antimicrobial Resistance Mechanisms of Bacteria," *AIMS Microbiology,* vol. 4, no. 3, pp. 482-501, 2018.

[15] E. Peterson and P. Kaur, "Antibiotic Resistance Mechanisms in Bacteria: Relationships Between Resistance Determinants of Antibiotic Producers, Environmental Bacteria, and Clinical Pathogens," *Frontiers in Microbiology,* vol. 9, pp. 1-21, 2018.

[16] R. E. W. Hancock and A. Rozek, "Role of Membranes in the Activities of Antimicrobial Cationic Peptides," *FEMS Microbiology Letters,* vol. 206, no. 2, pp. 143-149, 2006.

[17] S. Negin, B. A. Smith, A. Unger, W. M. Leevy and G. W. Gokel, "Hydraphiles: A Rigorously Studied Class of Synthetic Channel Compounds with In Vivo Activity," *International Journal of Biomedical Imaging,* pp. 1-11, 2013.

[18] S. Negin, M. B. Patel, M. R. Gokel, J. W. Meisel and G. W. Gokel, "Antibiotic Potency against E. coliis Enhanced by Channel-Forming Alkyl Lariat Ethers," *ChemBioChem,* vol. 17, pp. 2153-2161, 2016.

[19] M. R. Gokel, M. McKeever, J. W. Meisel, S. Negin, M. B. Patel, S. Yin and G. W. Gokel, "Crown Ethers having Side Arms: A Diverse and Versatile Supramolecular Chemistry," *Journal of Coordination Chemistry,* vol. 74, no. 1-3, pp. 14-39, 2021.

[20] M. B. Patel, J. W. Meisel, S. Negin, M. R. Gokel and G. W. Gokel, "Resensitization of Resistant Bacteria to Antimicrobials," *Annals of Pharmacology and Pharmaceutics,* vol. 2, no. 10, pp. 1-5, 2017.

[21] J. W. Meisel, M. B. Patel, E. Garrad, R. A. Stanton and G. W. Gokel, "Reversal of Teracycline Resistance in Escherichia coli by Noncytotoxic

bis(Tryptophan)s," *Journal of the American Chemical Society,* vol. 138, pp. 10571-10577, 2016.

[22] M. Patel, S. Negin, J. Meisel, S. Yin, M. Gokel, H. Gill and G. Gokel, "Bis(Tryptophan) Amphiphiles Form Ion Conducting Pores and Enhance Antimicrobial Activity against Resistant Bacteria," *Antibiotics,* vol. 10, no. 1391, pp. 1-18, 2021.

[23] S. H. Yalkowsky, "Carnelley's Rule and the Predicition of Melting Point," *Journal of Pharmaceutical Sciences ,* vol. 103, pp. 2629-2634, 2014.

[24] Y. Zhang and E. J. Maginn, "Molecular Dynamics Study of the Effect of Alkyl Chain Lngth on Melting Pointd of [CnMIM][PF6] Ionic Liquids," *Physical Chemistry Chemical Physics,* vol. 16, pp. 13489-13499, 2014.

[25] M. S. Smyth and J. H. J. Martin, "X Ray Crystallography," *Journal of Clinical Pathology: Molecular Pathology,* vol. 53, pp. 8-14, 2000.

[26] P. Muller, "Growing Quality Crystals," 2018. [Online]. Available: http://web.mit.edu/x-ray/cystallize.html. [Accessed 13 February 2022].

[27] W. M. Leevy, M. E. Weber, M. R. Gokel, G. B. Hughes-Strange, D. D. Daranciang, R. Ferdani and G. W. Gokel, "Correlation of Bilayer Membrane Cation Transport and Biological Activity in Alkyl-substituted Lariat Ethers," *Organic Biomolcular Chemistry,* vol. 3, pp. 1647-1652, 2005.

Chapter 3

Biological Activity of *Bis*(Tryptophan) Amphiphiles

3.1 Introduction

An important aim of this research was to determine if the *bis*(tryptophan) amphiphiles (BTs) are biologically active. While no specific microbe is the target of this research, it would be preferred if the compounds were active against both Gram-negative and Gram-positive bacteria. These two classes of bacteria have significantly different cell envelope structures (**Fig. 3.1**). [1]

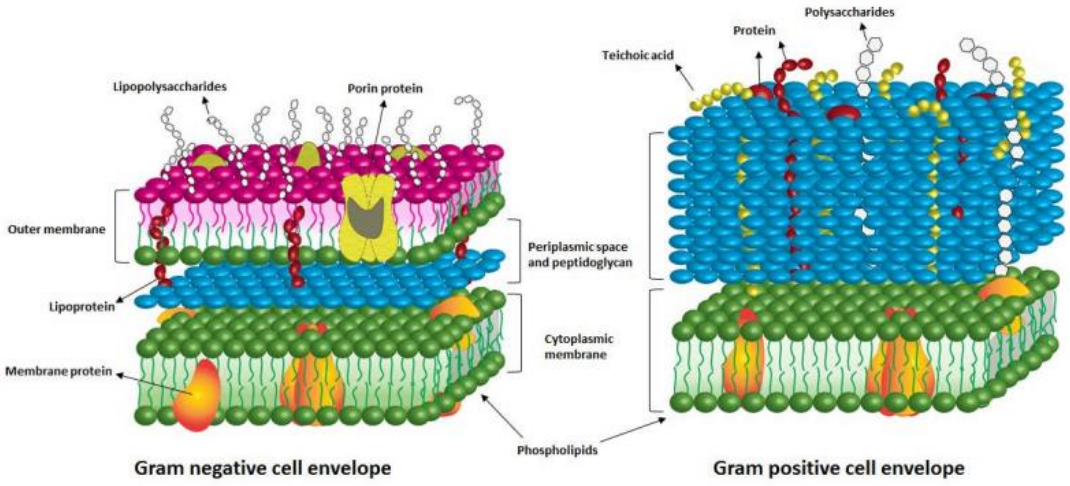

Figure 3.1. Schematic representations of the cell envelopes of Gram-negative and Gram-positive bacteria as illustrated by Heger et al. [1]

It is known that the cell membrane provides a barrier to entry in the bacterial cell against foreign materials, such as toxins or drugs. [2] If the BTs are to target the cell membrane, or if they need to pass through the membrane, then their efficacy as antibacterial agents may be altered depending on the type of cell membrane. As seen in **Fig. 3.1**, the Gram-negative cell envelope has two

membrane layers. Both of these layers may need to be penetrated or disturbed by the BTs if they are to be bactericidal. The amphiphilic nature of the cell membranes is part of their success as barriers into the cell. Two such membranes make the cell more difficult to penetrate. The Gram-negative bacteria have a relatively small number of peptidoglycans in the periplasmic space between the inner and outer membranes. The Gram-positive bacterial envelope is different as it lacks an outer membrane. Instead, it has a significantly more complex peptidoglycan layer on the outside of the cytoplasmic membrane. This peptidoglycan layer can be up to 80 nm in thickness, which can be 10 times as thick as the peptidoglycan layer in Gram-negative bacteria. [1] Because of the differences in cell envelope structure, the efficacy of BTs against both Gram-negative and Gram-positive bacteria were explored.

The international concern over antibiotic resistance is justified. The World Health Organization (WHO) has designated antimicrobial resistance (AMR) as one of the ten greatest health crises facing humanity. [3] One component of AMR is the evolution of bacteria into strains that possess multi-drug resistance (MDR). Therefore, in this research, the efficacy of the BTs against a multi-drug resistant strain of bacteria will also be investigated. This will be a MDR strain of *E. coli*, (BAA-3058 from American Type Culture Collection). This strain is resistant to a range of antibiotics including aztreonam, ciprofloxacin, levofloxacin and cefepime (**Fig 3.2**)**.** It is susceptible to some AMPs such as colistin. [4]

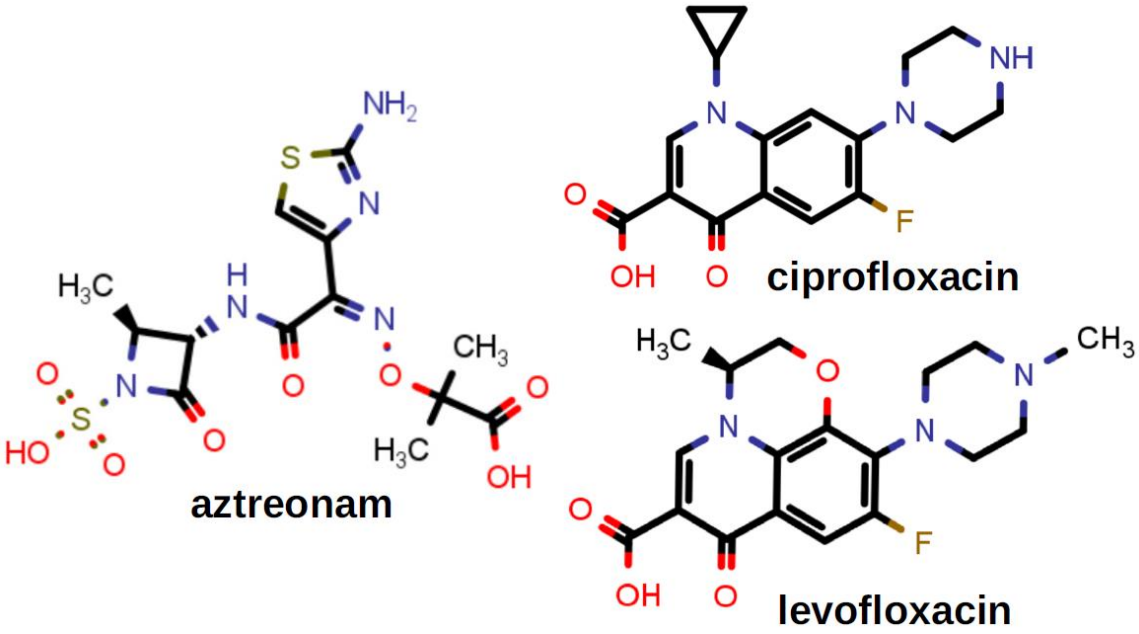

Figure 3.2 Structures of aztreonam, ciprofloxacin and levofloxacin

To assess the efficacy of the BTs against bacteria, minimum inhibitory concentration (MIC) studies were conducted. These studies were conducted in accordance with the methods described by the Clinical and Laboratory Standards Institute. [5] The bacterium being used in the investigation was grown to a specified optical density and added to the *bis*(tryptophan) that was serially diluted by halves until the growth is inhibited by greater than 90% (MIC_{90}), detected spectroscopically. Each of the BTs were dissolved in DMSO, and the solvent concentration was kept constant at 0.5% by volume in all experiments. The BTs investigated were C_3BT, C_4BT, C_6BT, C_8BT, $C_{10}BT$, $C_{12}BT$ and $C_{14}BT$. The data reported here included two replicates and a minimum of three trials each. All MICs are reported in µM with a value of >128 µM meaning that no growth inhibition was observed up to 128 µM. The MIC could be much higher, but such

values are usually not biologically useful.

The MIC experiments were conducted in 96-well plates. **Fig. 3.3** shows how the plates are set-up. Phosphate buffered saline (PBS) solution is placed in each of the wells on the perimeter of the plate. This helps mitigate the evaporation which may occur when the plates are in the incubator. In the second column from the left, media is placed in each of the wells, without any bacterial cells. The specific media used is Mueller-Hinton broth II (MHII). It contains casein acid hydrolysate (1.75% w/v), beef extract (0.30% w/v) and starch (0.15% w/v). The wells in this second column act as the negative control (absence of cell growth). The third column of wells have media and bacterial cells present and demonstrate the growth of the bacteria without any of the BTs being present (positive control). In the next four columns, the wells contain media, cells, and varying concentrations of the first test compound (C_8BT is used as an example). The BT concentration range used is 128 µM to 0.125 µM. Duplicates are produced at the same time to eliminate error. The wells in the remaining four columns contain the second compound being investigated (C_{10}BT). The same plate set-up is used for all of the MIC studies in this research, with the only differences being the bacterial cell line or BT being used. All MIC studies were reproduced in triplicate.

MIC: Plate Set-Up

			C8BT				C10BT				
PBS	PBS	PBS	PBS	PBS	PBS	PBS	PBS	PBS	PBS	PBS	PBS
PBS	Media	Cells	128	128	4	4	128	128	4	4	PBS
PBS	Media	Cells	64	6	2	2	64	64	2	2	PBS
PBS	Media	Cells	32	32	1	1	32	32	1	1	PBS
PBS	Media	Cells	16	16	0.5	0.5	16	16	0.5	0.5	PBS
PBS	Media	Cells	8	8	0.25	0.25	8	8	0.25	0.25	PBS
PBS	Media	Cells	4	4	0.125	0.125	4	4	0.125	0.125	PBS
PBS	PBS	PBS	PBS	PBS	PBS	PBS	PBS	PBS	PBS	PBS	PBS

Figure 3.3 Diagram showing the plate set-up used for the MIC experiments. All concentrations of BT being used are given in µM. The bacterial strain and compounds being investigated will vary.

3.2 Efficacy against Gram-negative Bacteria

The most widely used microorganism in biological research laboratories is *E. coli*. The *E. coli* (K-12) cell line is known for its fast-growth capabilities in inexpensive media. [6] As such, it has been used in this research as the bacterial strain to investigate the antibacterial activity of the BTs against Gram-negative bacteria and the first screening of the BTs for biological activity.

Table 3.1 shows the MICs of the aliphatic BTs against *E. coli* (K-12). The most potent of the compounds is the compound with the longest hydrocarbon chain, C_{14}BT. As the length of the carbon chains decrease from C_{14}BT to C_8BT, the MICs increase from 8 µM to 128 µM. C_3BT, C_4BT and C_6BT are considered virtually inactive against *E. coli* (K-12), for the purposes of this research because of their MIC values are 128 µM or greater. The structures of the BTs are shown in **Fig. 3.4**.

Table 3.1 Minimum Inhibitory Concentrations (MICs) against *E. coli* (K-12)

Compound	MIC (µM)
C_3BT	>128
C_4BT	>128
C_6BT	>128
C_8BT	128
C_{10}BT	32-64
C_{12}BT	8-16
C_{14}BT	8

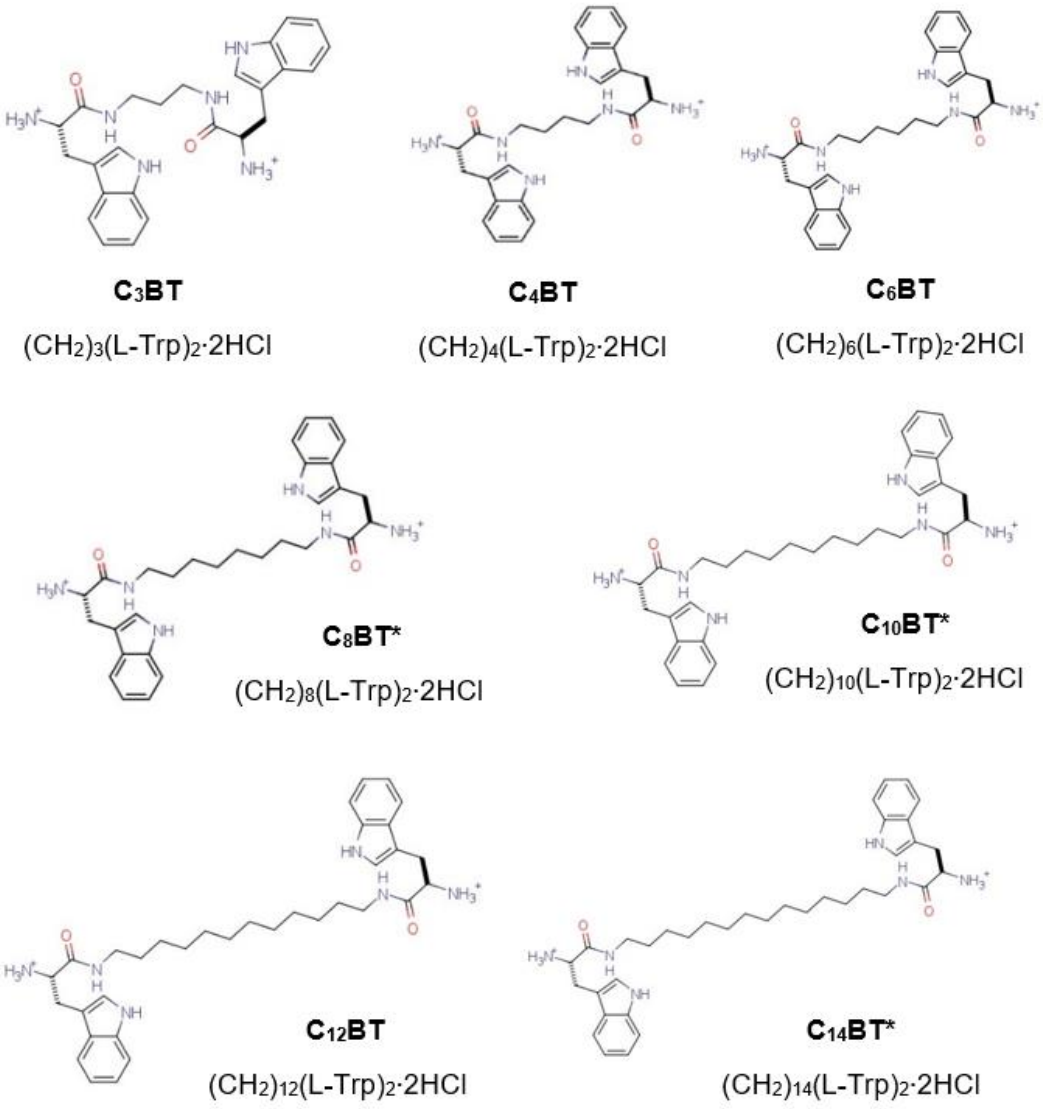

Figure 3.4 Names and structures of the BTs investigated. The compounds that were first prepared as part of this research are marked with an asterisk (*)

The apparent trend in potency for these compounds suggests that antibacterial potency of the BTs correspond to the length of the hydrocarbon chain. Why this might be the case is less than obvious. The estimated thickness of the hydrocarbon portion of a bilayer membrane is approximately 35 Å, which

would still exceed the anticipated length of even the longest of the BTs, C_{14}BT. [7] The *E. coli* cells have two such membranes in their cell envelope, (**Fig. 3.1**) in addition to a peptidoglycan layer separating the membranes. [1] It is not reasonable for the BTs to be able to span the entire cell envelope or create a channel or pore without some sort of secondary structure or self-assembly. In previous work, the Gokel lab showed that some other BTs form ion-conducting pores in bilayer membranes, which may, at least in part, be responsible for the antimicrobial properties of the BTs. [7]

Many amphiphiles are known to aggregate, most commonly forming micelles, but also forming various other structures. [8] Cell membranes, for example, are an aggregation of amphiphiles. [9] Antimicrobial peptides (AMPs) are known to disrupt ion homeostasis in microbes, including bacteria, by forming channels or pores in the cell membrane. [10] It may be possible that the BTs are forming pores or channels in the *E. coli* membranes via aggregation. This will be discussed further later in the next chapter.

3.3 Efficacy against Gram-positive Bacteria

After the initial screening with a Gram-negative bacterium*, E. coli*, a second screening of the BTs was completed. On this occasion the Gram-positive *S. aureus* was used. The specific strain (BAA-1720) is a methicillin-resistant *S. aureus* (MRSA) strain.

MRSA is most commonly known as a persistent, hospital-acquired bacterial infection, which has proven difficult to treat. [11] It was first recognized in the 1960's but has become a more significant concern over time. In 2014, the WHO gave considerable attention to the global threat of MRSA, in their first global report on antibiotic resistance. [12] It was noted that those with MRSA were 64% more likely to die than those infected with a non-resistant strain. In 2005, there were over 90,000 invasive MRSA infections in the US alone. [13] In the EU, more than 150,000 patients annually are affected by MRSA with an estimated cost of almost €400M ($440M) to the healthcare systems. [14] Undoubtedly, potency against MRSA would be an exciting attribute for our BT compounds.

Table 3.2 shows the MICs of the aliphatic BTs against MRSA (BAA-1720). The results show that the MICs for the C_3BT, C_4BT and C_6BT are once again too high for those compounds to be considered biologically relevant. The C_8BT, C_{10}BT, C_{12}BT and C_{14}BT all show potency at 64 µM or lower. The activity of the C_{12}BT and C_{14}BT are particularly interesting. Potency below 10 µM is of particular interest as biological activity is more likely to be observed at concentrations which are not toxic to mammalian cells. In previous work, the

Gokel lab established that human embryonic kidney cells (HEK-293) and *Cercopithecus aethiops* kidney cells (Cos-7) had an 80-100% survival rate when exposed to 10 μM C_{12}BT for 24 hours. [15]

Table 3.2 Minimum Inhibitory Concentrations (MICs) against *S. aureus*

Compound	MIC (μM)
C_3BT	128-256
C_4BT	1024
C_6BT	512
C_8BT	32-64
C_{10}BT	16
C_{12}BT	4-8
C_{14}BT	≤4

Similar to the results against the *E. coli* (K-12) (**Table 3.1**) it is notable that as the hydrocarbon chain length in the BT increases, the MIC against the bacterial strain decreases and potency increases. This suggests a correlation between the length of the BT and the potency against the bacterium. Although *S. aureus* bacteria have only one cell membrane, there is also a thick layer of peptidoglycans on the exterior of the cell to contend with. As previously mentioned, the peptidoglycan structure of Gram-positive bacteria can be up to 80 nm, however, the peptidoglycan layer in *S. aureus* is known to be approximately 20-30 nm thick. [16] In either case, the thickness of the cell envelope of the

bacterium is far greater than the estimated length of our longest BT. This again poses the question of how the BTs might be disrupting the cell membrane.

3.4 Efficacy against MDR Bacteria

Following the various successes of the BTs against the *E. coli* (K-12) and the methicillin-resistant *S. aureus* (BAA-1720) bacteria, it was decided that the efficacy of the compounds against a multi-drug resistant (MDR) bacterial strain would be investigated. MDR bacteria may have a plethora of antibiotic resistance mechanisms. In addition to the cell membrane, many bacteria achieve resistance through the development of efflux pumps. Efflux pumps are efficient as extrusion of the antibiotic/toxin from the cell can occur before any damage has been exerted on the bacterium. [17] Approximately 70% of methicillin-resistant *S. aureus* bacteria are known to possess efflux pumps. [18] It is speculated that the bactericidal properties of the BTs may be a result of pores in the bacterial membranes caused by the BTs. Increasing membrane permeability may disrupt ion homeostasis within the bacterial cell, which is essential for many cell functions including utilization of efflux pumps. [19] If the BTs are disrupting cell membranes and therefore disrupting ion homeostasis, it is suggested they might also show potency against MDR bacteria.

In 2017, the WHO published a list of the bacteria for which new drugs were needed most urgently. MRSA and MDR Gram-negative bacteria were both included on the list. [20] The third bacterial strain against which antibiotic activity of the BTs was screened was MDR *E. coli* (BAA-3058), a Gram-negative bacterial strain. The results are shown in **Table 3.3**.

Table 3.3 Minimum Inhibitory Concentrations (MICs) against MDR *E. coli*	
Compound	**MIC (μM)**
C_3BT	256
C_4BT	512
C_6BT	>1024
C_8BT	32-64
C_{10}BT	64-128
C_{12}BT	>128
C_{14}BT	>128

The efficacy of the BTs against MDR *E. coli* were generally poor and did not follow the same trend observed for efficacy against the two other bacterial strains. In this case, the most potent of the compounds was C_8BT (MIC = 32-64 μM). The two BTs with the longest chains showed significantly lower potency against the bacterium (MIC >128 μM). The compounds with shorter hydrocarbon chains, C_3BT, C_4BT and C_6BT were also less potent against the MDR *E. coli* than the C_8BT. The MIC for the C_{10}BT was 64-128 μM, which was similar to the MIC observed for C_8BT.

Although there is no obvious trend in the results obtained for the BTs against MDR *E. coli,* there is evidence of modest activity against this strain in the micromolar concentration range. The ability of the C_8BT and C_{10}BT to impede the growth of the MDR *E. coli* at all suggests the bacterial cell's integrity or essential functions have been disrupted by the BTs.

3.5 Conclusion

Throughout the bacterial studies, it was hoped that the compounds would show efficacy against bacteria in the low micromolar concentration range, well below 128 µM. The C_3BT, C_4BT and C_6BT were inactive at MICs below 128 µM against any of the three bacterial strains. The C_8BT, C_{10}BT, C_{12}BT and C_{14}BT all showed activity below 128 µM for at least two of the three bacteria used for screening. Among the compounds tested, only C_{10}BT showed activity against all three bacterial strains.

The C_{12}BT and C_{14}BT are the compounds with the longest hydrocarbon chains. They each were potent against Gram-negative and Gram-positive bacteria, with MICs of 12 µM (±4 µM) or lower. Surprisingly, both compounds failed to show activity below 128 µM against the MDR *E. coli* bacteria. In contrast, the C_8BT, which had a MIC of 128 µM against the Gram-negative *E. coli* (K-12) strain, showed the most potency of all the BTs against the MDR *E. coli* strain (MIC = 32-64 µM). This could be explained in number of ways. The mechanism of action of the C_8BT may be different than the C_{12}BT and C_{14}BT. The efflux pump of the MDR *E. coli* might be capable of extruding the C_{12}BT and C_{14}BT, but not the C_8BT. The C_8BT may block the efflux pumps, whereas C_{12}BT and C_{14}BT might not. C_8BT might form aggregates capable of disrupting the membrane of the MDR *E. coli*, which are relatively incapable of disrupting the membrane of the K-12 *E. coli*. Bacteria and cell membranes can be incredibly complex, so all of these possibilities remain speculative.

The compound that showed consistent activity against all three bacterial

strains was C_{10}BT. This may suggest it has the greatest potential against a range of bacteria. It was not, however, the most potent against any of the individual strains of bacteria.

The differences observed in the potency of the BTs against all three bacterial strains is interesting. A mechanism of action can be hypothesized. In earlier work by the Gokel group, BTs were shown to form pores in bilayer membranes. [7] In addition, the Gokel group had previously demonstrated *E. coli* cell membrane disruption , using fluoresceine diacetate (FDA) and propidium iodide (PI). Confocal microscopy was used to show the cell membrane was compromised in the presence of either *m*-PhBT or C_{12}BT at ½ MICs. PI does not normally pass through the membrane into *E. coli* cells, yet could be detected, via fluorescence, intercalated with DNA within the cell. [15] Penetration of the cell membrane is made possible by BTs.

Pores or channels in the cell membrane can disrupt ion homeostasis. As mentioned previously, ion homeostasis is essential for many cell functions, including the function of efflux pumps. [19] [21] Therefore, membrane disruption caused by the BTs could result in biological activity, including activity against antibiotic resistant bacterial strains. The length of any of the individual BTs is known to be too short to span any of the membranes or envelopes. Pores or channels, if they exist, must be formed by aggregation or organization of the molecules at the cell membrane.

Antimicrobial peptides (AMPs) commonly facilitate bacterial cell death by disrupting cell membranes or hindering other functions essential for cell survival.

[22] AMPs may promote bacterial aggregation or may indeed self-associate and form aggregates of their own. [23] AMPs most often are known to self-aggregate when they are rich in arginine (Arg) and tryptophan (Trp) residues, due to the cation-π and π-π stacking interactions. The BTs are rich in tryptophan by design. In all cases where AMPs are bactericidal, they first interact and interfere with the inner and / or outer cell membrane(s) of the bacterium. [24]

There are a number of ways in which AMPs may form aggregates while interacting with the cell membrane. **Fig. 3.5** shows various models of such modes of aggregation which may occur for AMPs. These aggregation models facilitate bactericidal activity. [24]

The diagram at the top, left-hand side of **Fig. 3.5** shows AMP molecules bound parallel to the lipid membrane. This typically happens at low peptide / lipid ratios (low concentrations of AMP). As the concentration of the AMP is increased, the peptide orients perpendicular to the lipid membrane, inserts into the membrane and forms pores or channels (known as the I state). Peptide / lipid ratios, along with a host of other factors influence the types of pores or channels that are formed. [25]

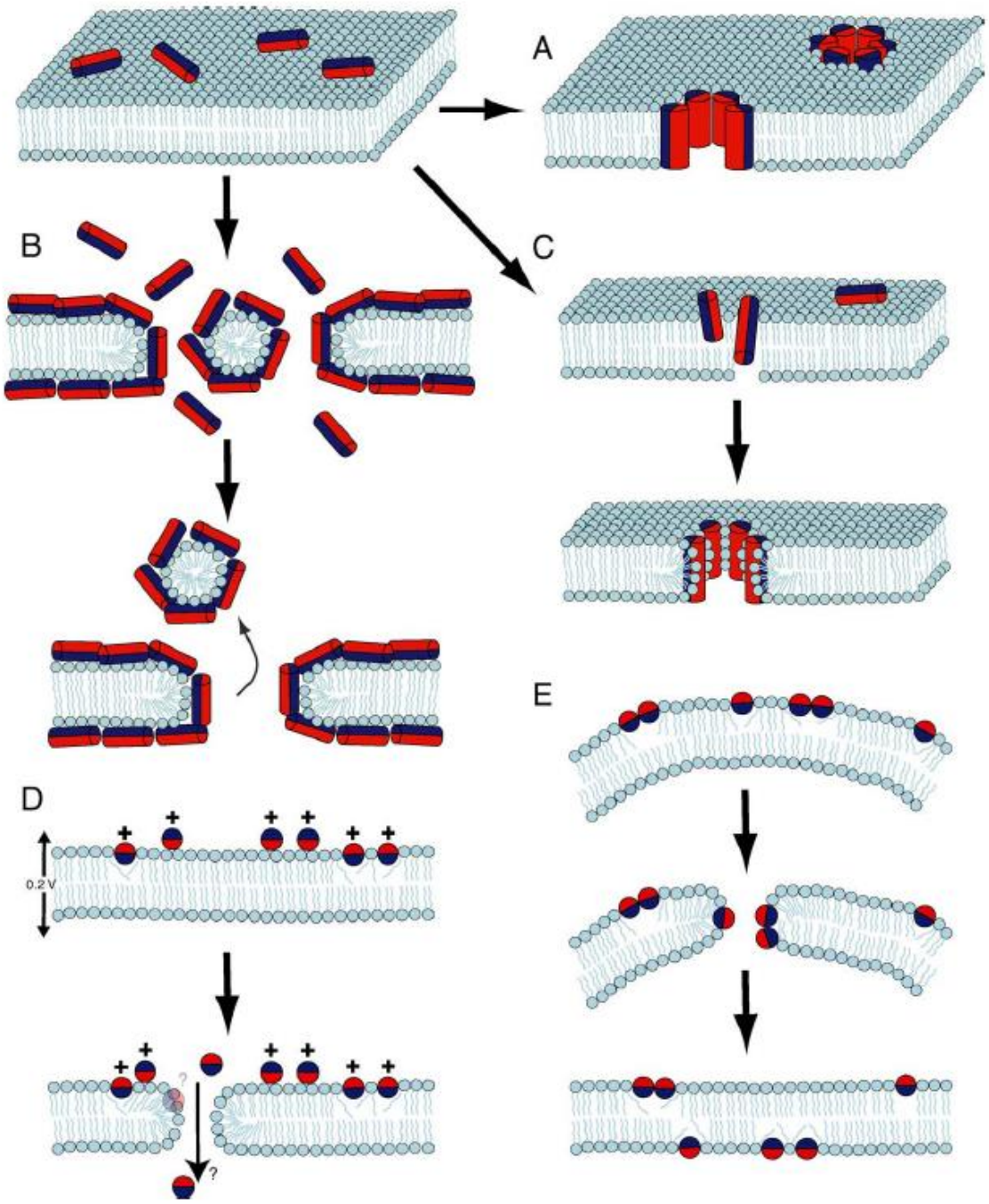

Figure 3.5 Five different models describing AMP activity at cell membranes. (A) Barrel-Stave Model. (B) Carpet Model. (C) Toroidal Pore Model. (D) Molecular Electroporation Model (E) Sinking Raft Model. Schematic produced by Vogel et al. [24]

Model A shows the barrel-stave mode of aggregation. This is one of the most common aggregation types and is seen in the widely studied ionophore, alamethicin (Alm) (Acetyl-Aib-Pro-Aib-Ala-Aib-Ala-Gln-Aib-Val-Aib-Gly-Leu-Aib-Pro-Val-Aib-Aib-Glu-Gln-phenylalaninol) (**Fig. 3.6**). In this model, the peptide helices bundle together in the membrane and a central lumen forms. The lumen represents the barrel held together by the peptide "staves." The hydrophobic regions of the peptide match up with the core lipid region of the membrane and the hydrophilic regions of the peptide form the interior of the newly formed membrane pore. Alm pores of this nature have channel walls (staves) approximately 1.1 nm thick. [25]

In 1993, the Parsegian group established that the difference in lipids found in the membranes greatly varied the activity of the membrane channels formed by alamethicin. [26] It was noted that the concentration of the compound required to form channels in the first place could vary by 10-fold. There was a striking difference not only in the activity of the channels formed, but whether the channels formed at all when the lipids of the membrane were varied. It is proposed that the differences in channel formation and activity can be associated with the repulsive forces of the head groups in the phospholipid bilayer and a disparity that may exist in terms of hydrophobicity among thicker *vs*. thinner membranes with the aggregates. [27]

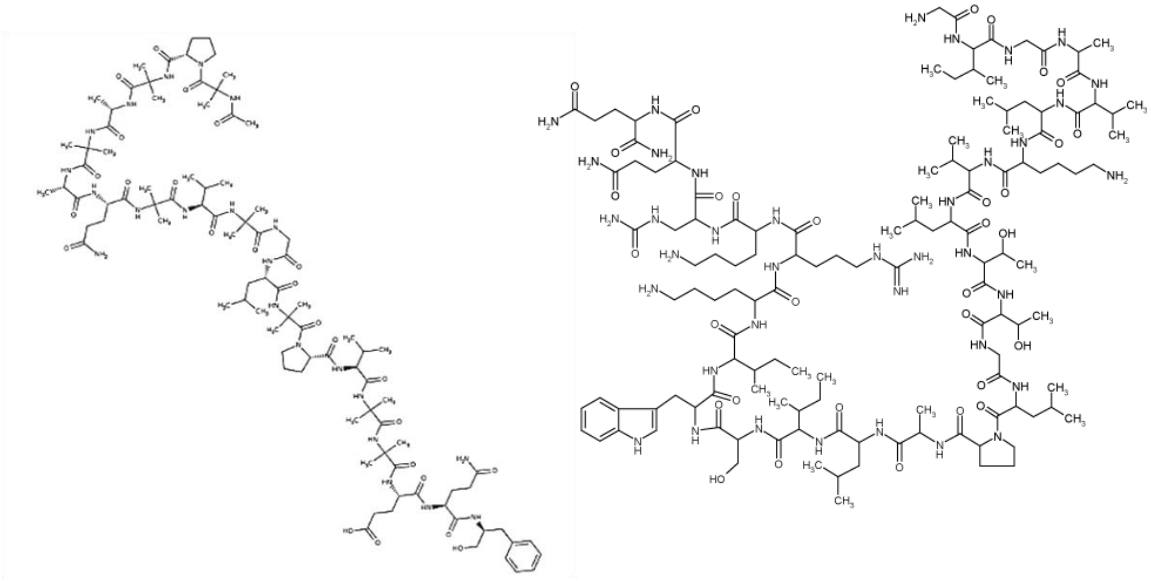

Figure 3.6 Chemical structures of Alamethicin (left) [30] and melittin (right) [31]

Model B in **Fig. 3.5** shows the carpet-model. This occurs when AMPs accumulate on the surface of the membrane, orienting parallel to the surface. Ovispirin (NH_2-Lys-Asn-Leu-Arg-Arg-*Ile*-*Ile*-Arg-Lys-Ile-*Ile*-His-*Ile*-Ile-Lys-Tyr-*Gly*-COOH) is an example of an AMP that aggregates this way. There is electrostatic attraction between the anionic phospholipid head groups and the peptide. At higher concentrations, the peptides disrupt the membrane in a similar manner to detergents and form micelles. This allows for holes to occur in the membrane, allowing more peptides to interact with the membrane and to form more micelles. Eventually, the membrane has been disintegrated entirely. [25]

Model C in Figure 3.4 shows the toroidal-pore model, often resulting from interactions of membranes with protegrins or melittin (NH_2-Gln-Gln-Arg-Lys-Arg-Lys-Ile-Trp-Ser-Ile-Leu-Ala-Pro-Leu-Gly-Thr-Thr-Leu-Val-Lys-Leu-Val-Ala-Gly-Ile-Gly-COOH) (**Fig. 3.6**). The AMPs insert into the membrane causing the layers

of the membrane to bend. This opens up an aqueous core surrounded by both the peptide and the phospholipid head groups. The polar regions of the AMPs associate with the polar regions the phospholipid head groups. This orientation allows for cationic peptide charges to be masked. [25]

Model D is somewhat different than the previous three models. It represents molecular electroporation. The association of cationic peptides with the negatively charged bacterial membrane can produce an electrical potential. It is proposed that when a membrane potential difference is greater than 0.2 V, pores form and the membrane is compromised. [24] Although the BTs are likely protonated at the two primary nitrogen atoms, this is not entirely sufficient for the electroporation model to be relevant.

The final model described, Model E, represents the sinking raft model. In this model, the amphiphile, AMP, integrates into and binds with the cell membrane. The binding causes an imbalance in terms of mass and so the membrane begins to bend and bow. This allows the AMP molecules to self-associate and create pores within the cell membrane. [28]

At this time, the mechanism of antimicrobial action of any of our compounds against the three bacteria remains unclear. The high proportion of tryptophan residues in the BTs suggests that self-association and the formation of aggregates is viable. It is also possible that these properties allow the formation of pores or channels through the cell membrane(s). Planar bilayer conductance has been observed for several of the BTs in phospholipid bilayer. To be sure, these bilayers are far simpler than any bacterial boundary layer, but

these results are suggestive of membrane penetration. The next section of this research will investigate some of the properties of BTs further using dynamic light scattering (DLS), scanning electron microscopy (SEM) and UV-Vis spectroscopy.

3.6 Experimental Details

3.6.1 Bacterial Strains Used. The K-12 *E. coli* (ATCC 700926), *S. aureus* (BAA-1720) and MDR *E. coli* (BAA-3058) were all purchased from American Type Culture Collection (ATCC). All bacterial strains were grown in Mueller Hinton II (MHII) media (Sigma-Aldrich).

3.6.2 MIC Experiments. MIC experiments were performed according to the Clinical and Laboratory Standards Institute protocols for microdilutions. [5] The bacteria from one colony-forming unit (CFU) were grown overnight (18-20 hours) at 37 °C, in MHII media. The next day, the media are knocked back to O.D. at λ = 600 nm = 0.500 in the same media. The bacteria, now in the exponential growth phase, are diluted in the media to achieve $4x10^8$ CFU / mL. The 96-well plates were set up according to **Fig 3.2** using MHII media and the serially diluted BT compounds. The BT compounds were dissolved in DMSO with the final DMSO concentration in each well-kept constant at 0.5% (v / v). The contents of the wells were mixed thoroughly before the cells were added (20 µL giving $4x10^5$ CFU / mL per well). The plates were incubated (37 °C, 200 RPM, 20 hours) and the results collected on the Biotek Cytation 3 plate reader. O.D was determined at λ = 600 nm. Media alone was considered as 100% inhibition and cells with media considered 0% inhibition. Inhibition greater than 90% was considered the MIC for that compound. All results were duplicated and then reproduced three times before reporting.

3.7 References

[1] Y. Liu, R. Qin, S. A. J. Zaat, E. Breukink and M. Heger, "Antibacterial Photodynamic Therapy: Overview of a Promising Approach to Fight Antibiotic-resistant Bacterial Infections," *Journal of Clinical and Tranlational Research,* vol. 1, no. 3, pp. 140-167, 2015.

[2] F. Ranow, J. D. MacMicking and L. C. James, "Cellular Self-Defense: How Cell-Autonomous Immunity Protects Against Pathogens," *Science,* vol. 10, no. 340, pp. 701-706, 2013.

[3] "World Health Organization Antimicrobial Resistance," 17 November 2021. [Online]. Available: https://www.who.int/news-room/fact-sheets/detail/antimicrobial-resistance.

[4] ATCC, "Escherichia coli (Migula) Castellano and Chalmers BAA-3028," 2022. [Online]. Available: https://www.atcc.org/products/baa-3058. [Accessed 25 March 2022].

[5] Clinical and Laboratory Standards Institute, "Methods for Dilution Antimicrobial Susceptibility Tests for Bacteria that Grow Aerobically," 9th ed., vol. 32, 2012.

[6] K. Marisch, K. Bayer, T. Scharl, J. Mairhofer, P. M. Krempl, K. Hummel, E. Razzazi-Fazeli and G. Striedner, "A Comparative Analysis of Industrial E. coli K-12 and B Strains in High-Glucose Batch Cultivations on Process-, Transciptome- and Proteome Level," *PLOS One,* vol. 8, no. 8, pp. 1-16, 2013.

[7] M. Patel, S. Negin, J. Meisel, S. Yin, M. Gokel, H. Gill and G. Gokel, "Bis(Tryptophan) Amphiphiles Form Ion Conducting Pores and Enhance Antimicrobial Activity against Resistant Bacteria," *Antibiotics,* vol. 10, no. 1391, pp. 1-18, 2021.

[8] J. Israelachvili, Intermolecular and Surface Forces, 2nd ed., Academic Press Ltd, 1992, pp. 366-382.

[9] T. Heimburg, "Physical Properties of Biological Membranes," 16 February 2009. [Online]. Available: https://www.nbi.ku.dk/membranes/pdf/2009_Heimburg_arXiv. [Accessed 04 February 2022].

[10] K. A. Brogden, "Antimicrobial Peptides: Pore Formers or Metabolic Inhibitors in Bacteria?," *Nature Reviews,* vol. 3, pp. 238-250, 2005.

[11] E. Y. Garoy, Y. B. Gebreab, O. O. Achila, D. G. Tekeste, R. Kesete, R. Ghirmay, R. Kiflay and T. Tesfu, "Methicillin-Resistant Staphylococcus aureus (MRSA): Prevalance and Antimicrobial Senstitivity Pattern among Patients - A Multicenter Study in Asmara, Eritrea," *Canadian Journal of Infectious Diseases and Medical Microbiology,* vol. 2019, pp. 1-9, 2019.

[12] WHO, "WHO's First Gloabl Report on Antibiotic Resistance.," Geneva, Switzerland, 2014.

[13] R. M. Klevens, M. A. Morrison, J. Nadle, S. Petit, K. Gershman, S. Ray, L. H. Harrison, R. Lynfield, G. Dumyati, J. M. Townes, A. S. Craig, E. R. Zell, G. E. Fosheim, L. k. McDougal, R. B. Carey and S. K. Fridkin, "Invasive Methicillin-Resistant Stapylococcus aureus Infections in the United States," *Journal of the American Medical Association ,* vol. 298, no. 15, pp. 1763-1771, 2007.

[14] R. Kock, K. Becker, B. Cookson, J. E. van Gemert-Pijnen, S. Harbath, J. Kluytmans, M. Mielke, G. Peters, R. L. Skov, M. J. Struelens, E. Tacconelli, A. Navarro Torne, W. Witte and A. W. Friedrich, "Methicillin-resistant Staphylococcus aureus (MRSA): Burden of Disease and Control Challenges in Europe," *Euro Surveillance,* vol. 15, no. 41, pp. 1-9, 2010.

[15] J. W. Meisel, M. B. Patel, E. Garrad, R. A. Stanton and G. W. Gokel, "Reversal of Teracycline Resistance in Escherichia coli by Noncytotoxic bis(Tryptophan)s," *Journal of the American Chemical Society,* vol. 138, pp. 10571-10577, 2016.

[16] S. Sharif, M. Singh, S. J. Kim and J. Schaefer, "Staphylococcus aureus Peptidoglycan Tertiary Structure from Carbon-13 Spin Diffusion," *Journal of the American Chemical Society ,* vol. 131, no. 20, pp. 7023-7030, 2009.

[17] W. C. Reygaert, "An Overview of the Antimicrobial Resistance Mechanisms of Bacteria," *AIMS Microbiology,* vol. 4, no. 3, pp. 482-501, 2018.

[18] S. Hassanzadeh, R. Mashhadi, M. Yousefi, E. Askari, M. Saniei and M. R. Pourmand, "Frequency of Efflux Pump Genes mediating Ciprofloxacin and Antiseptic Resistance in Methicillin-resistant Stapyhlococcus aureus Isolates," *Microbial Pathogenesis,* vol. 111, pp. 71-74, 2017.

[19] P. Chandrangsu, C. Rensing and J. Helmann, "Metal Homostasis and Resistance in Bacteria," *Nature Reviews Microbiology,* vol. 15, pp. 338-350, 2017.

[20] WHO, "WHO Publishes List of Bacteria for which New Antibiotics are Urgently Needed," 27 February 2017. [Online]. Available:

https://www.who.int/news/item/27-02-2017-who-publishes-list-of-bacteria-for-which-new-antibiotics-are-urgently-needed. [Accessed 17 March 2022].

[21] M. Moustakas, "The Role of Metal Ions in Biology, Biochemistry and Medicine," *Materials,* vol. 14, no. 549, pp. 1-4, 2021.

[22] C. F. Le, C. M. Fang and S. D. Sekaran, "Intracellular Targeting Mechanisms by Antimicrobial Peptides," *Antimicrobial Agents and Chemotherapy,* vol. 61, no. 4, 2017.

[23] S. U. Gorr, J. B. Sotsky, A. P. Shelar and D. R. Demuth, "Design of Bacteria-agglutinating Peptides derived from Parotid Secretory Protein, a Member of the Bactericidal/Permeability Increasing-like Protein Family," *Peptides,* vol. 29, no. 12, pp. 2118-2127, 2008.

[24] D. I. Chan, E. J. Prenner and H. J. Vogel, "Tryptophan- and Arginine-rich Antimicrobial Peptides: Structure and Mechanisms of Action," *Biochemica et Biophysica Acta,* vol. 1758, no. 9, pp. 1184-1202, 2006.

[25] K. A. Brogden, "Antimicrobial Peptides: Pore Formers or Metabolic Inhibitors in Bacteria?," *Nature Reviews,* vol. 3, pp. 238-250, 2005.

[26] S. L. Keller, S. M. Bezrukov, S. M. Gruner, M. W. Tate, I. Vodyanoy and V. A. Parsegian, "Probability of Alamethicin Conductance States Varies with Nonlamellar Tendency of Bilayer Phospholipids," *Biophysical Journal,* vol. 65, pp. 23-27, 1993.

[27] R. S. Cantor, "Size Distribtion of Barrel-Stave Aggregates of Membrane Peptides: Influence of the Bilayer Lateral Pressure Profile," *Biophysical Journal,* vol. 82, pp. 2520-2525, 2002.

[28] A. Pokorny and P. F. F. Almeida, "Permeabilization of Raft-Containing Lipid Vesicles by delta-Lysin: A Mechanism for Cell Sensitivity to Cytotoxic Peptides," *Biochemistry,* vol. 44, pp. 9538-9544, 2005.

[29] R. E. W. Hancock and A. Rozek, "Role of Membranes in the Activities of Antimicrobial Cationic Peptides," *FEMS Microbiology Letters,* vol. 206, no. 2, pp. 143-149, 2006.

[30] Fisher Scientific, "Alamethicin," 2022. [Online]. Available: https://www.fishersci.it/shop/products/alamethicin-2/15465989. [Accessed 28 03 2022].

[31] Enzo Life Sciences, "Melittin (natural)," 2022. [Online]. Available: https://www.enzolifesciences.com/ALX-162-006/melittin-natural/. [Accessed 28 03 2022].

Chapter 4

Characterization of Properties of *Bis*(Tryptophan) *Amphiphiles*

4.1 Introduction

Following the successful outcomes of the *bis*(tryptophan) amphiphiles (BTs) against the three bacterial strains, the interest in the potential mechanisms of action of these compounds was piqued further. Commonly proposed mechanisms of antimicrobial peptides (AMPs) include disruption of cell membrane structures, hindrance of cell membrane functions or indeed penetration into the cytoplasm of the bacterial cell and subsequent targeting of organelles and functions within the cell (**Fig. 3.4**). [1] [2] AMPs are also known to promote bacterial cell death by facilitating bacterial aggregation. [3] Furthermore, AMPs rich in tryptophan (Trp) and arginine (Arg) residues are known to readily self-associate. The cation-π and π-π stacking capabilities allow for the formation of various aggregates and nanostructures. [2] It was therefore decided that the potential aggregation of the BTs should be explored. Dynamic light scattering (DLS) is a method that will detect the presence of aggregates. If they are present, aggregate size is also estimated. Detection of aggregation can then be confirmed via scanning electron microscopy (SEM). SEM would also allow for the shape of aggregates to be observed.

The Gokel group has developed hydraphiles that act as ion channels once inserted into bacterial cell membranes. [4] [5] They have also developed lariat ethers that can act as ion carriers when donor groups are present in the side arms. The lariat ethers can also form pores in cell membranes in the absence of

donor groups. [6] The Gokel group has previously conducted planar bilayer lipid membrane (BLM) studies on BTs (**Fig. 4.1**) This trace shows classical open-close behavior with two stable open states observed. It is possible that two open channels formed or that aggregate formation was observed of the BT. It should be stated that this experiment involves passage of ions across a synthetic membrane and is not conducted within a bacterial cell. At least two of the BTs [*ortho*-C_6H_4(L-Trp)$_2$·2HCl and *meta*-C_6H_4(D-Trp)$_2$·2HCl] displayed ion channel activity. [7]

Figure 4.1 Planar bilayer voltage clamp trace produced by the Gokel lab for *m*-PhBT [*meta*-C_6H_4(D-Trp)$_2$·2HCl] in azolectin bilayers. Voltage applied = 30 mV, 10 mM HEPES buffer, [KCl] = 450 nM [7]

The maximal length of any of the BTs is significantly shorter than the cell envelope of the bacterial strains used in this work. If the BTs are active via the mechanism observed in the BLM study, it is likely that the BTs form these channels by some type of self-assembly

4.2 Dynamic Light Scattering (DLS)

4.2.1 Introduction to DLS. Dynamic light scattering is used to determine the effective diameter (Z-diameter) of particles in solution. The Z-diameter is the average diameter size detected of all aggregates detected in the sample at that time. Theoretically, the hydrodynamic diameter (d_h) of a particle in solution is inversely related to the rate of diffusion, according to the Stokes-Einstein equation: $D_t = K_b T / 3\pi\eta d_h$, where D_t is the translational diffusion coefficient, K_b is the Boltzmann constant, **T** represents the temperature, and **η** is the viscosity of the bulk solution. [8]

The DLS instrument operates by projecting monochromatic light into the sample at a 90° angle. The scattered light is collected and transformed into an autocorrelation function, which is then used to determine the size distribution. There are a number of limitations to the application of DLS. The limitations that are important for this research include maintaining a constant temperature and recognizing that the instrument operates at low resolution and therefore cannot distinguish between closely related molecules (for example, monomers and dimers). The instrument is also sensitive to dust particles, thus minimizing the exposure to dust is of paramount importance. The steps taken to reduce the impact of dust particles are detailed in the experimental section. [8] DLS measurements were obtained for all of the BTs in the library used and developed in this research.

4.2.2 DLS Results and Discussion. The initial library of BTs synthesized by the Gokel lab yielded several biologically active compounds. Among those

was the $C_{12}BT$ [$(CH_2)_{12}$(L-Trp)$_2$·2HCl]. This compound was the most potent of the BTs and more data has been accumulated for this compound than any of the other BTs. It was decided that exploration of the aggregation of the BTs should start with $C_{12}BT$.

At the beginning of the DLS investigations, the amount of time used for the collection of data was arbitrarily assigned at 30 minutes. It was noted that the size of aggregates forming continued to increase with time. It was important, from a chemical standpoint, to establish a timeframe within which the maximal size of aggregates could be determined. It was found that within a four-hour window, the aggregation size usually stabilized, and a maximal aggregation size could be established. This four-hour aggregation window is more chemically than biologically relevant. Consequentially, the DLS experiments for all BTs were conducted for four hours. The data depict the Z-diameter of the particles detected in the solution.

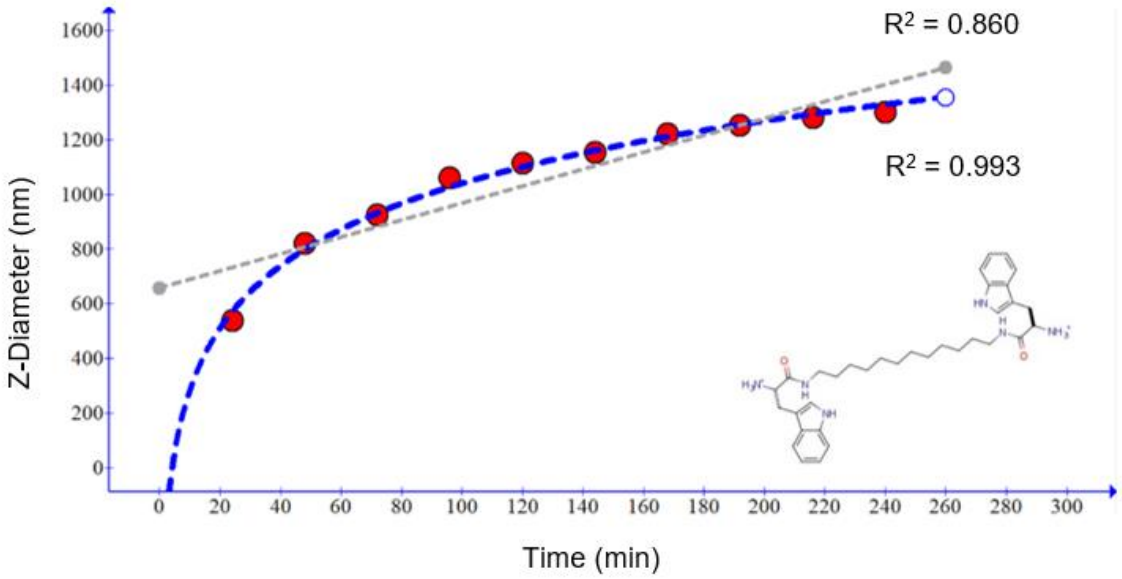

Figure 4.2 Aggregation of 128 µM $C_{12}BT$ [$(CH_2)_{12}$(L-Trp)$_2$·2HCl] over 4 hours in PBS solution. A Logarithmic trendline (blue) and linear trendline (grey) are shown.

The results for the aggregation of 128 µM C_{12}BT in phosphate buffered saline (PBS) solution over 4 hours can be seen in **Fig. 4.2**. PBS solution was chosen as the initial solvent as it most closely mimics physiological conditions. The results show that the Z-diameter of the aggregates formed increases over time and continued to increase to a maximum size of 1300 nm achieved at 240 minutes. This data suggested that some aggregates could be as large, or even greater in size than the bacterial cells used (*E. coli* are approximately 3000 nm long and 1000 nm in diameter). [9] The increase in aggregation size over time is not unique to BTs. Proteins, such as monoclonal antibodies, in a buffer solution will also aggregate over time. [10] It is important to acknowledge that the Z-diameter is an average measurement based on the sizes of all particles detected. Many smaller molecules and aggregates will undoubtedly exist which may be more important for biological activity than the aggregates which are larger than the bacterial cell. We speculate that these smaller aggregates may interact with the bacterial surface, perhaps inserting into the lipid membrane, causing disruption or pore formation.

Various trend lines were applied to the data in **Fig. 4.2**. The linear trendline (grey) and a logarithmic trendline (blue) are shown. A linear relationship exists when there is a steady increase in the aggregate sizes over time. A logarithmic relationship exists when there is a sharp increase in the aggregate sizes, which then levels off over time. The coefficient of determination (R^2) was calculated for each trend. An R^2 value of 1 indicates that the trendline perfectly fits the data. The R^2 for the linear fit was 0.86, however the R^2 for the logarithmic

trendline was significantly better, 0.993. The logarithmic trendline was the best fit for the relationship between aggregation size and time for all of the BTs in PBS in this study. The aim of the longer trial time for the DLS studies was to determine when a maximal aggregate size was achieved. The DLS data show that there is a fast increase in aggregate size observed initially but over sufficient time, the aggregate sizes no longer increase beyond a certain point.

The biological activity of the C_{12}BT, and the other BTs, is based upon the concentration of compound to which the bacteria are exposed. DLS data were collected to find if changing concentration of C_{12}BT had any impact on the size of aggregates formed, as shown in **Fig. 4.3**.

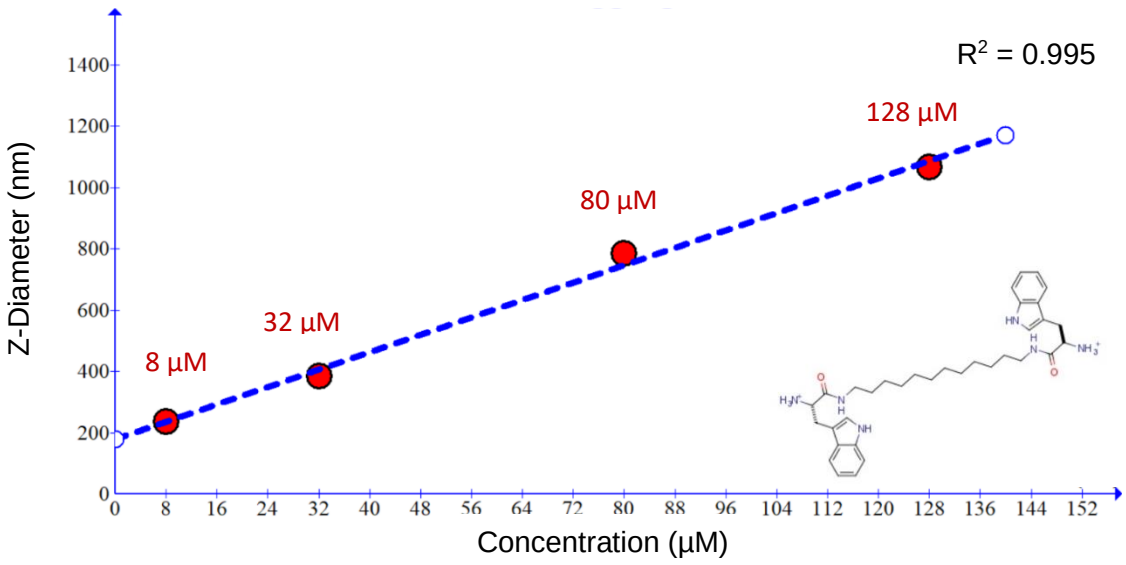

Figure 4.3 Effect of concentration on the size of aggregates formed of C_{12}BT [$(CH_2)_{12}$(L-Trp)$_2$·2HCl] over 4 hours in PBS solution.

The concentration range studied was from 8 µM – 128 µM, to reflect the concentrations at which the C_{12}BT was biologically active. There is a linear relationship between concentration and the Z-diameter of aggregates with an R^2 value of 0.995. This linear relationship shows that as the concentration increases, so too does the average size of aggregates formed. This is the expected relationship between concentration of BTs and the size of aggregates formed. Increasing the concentration of the BT in solution facilitates increased probability of collisions and, therefore, aggregates are likely to form larger sized molecules. [10]

In addition to investigating the aggregation of C_{12}BT in PBS solution, aggregation was also monitored for the compound in 18.2 MΩ H_2O and in MHII (Mueller Hinton Broth II) media (**Fig. 4.4**).

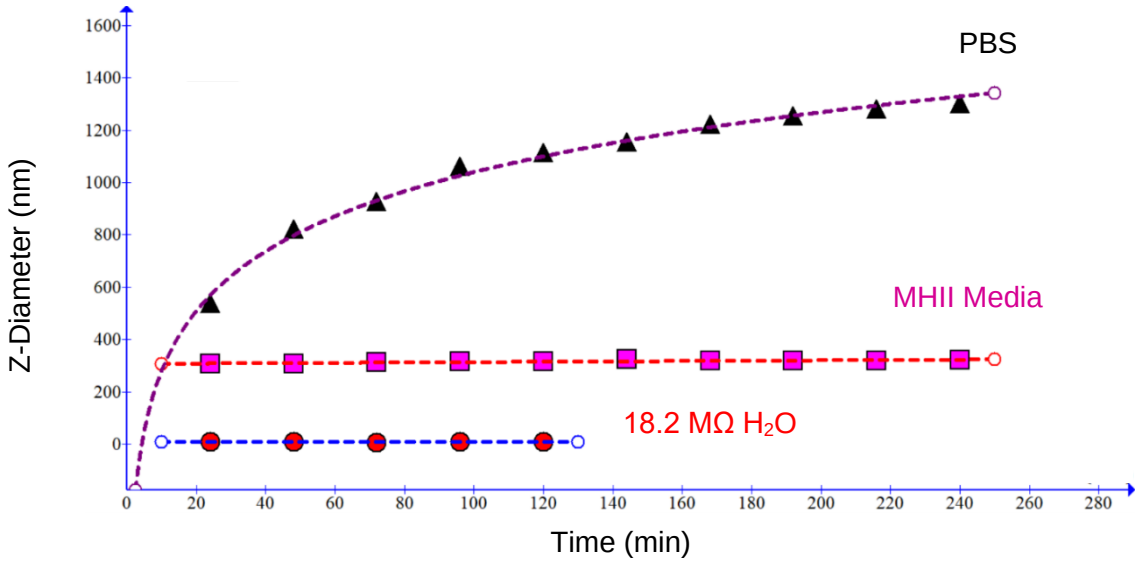

Figure 4.4 Effect of solvent on the size of aggregates formed from 128 µM C_{12}BT [$(CH_2)_{12}$(L-Trp)$_2$·2HCl] as a function of time.

The DLS studies for $C_{12}BT$ in de-ionized water showed no evidence for aggregation. Within two hours, aggregates over 1000 nm in diameter were observed in the PBS solution, whereas no aggregation was detected during the same time in 18.2 MΩ H_2O. This suggests that the ions present in the PBS solution (Na^+, K^+, Cl^-, $[HPO4]^-$, $[H_2PO4]^{2-}$) may contribute to the amphiphile's ability to form sizeable aggregates. The BTs may coordinate around the ions. For example, the positively charged ions may coordinate with indole groups from the tryptophan residues. It is also possible the NH_3^+ coordinates with anions in solution. Aggregation may depend on interactions such as these occurring between "layers" of amphiphiles.

When the MHII media, consisting of meat extract, casein hydrolysate and starch, was used instead of PBS solution, aggregates of about 350 nm in diameter were observed. MHII media also contains many ions (including Na^+, H^+, Cl^-, $CH_3CH(OH)COO^-$). It was expected that the $C_{12}BT$ in MHII would form aggregates due to the presence of these ions. Over the 4-hour timeframe, the aggregates formed did not increase in size. The 350 nm size is significantly smaller than the 1300 nm diameter observed in PBS solution. One reason may be the viscosity of the media solution compared to the PBS. In a more viscous solution, it may be reasonable to observe aggregates forming over a longer time period. [10] The MHII media contains a vast array of molecules compared to the PBS solution. The presence of starch, various amino acids and many other organic and inorganic materials common to meat extracts, will impact the viscosity, availability of ions and presumably the aggregation rate of $C_{12}BT$

amphiphiles. To investigate this further, DLS measurements were taken of the C_{12}BT in MHII media over a 2-week time period, **Fig. 4.5**. The objective of the longer aggregation window was to determine if a similar maximal aggregation size would be observed over a longer time period as the viscosity of the media was thought to be slowing the rate of aggregation.

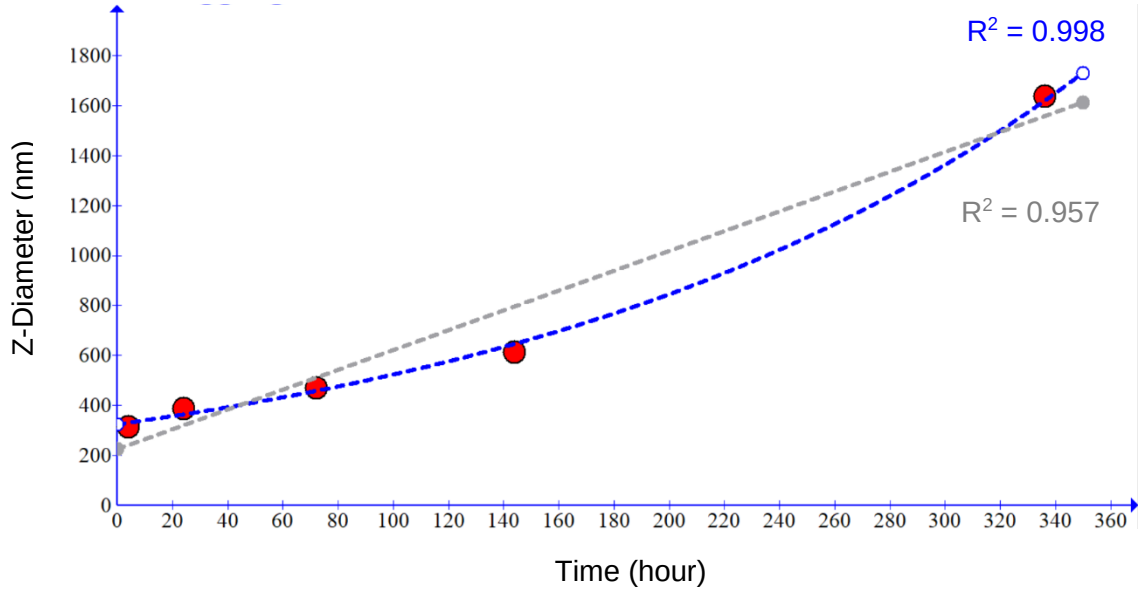

Figure 4.5 Aggregation of 128 µM C_{12}BT [$(CH_2)_{12}$(L-Trp)$_2$·2HCl] in MHII media solution over 2 weeks.

The aggregate growth trend for C_{12}BT in MHII media most closely matched an exponential growth trend (R^2 = 0.998). The Z-diameter of the aggregates reached over 1600 nm after two weeks. In PBS solution, the C_{12}BT reached a comparable 1300 nm Z-diameter size after four hours. The concave curve is a result of the exponential increase in aggregate size over two weeks. This is an unexpected trend. The aggregate formation in PBS solution was much quicker initially, reaching a maximal Z-diameter within four hours. Therefore, a

convex curve was observed as a plateau was reached for the C_{12}BT in PBS solution .The aggregation curve for the C_{12}BT in MHII media (**Fig 4.5**) suggests that the viscosity of the media led to slower rates of aggregation but did not prevent aggregation. A slower rate of aggregation does not explain an exponential growth curve. It would be expected that the trend may be linear. As the rate of aggregation was decreased due to viscosity, the rapid increase in aggregate size would not be observed. Instead, a steady increase in aggregate size would be expected until a maximal aggregate size is observed. A concern in this case is that the MHII media containing the amphiphile is not entirely transparent. A lack of transparency of the solution can prevent the DLS instrument from accurately determining the size of the aggregates. [8] It is therefore suggested that the media does indeed facilitate aggregation of the C_{12}BT at a slower rate, but the size of aggregates may be obscured by media particulates. Obtaining aggregate sizes between 144 hours and 336 hours (one week and two weeks) might have helped understand the rate of aggregation and the trendline observed. Those additional data points could help determine if the growth trend was more linear or if the convex trend was more accurate.

The next logical step in the utilization of DLS was investigating if aggregation could be observed for any other BTs. The C_8BT, C_{10}BT and C_{14}BT were all biologically active. DLS was used to explore any potential aggregation in PBS solution for each of these BTs.

The DLS experiments for C_8BT in PBS showed that aggregates did form over 4 hours. **Fig. 4.6** shows that an effective aggregate diameter as large as 2700 nm was observed for C_8BT at 128 µM concentration over this time period. The maximal Z-diameter for C_8BT is twice that of the C_{12}BT (1300 nm). This shows that the length of the hydrocarbon chain of the amphiphile has an impact on the size of aggregates being formed. It is speculated that the way in which the C_8BT and longer chain BTs are aggregating is different. It is speculated that the C_{12}BT folds and so both the tryptophan residues are at the same "end" while in shorter chains, such as C_8BT, the chain may not fold. Both C_{12}BT and C_8BT are active against both Gram-negative and Gram-positive bacteria, however, C_{12}BT is more potent in the MIC studies conducted in this research. For example, C_{12}BT has a MIC of 12 µM (± 4 µM) against *E. coli* (K-12), whereas the MIC of C_8BT for the same bacterial strain is 128 µM. Similarly, while C_8BT has a MIC of 50 µM (± 18 µM) against MRSA, the MIC of C_{12}BT is significantly lower at 6 µM (± 2 µM). It appears that while aggregation may enhance the antimicrobial effects of these amphiphiles, larger aggregates may not suggest greater potency. As mentioned previously, the larger aggregates may be too large to have any biological effect. The number of smaller aggregates formed may be more relevant to biological activity as they may be capable of disrupting the bacterial cell membranes.

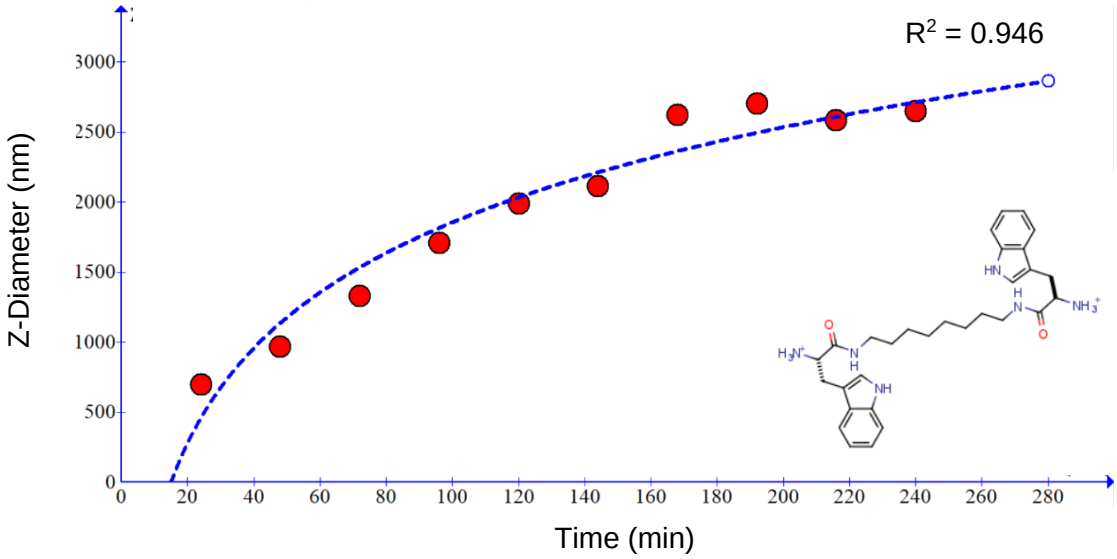

Figure 4.6 Aggregation of 128 µM C_8BT [$(CH_2)_8$(L-Trp)$_2$·2HCl] over 4 hours in PBS solution

The aggregation of C_8BT follows a similar trend to C_{12}BT when concentration is varied. **Fig. 4.7** shows that increasing the concentration of C_8BT leads to an increased Z-diameter of the aggregates formed. Unlike the C_{12}BT, at 8 µM, the C_8BT does not form any aggregates, whereas the C_{12}BT forms aggregates with diameters greater than 200 nm at 8 µM (**Fig. 4.3**). **Fig. 4.7** shows that aggregates are observed at 32 µM C_8BT, suggesting the critical aggregate concentration (CAC) of the C_8BT is greater than 8 µM but less than 32 µM (8 µM < CAC < 32 µM). Interestingly, no antibacterial activity was observed below 32 µM. This was true for both Gram-positive and Gram-negative strains. The data comport with the suggestion that aggregation may be linked to the antimicrobial properties of the *bis*(tryptophan) amphiphiles.

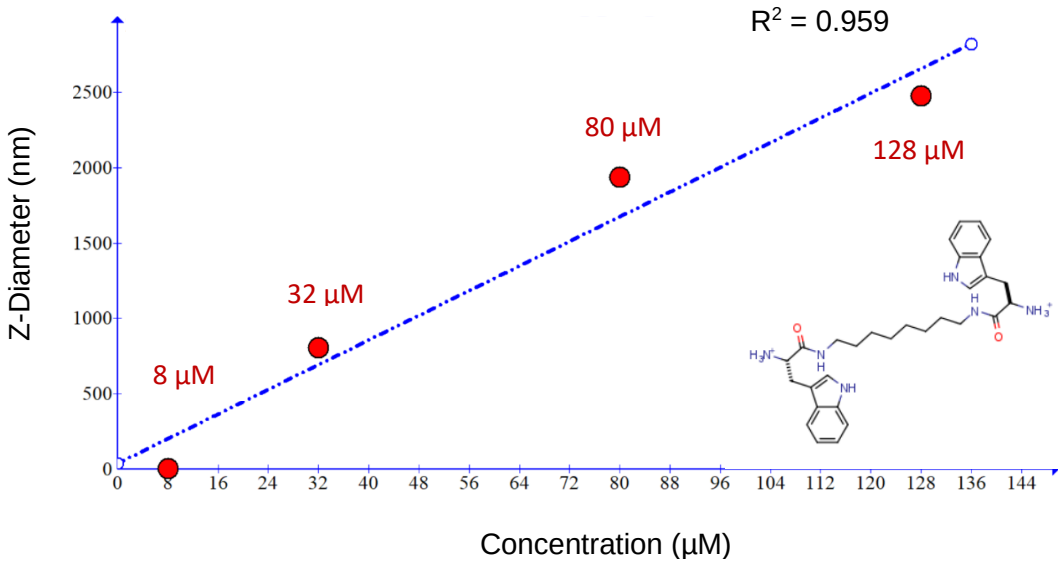

Figure 4.7 Effect of concentration on the size of aggregates formed of C_8BT [$(CH_2)_8$(L-Trp)$_2$·2HCl] over 4 hours in PBS solution.

The $C_{10}BT$ aggregates formed in PBS solution (~1500 nm) were more similar in size to the $C_{12}BT$ (1300 nm at 128 µM), than the C_8BT aggregates (2700 nm at 128 µM) (**Fig. 4.8**). The data show that the aggregate sizes of 128 µM $C_{10}BT$ in PBS solution increase over time, reaching a plateau during four hours. This trend is similar to the one observed for $C_{12}BT$ (**Fig. 4.2**) and C_8BT (**Fig. 4.6**).

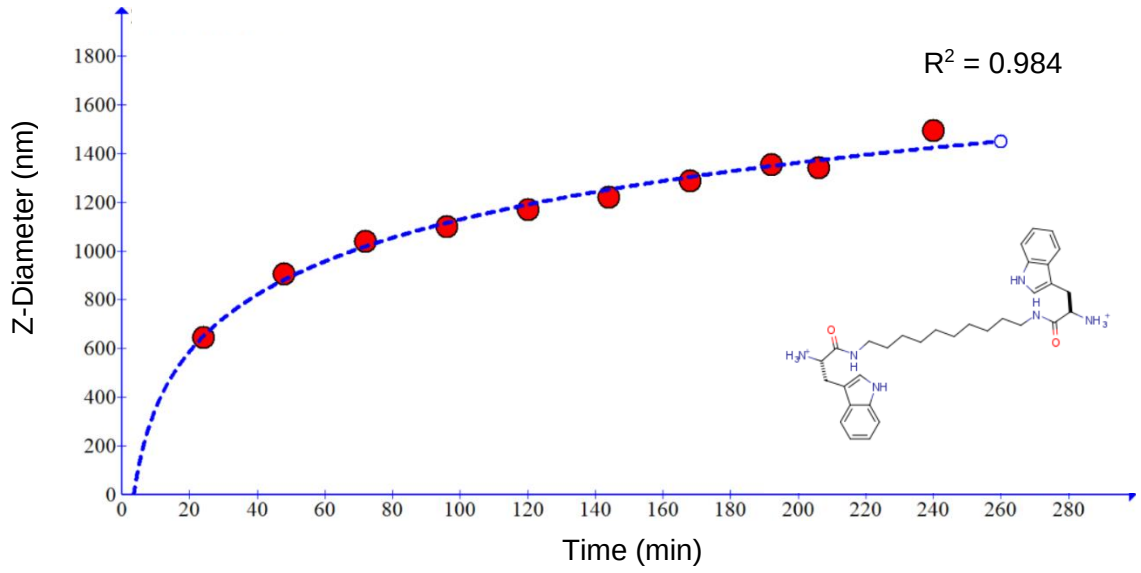

Figure 4.8 Aggregation of 128 µM C_{10}BT [$(CH_2)_{10}$(L-Trp)$_2$·2HCl] over 4 hours in PBS solution.

The relationship between the concentration and the Z-diameter of the aggregates of C_{10}BT was also investigated by DLS. **Fig. 4.9** shows the increasing aggregate size as the concentration of the amphiphile is increased. In this system a linear relationship also exists between concentration and the size of the aggregates formed. At 8 µM the C_{10}BT forms large aggregates. The C_{10}BT falls between the C_8BT and C_{12}BT in terms of chain length. Aggregates were not detected until 32 µM for C_8BT (**Fig. 4.7**), however the C_{12}BT showed clear aggregation from 8 µM (**Fig. 4.3**). The lowest MIC observed for the C_{10}BT against *E. coli* was 32 µM, however the MIC against the Gram-positive MRSA bacterium was as low as 16 µM.

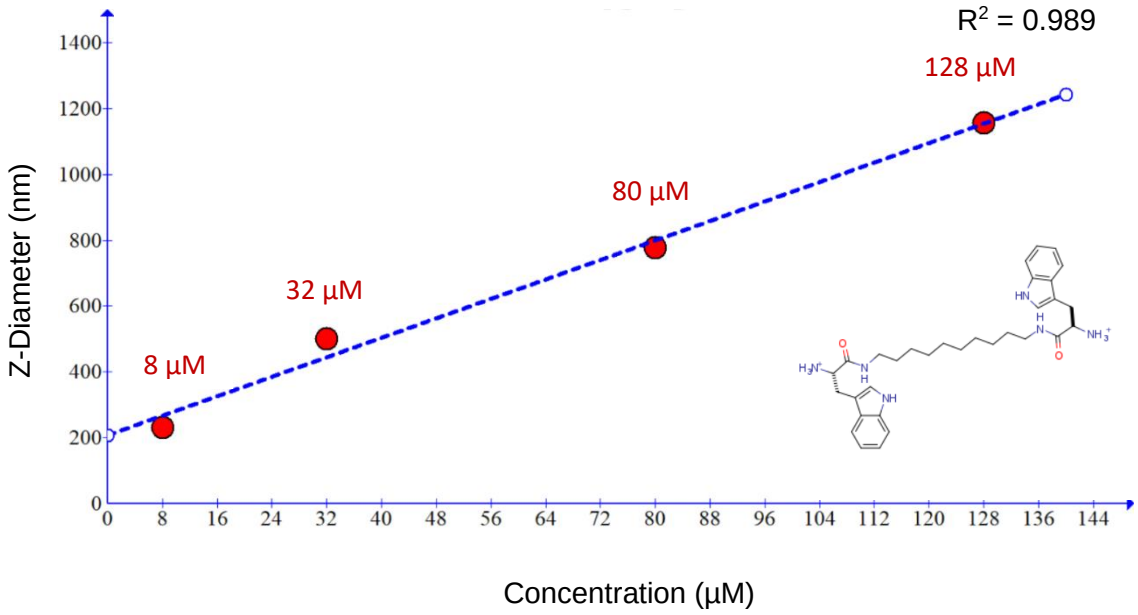

Figure 4.9 Effect of concentration on the size of aggregates formed of C_{10}BT [$(CH_2)_{10}$(L-Trp)$_2$·2HCl] over 4 hours in PBS solution.

The C_{14}BT was biologically active against *E. coli* (K-12) at 8 µM in these studies. DLS was used to determine the sizes of aggregates formed from C_{14}BT in PBS solution. The maximal Z-diameter of aggregates at 128 µM is approximately 1600 nm (**Fig. 4.10**). These aggregates are again significantly smaller than the aggregates observed for the C_8BT (2700 nm at 128 µM). It is notable that the C_{10}BT, C_{12}BT and C_{14}BT all form aggregates of a more similar size than the C_8BT, at 128 µM in PBS solution.

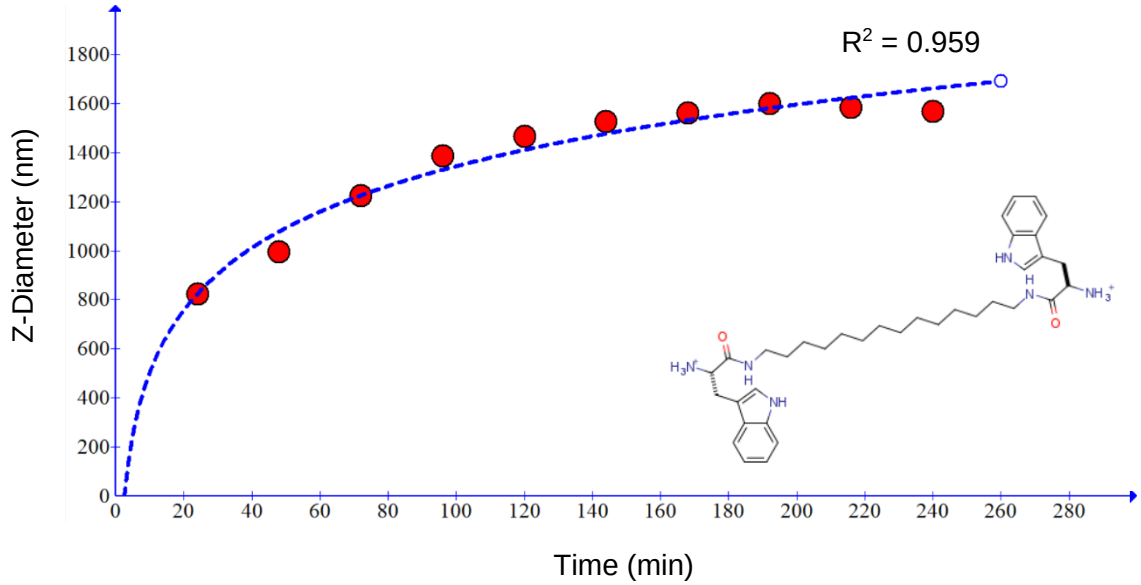

Figure 4.10 Aggregation of 128 µM C_{14}BT [$(CH_2)_{14}$(L-Trp)$_2$·2HCl] over 4 hours in PBS solution.

Further DLS studies were carried out on the C_{14}BT to investigate any relationship between concentration and the Z-diameter of the aggregates formed, (**Fig. 4.11**). The results were consistent with previous results for the aliphatic BTs. As the concentration of C_{14}BT in solution is increased, the size of the aggregates formed also increases. Significantly large aggregates were again observed at concentrations as low as 8 µM. The MIC for C_{14}BT against *E. coli* (K-12) is 8 µM and the MIC against MRSA is as low as 4 µM.

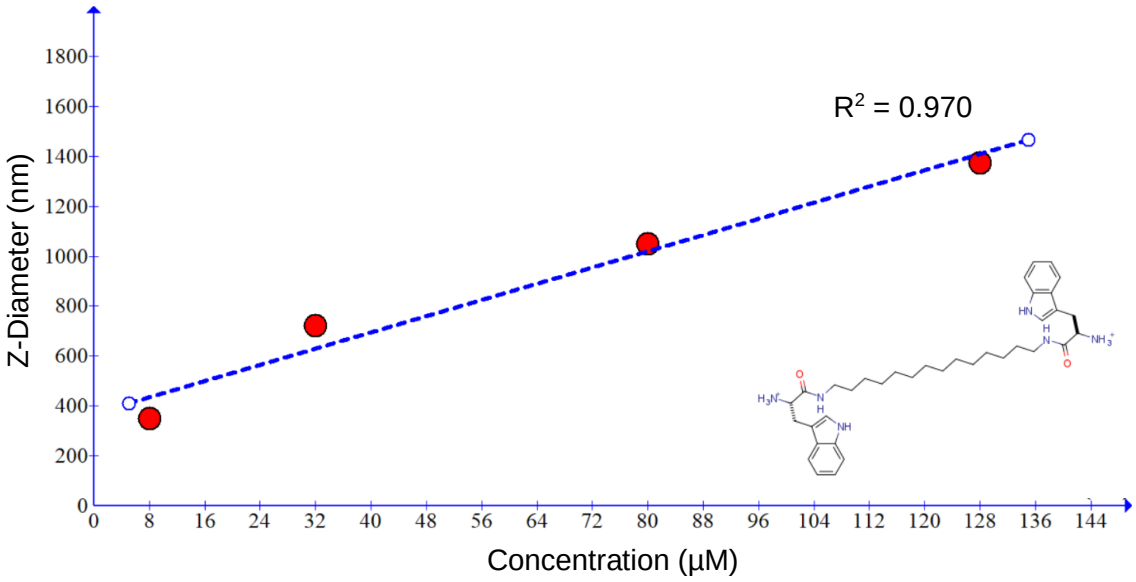

Figure 4.11 Effect of concentration on the size of aggregates formed of C_{14}BT [$(CH_2)_{14}$(L-Trp)$_2$·2HCl] over 4 hours in PBS solution.

From the DLS data collected from the aliphatic *bis*(tryptophan) amphiphiles, it is evident that each of the compounds form aggregates in PBS solution. It is also apparent that increasing the concentration of any of the BTs in solution leads to larger aggregates being formed, **Fig. 4.12**.

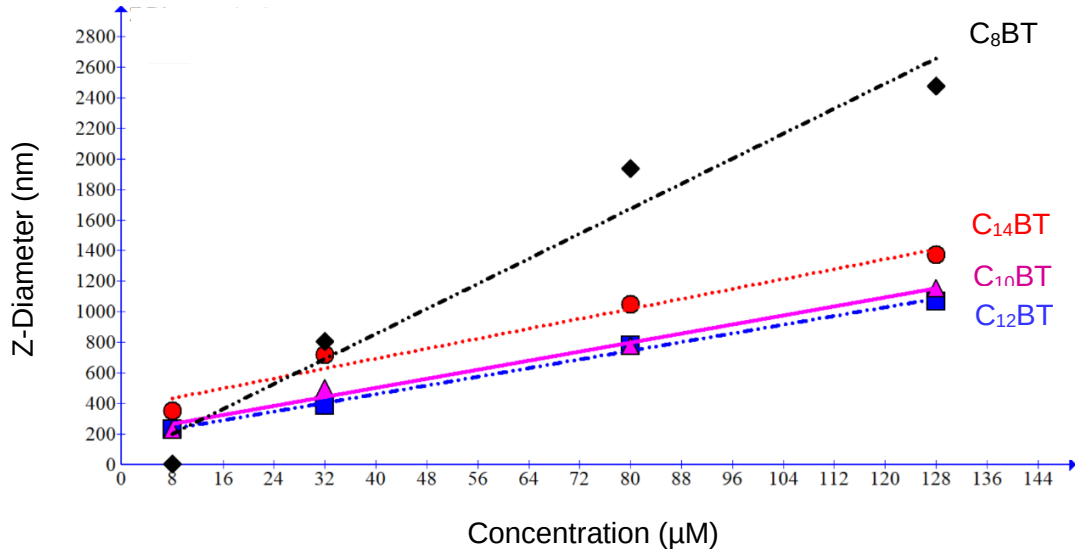

Figure 4.12 Effect of concentration on the size of aggregates formed of **C_8BT** [$(CH_2)_8$(L-Trp)$_2$·2HCl], **C_{10}BT** [$(CH_2)_{10}$(L-Trp)$_2$·2HCl], **C_{12}BT** [$(CH_2)_{12}$(L-Trp)$_2$·2HCl] and **C_{14}BT** [$(CH_2)_{14}$(L-Trp)$_2$·2HCl] over 4 hours in PBS solution.

The C_8BT, C_{10}BT, C_{12}BT and C_{14}BT all showed activity against at least two of the three bacterial strains investigated, at concentrations below 128 µM. These four compounds also all formed aggregates >1000 nm in diameter at concentrations of 128 µM or lower. The complexity of the cell membrane and its potential interactions with aggregates of other amphiphilic molecules, cannot be overstated. Three model systems, mentioned in Chapter 3, describing the potential interactions of AMPs with bacterial cell membranes, exemplified the possible methods of pore and channel formation. The barrel-stave, carpet, and toroidal-pore models are all possible mechanisms by which the BTs could be inserting into and disrupting bacterial cell membranes. [2] [11] [12] Important physical attributes for compounds to be capable of these mechanisms include amphiphilicity and the capability to engage in electrostatic interactions. The BTs are short chained amphiphiles that have been synthesized as hydrochloride

salts.

Two further mechanisms of action for AMPs were also previously described. The molecular electroporation and sinking raft models could be mechanisms by which the BTs express biological activity. [2] [13] Again, the ability to form electrostatic interactions with anionic species in the cell membrane and being amphiphilic in nature, would allow the BTs to potentially interact with the cell membrane by either of these two mechanisms. The tryptophan-rich nature of our small molecules may also encourage aggregation and facilitate membrane activity due to potential cation-π or π-π stacking. **Fig. 4.13** shows representative π stacking conformations for non-polar (A,B) and polarized (C) π-systems. [14]

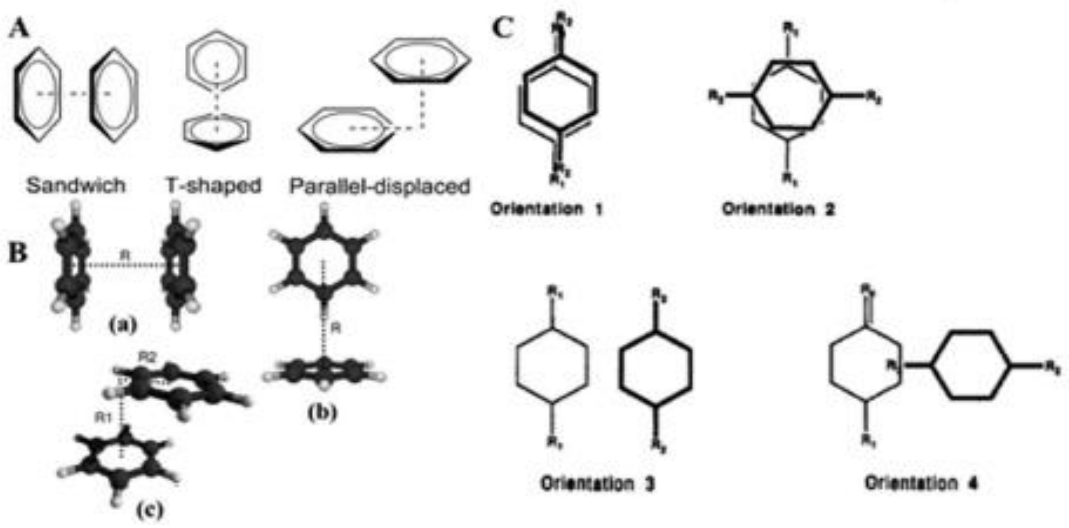

Figure 4.13 Schematic showing potential π stacking interactions of non-polar benzene rings (A and B) and polarized π-systems (C). Image created by Li et al. [14]

It is suggested that the indole groups of the tryptophan residues of the BTs are involved in π-cation-π stacking interactions, thus facilitating aggregation. Tryptophan residues are known to be involved in stacking with other ring systems and favor perpendicular ring interactions and a staggered stacking structure in proteins. [15] [16] When interactions of the tryptophan indole ring with the aromatic side chains of other tryptophan residues, histidine, tyrosine, and phenylalanine were analyzed, parallel packing was only observed 11% of the time. [16] The interaction of central negative charge of the ring system and the partial positive charges of hydrogens is one of the most simplistic explanations for stacking being observed and the specific spatial orientation of stacking [15] However, there was no aggregation observed in the absence of ions (**Fig 4.4**), when aggregation of C_{12}BT was measured in **18.2 MΩ H_2O. It is therefore suggested that** π-cation-π stacking interactions may be taking place.

Having established an apparent correlation between aggregation and biological activity, it was important to investigate if any of the biologically inactive BTs (MIC > 128 μM) also aggregated. C_4BT was chosen as the first biologically inactive compound to be investigated for aggregation, **Fig. 4.14**. The DLS data collected of 128 μM C_4BT in PBS control solution over 4 hours showed that no aggregates were forming. The 6-8 nm Z-diameter is what is observed for PBS solution alone. The only difference in the C_4BT structure compared with the biologically active BTs, is the shorter chain length compared to active compounds. It appears that the linker must be of a particular length to facilitate aggregation. It also seems that aggregation correlated to antibacterial activity.

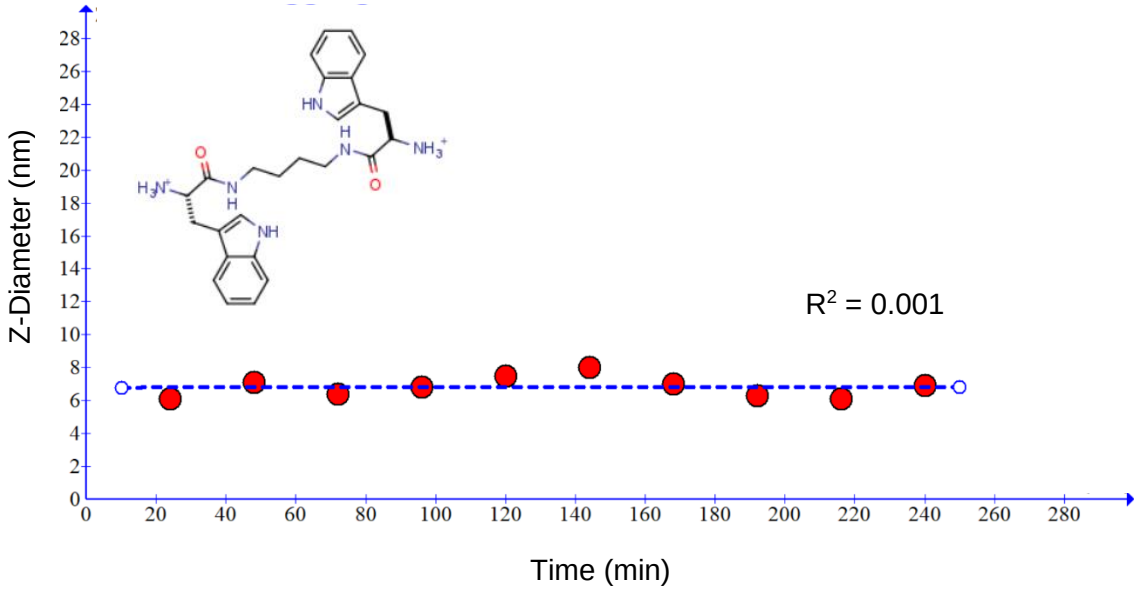

Figure 4.14 Aggregation of 128 μM C_4BT [$(CH_2)_4$(L-Trp)$_2$·2HCl] over 4 hours in PBS solution.

DLS data were also collected for 72 hours for the C_4BT, to ensure that aggregation was not happening at a slower rate. **Fig. 4.15** shows that there was no increase in the Z-diameter observed during this time, confirming a lack of aggregation.

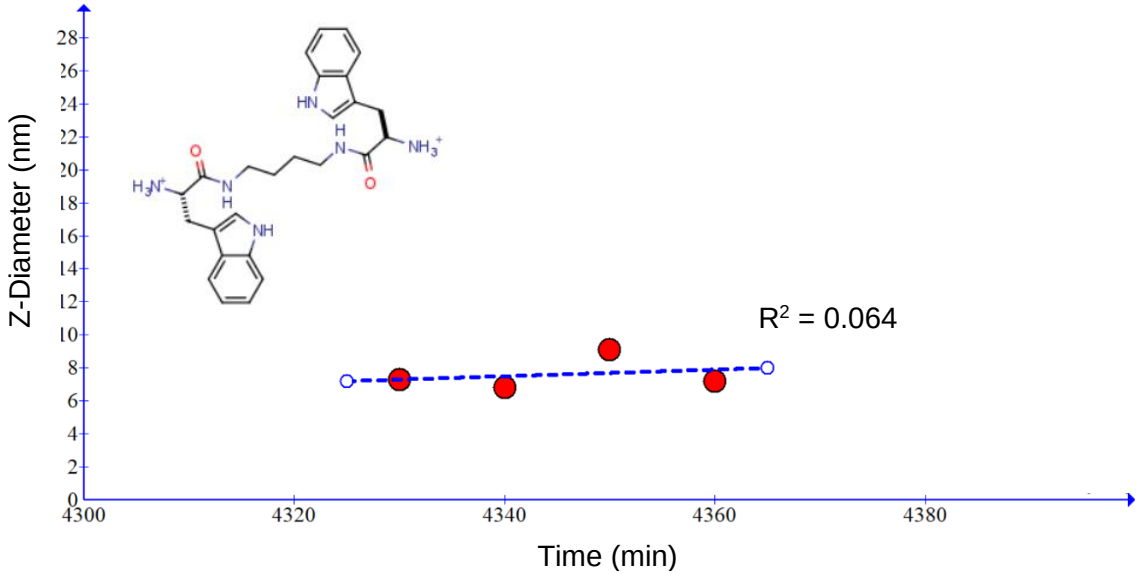

Figure 4.15 Aggregation of 128 μM C_4BT [$(CH_2)_4$(L-Trp)$_2$·2HCl] in PBS solution after 72 hours.

Although the longer-chain aliphatic BTs did not aggregate in 18.2 MΩ H_2O, an experiment was conducted to determine if the shorter-chain C_4BT behaved differently or not, **Fig. 4.16**. Over the course of 1 hour, no aggregates ≥ 8 nm were detected. For all the compounds that showed aggregation, DLS detected it almost instantly and certainly within the first 24 minutes. No aggregation was detected for the C_4BT, either in PBS solution or 18.2 MΩ H_2O.

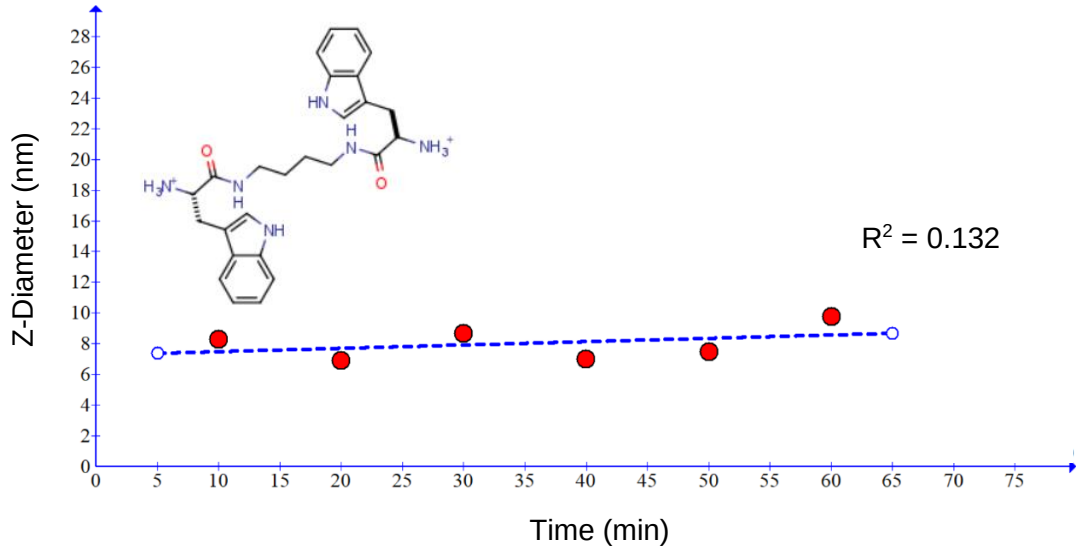

Figure 4.16 Aggregation of 128 µM C_4BT [$(CH_2)_4$(L-Trp)$_2$·2HCl] in 18.2 MΩ H_2O solution over 1 hour.

DLS data were next collected for the C_3BT. This compound showed no biological activity in the three-organism screen discussed above. It has a shorter carbon chain than any of the other BTs investigated up to this point. It was therefore expected that no aggregation would be detected for the C_3BT in PBS solution. **Fig. 4.17** shows the data obtained for 128 µM C_3BT in PBS solution over 100 minutes. As expected, there was no aggregation detected for the C_3BT in PBS solution.

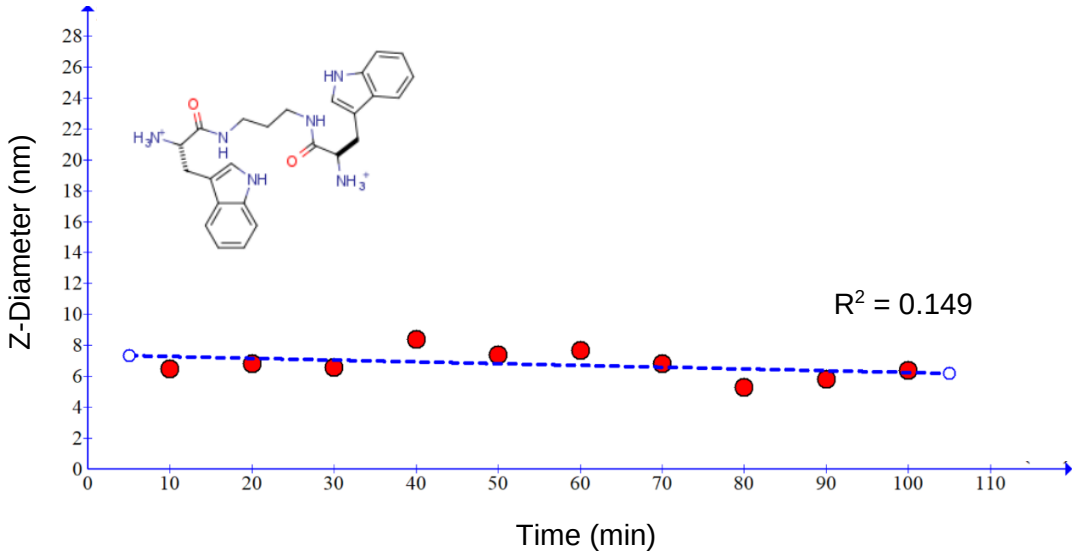

Figure 4.17 Aggregation of 128 µM C_3BT [$(CH_2)_3$(L-Trp)$_2$·2HCl] over 100 minutes in PBS solution.

The remaining aliphatic BT compound from this library is C_6BT. The chain length lies between that of the biologically inactive C_4BT and the active C_8BT. DLS was used to collect potential aggregation formation in PBS solution over 4 hours, **Fig. 4.18**. Similar to the other biologically inactive compounds, C_3BT and C_4BT, the C_6BT shows no signs of aggregate formation over 4 hours in PBS solution.

Based on the biological and DLS data collected for the aliphatic BTs, it can be concluded that the biologically active BTs (C_8BT, C_{10}BT, C_{12}BT and C_{14}BT) all form aggregates in the PBS solution. Similarly, it can also be concluded that the biologically inactive compounds (C_3BT, C_4BT and C_6BT) do not form aggregates in the PBS solution. The length of the carbon chain in the compounds appears to dictate formation of aggregates and biological activity against the three bacterial strains investigated. It is possible that the hydrocarbon

chain needs to be of a certain length to allow for the flexibility for π-π stacking, or other mechanisms of aggregation.

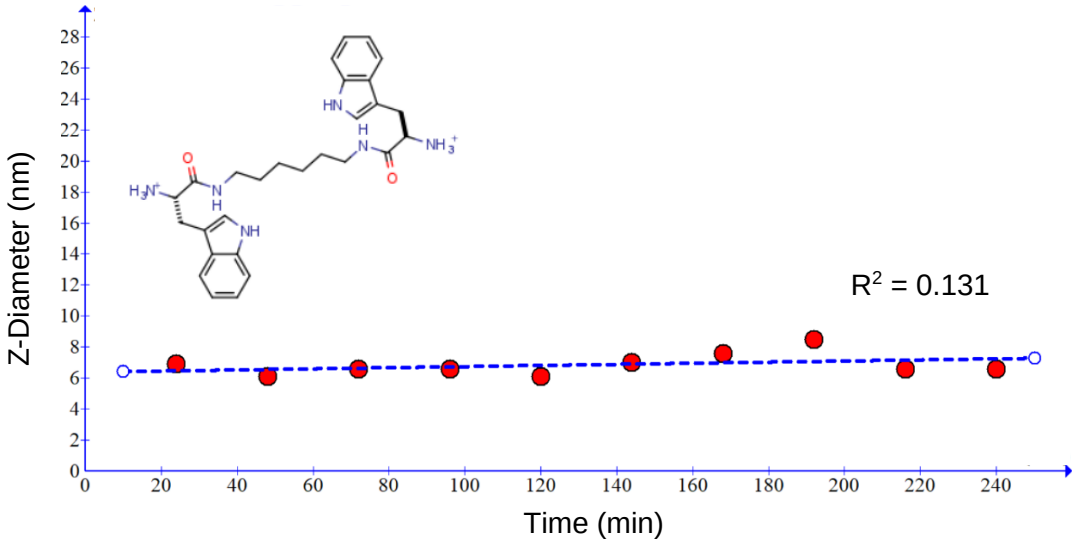

Figure 4.18 Aggregation of 128 μM C_6BT [$(CH_2)_6$(L-Trp)$_2$·2HCl] over 4 hours in PBS solution.

In previous work conducted by the Gokel lab, phenylene-linked BTs also showed potency against multiple bacterial strains. [7] The maximal length of any of these compounds is estimated to be ~9 Å, approximately 25% shorter than the C_{12}BT (~12 Å) and a similar length to the C_3BT and C_4BT. [7] DLS experiments were conducted for the *m*-PhBT [*meta*-C_6H_4(L-Trp)$_2$·2HCl] and *p*-PhBT [*para*-C_6H_4(L-Trp)$_2$·2HCl], **Fig. 4.19**. On this occasion, the experiments were conducted over three hours instead of four. A plateau in aggregate size was reached more quickly for each of the phenylene-linked BTs than the aliphatically-linked BTs. Despite their biological activity, (MIC = 64 μM and 128 μM against K-12 *E. coli* for *m*-PhBT and *p*-PhBT respectively), it was expected, based solely on their short chain length, the two phenylene-linked BTs would not form aggregates. Of

course, the phenylenes are fundamentally different than the C_nBTs.

The DLS data showed that both the *m*-PhBT and *p*-PhBT formed aggregates in PBS solution. The *p*-PhBT formed larger aggregates overall, with a maximal Z-diameter over 1300 nm, comparable to the aggregates seen for C_{12}BT. The *m*-PhBT formed aggregates about half as large, with a maximal Z-diameter of less than 800 nm.

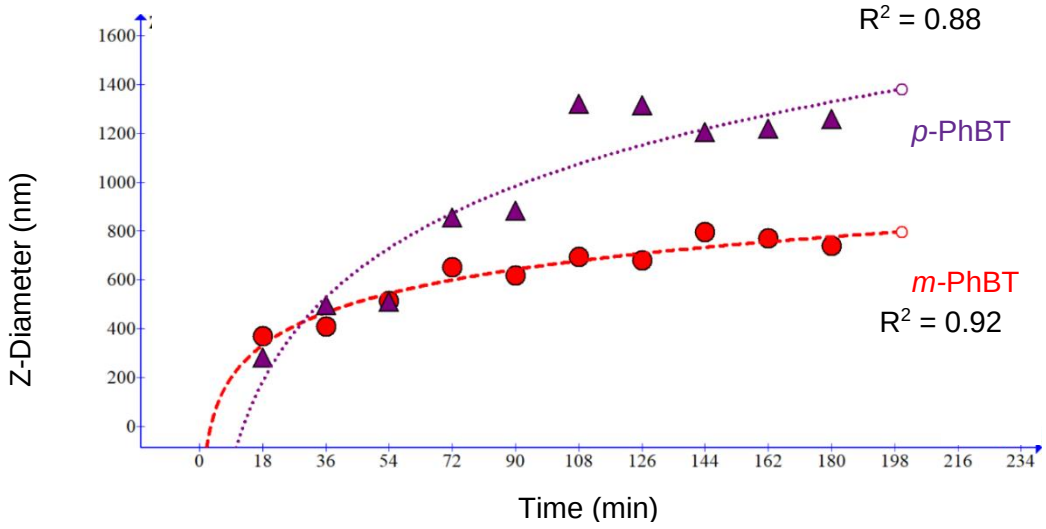

Figure 4.19 Aggregation of 128 µM ***m*-PhBT** [*meta*-C_6H_4(L-Trp)$_2$·2HCl] and ***p*-PhBT** [*para*-C_6H_4(L-Trp)$_2$·2HCl] over 3 hours in PBS solution.

The data suggest that the length of the molecule may be less important than the ability to form π-π or π - cation - π stacking interactions. It is possible that the short-chain aliphatic BTs are unable to form aggregates as the hydrocarbon chain does not allow for enough rotation to self-assemble. While the phenylene linker may be similar in length to the linker of the C_3BT and C_4BT, the phenylene-linked BTs appear to be able to aggregate. It is known that the indole group of the tryptophan interacts favorable with other ring systems. [15] [16] The

phenyl ring in the linker could promote π-π or π - cation - π stacking interactions (**Fig. 4.13**), thus forming aggregates.

The aggregation data from the phenylene-linked BTs do not correlate with the biological activity. The *p*-PhBT forms larger aggregates than the *m*-PhBT, however it is less active against *E. coli* (K-12) than the *m*-PhBT. It is unsurprising that aggregation size in PBS solution and the biological activity are not proportional. It is speculated that smaller aggregates may be integrating with the membrane and so the ultimate size of potential aggregates may not be relevant. The stability of the aggregates formed and their ability to integrate into the cell membrane are likely more important factors. It is also known that the composition of the cell membrane, along with other factors, will impact how the BT will interact with the bacterial cell. [11] [12] For example, the net charge at the membrane can prevent AMPs and other molecules penetrating. *S. aureus* is known to transport $_{D}$-alanine from the cytoplasm to the membrane to reduce the net negative charge near the membrane surface. Increased hydrophobic interactions can also prevent penetration into the cell. *Salmonella* species are capable of increasing the hydrophobic interactions between Lipid A acyl tails which reduces the fluidity of the membrane, making it more difficult to penetrate. [11]

4.3 Scanning Electron Microscopy (SEM)

4.3.1. Introduction to SEM. Scanning electron microscopy allows for the size and shape of molecules to be determined. It can also provide information on the surface topography and composition of the molecules. In SEM, the sample is adhered to or coated with conductive material (if necessary) and mounted on the stage. Within the microscope, a vacuum is produced, and the sample is subjected to a focused electron beam. The vacuum allows for high quality imaging, but also protects the electron source from noise and vibrations. The sample is scanned by the electron beam in a raster pattern, interacting with the atoms at the surface of the sample. Signals in the form of secondary electrons and backscattered electrons are produced. These are collected and interpreted by detectors and the images are produced on the screen. [17]

4.3.2 SEM Results and Discussion. Electron microscopy images were taken to confirm the size of *bis*(tryptophan) aggregates determined by DLS, and to investigate the shape of the molecules forming. The C_{12}BT [$(CH_2)_{12}$(L-Trp)$_2$·2HCl] was used for the initial images. **Fig. 4.20** and **Fig. 4.21** show the SEM images collected of C_{12}BT aggregates which were formed in PBS solution. Before images were taken, they were dried and mounted on conductive carbon tape.

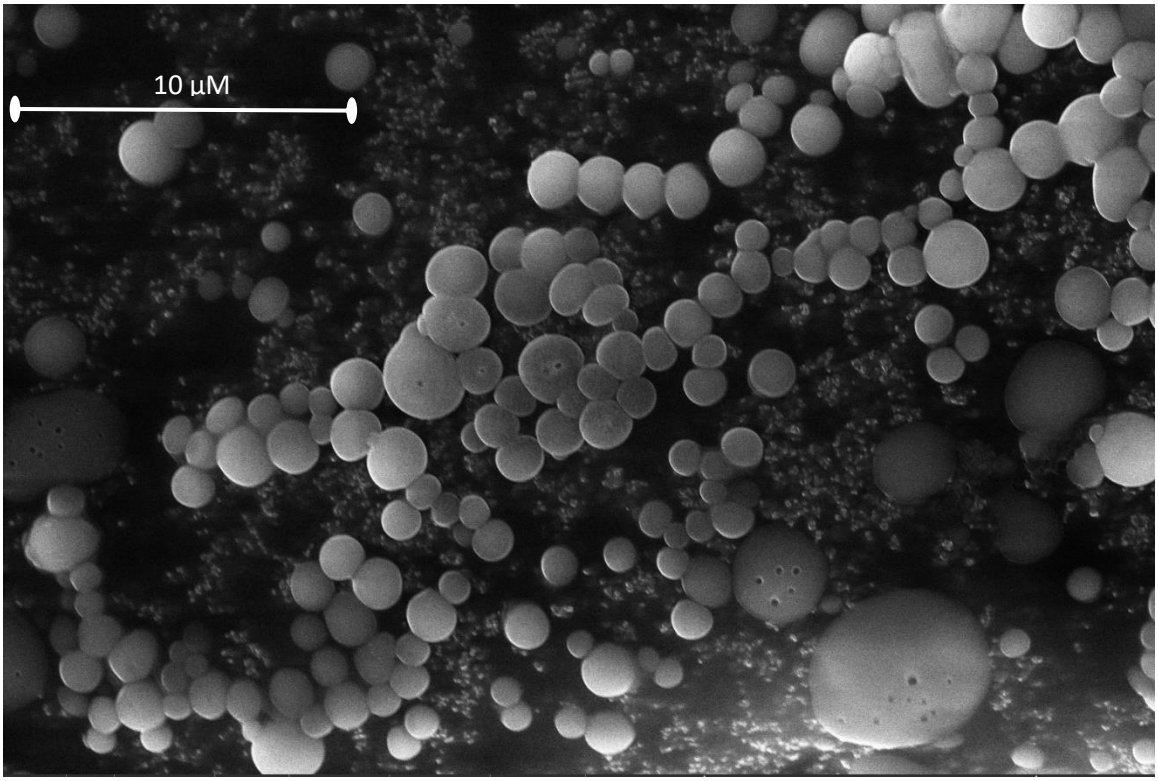

Figure 4.20 Scanning Electron Micrograph of C_{12}BT aggregates

Fig. 4.20 shows a great number of aggregates, many of which are clustering and potentially fusing with one another to form larger structures, such as the one shown at the bottom right-hand corner of the micrograph. The image shows that holes, or pores, exist in some of the larger structures. This may be indicative of the types of pores formed when the BT amphiphile interacts with the cell membrane, although this is obviously speculative. The range of sizes and the number of molecules was vast with all aggregates appearing spherical in shape.

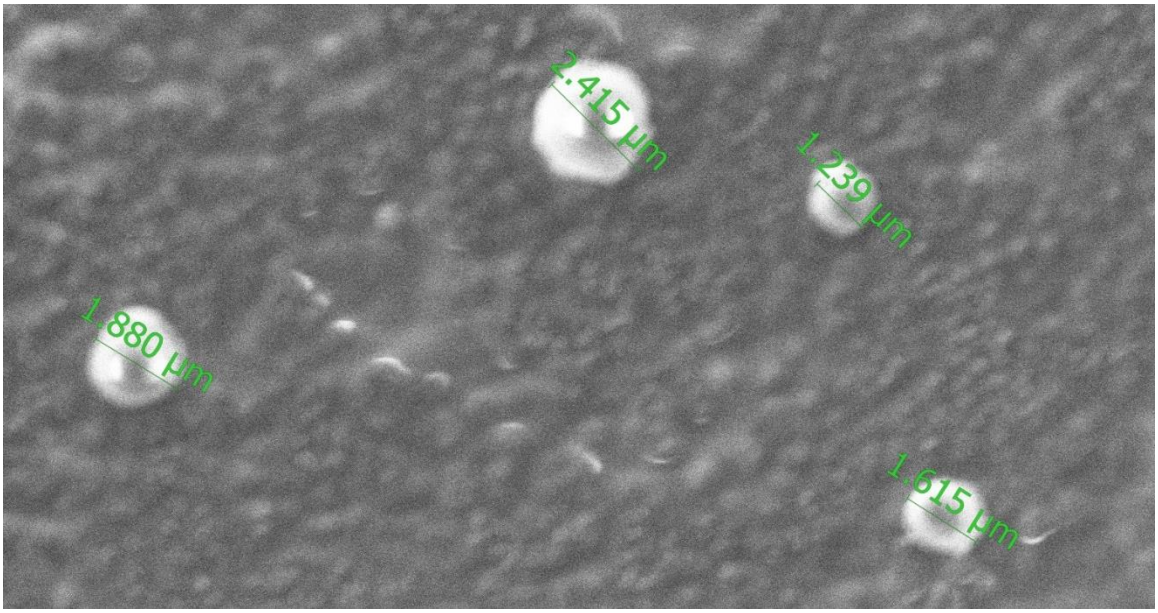

Figure 4.21 Scanning Electron Micrograph of C_{12}BT aggregates. Particle sizes were measured using the electron microscope. Overall average particle sizes determined to be 1.787 µm.

Fig. 4.21 shows some isolated C_{12}BT aggregates. This micrograph is a good representation of the typical particle sizes detected with SEM. The average diameter size of particles was determined to be 1787 nm. This is ~ 40% larger than the 1300 nm effective diameter (Z-diameter) calculated by DLS. The smaller particles are more difficult to focus in on using SEM, electron charging often results, obscuring the image. For this reason, it is anticipated that many of the smaller aggregates were not considered when measuring the particle sizes using SEM. This would skew the average diameter to a size larger than it really is. The use of sputter coating could have helped overcome the electron charging impacting the imaging, however, instrumental limitations prevented this.

The phenylene-linked BTs also formed aggregates, despite being considerably shorter in length. SEM images were collected for both the *m*-PhBT

[*meta*-C_6H_4(L-Trp)$_2$·2HCl] and *p*-PhBT [*para*-C_6H_4(L-Trp)$_2$·2HCl], **Fig. 4.22** and **Fig. 4.23**.

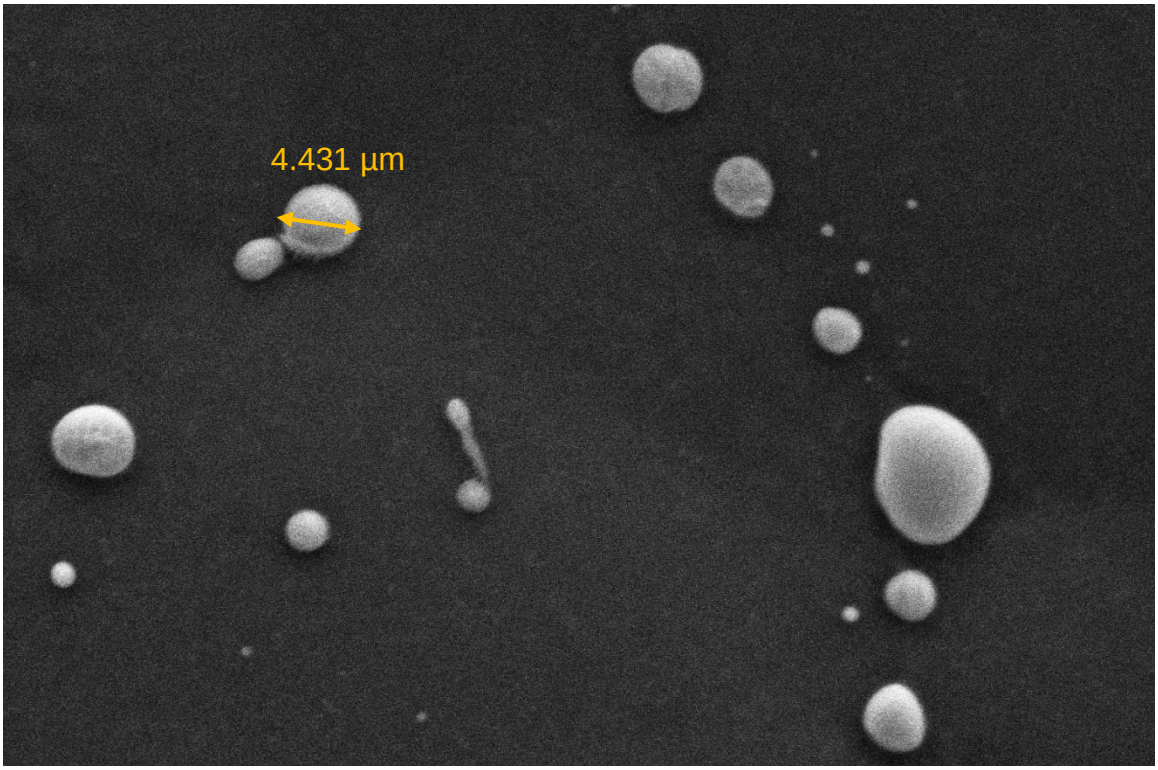

Figure 4.22 Scanning electron micrograph of *m*-PhBT aggregates.

The SEM images for the *m*-PhBT showed that fewer aggregates were detected, **Fig. 4.22**. The distribution of the sizes of the aggregates detected was more bimodal than those observed with C_{12}BT. The aggregates were generally large or small, with few in the 1000 - 3000 nm range. The *m*-PhBT aggregates appeared to fuse together rather quickly, forming several very large structures, and then leaving smaller aggregates that had yet to merge. Many aggregates, estimated to be 500 nm or less were observed. The aggregates were mostly spherical in shape although the integrity of the structures appeared to be questionable. Instead of uniformly shaped spheres, the *m*-PhBT aggregates

appeared to more irregular in shape. These aggregates showed fluidity, whereas the C_{12}BT aggregates resembled more rigid structures.

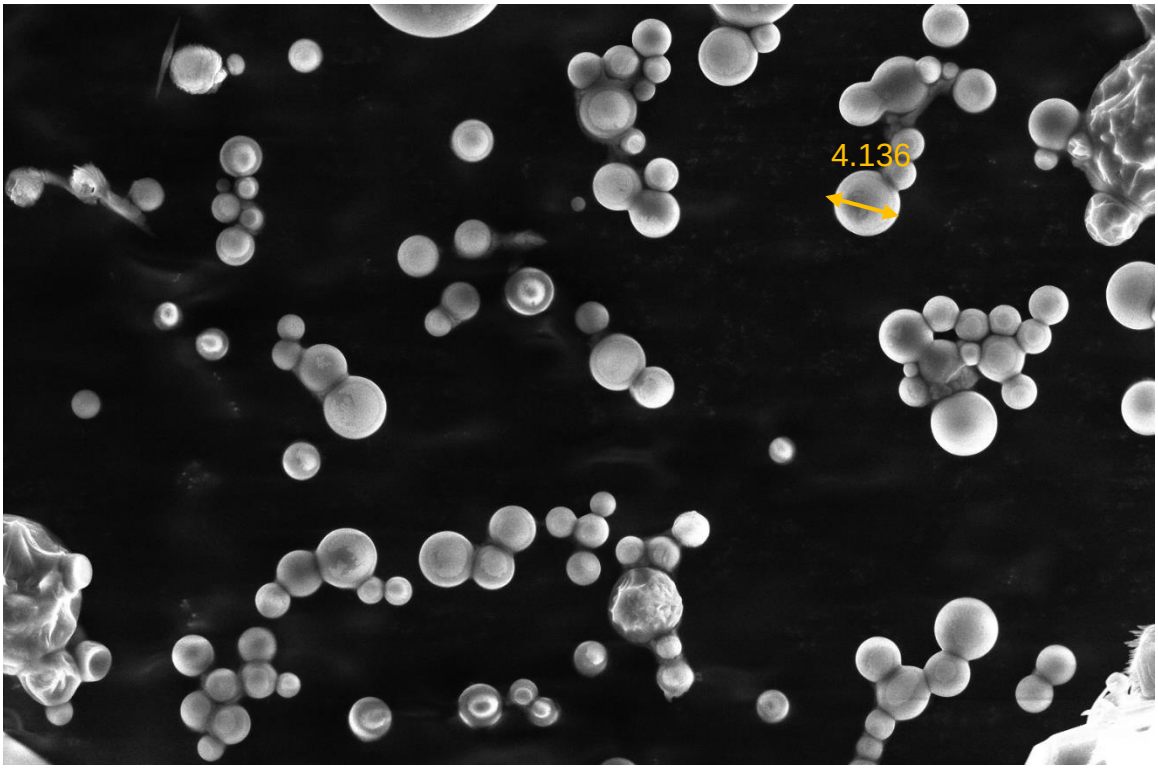

Figure 4.23 Scanning electron micrograph of *p*-PhBT aggregates.

The aggregates detected for the *p*-PhBT are larger than the aggregates detected for the C_{12}BT, **Fig. 4.23**.Unlike the *m*-PhBT, the aggregates of the *p*-PhBT are greater in number and span a range of diameters. Clustering of the aggregates can be seen, suggesting that aggregates fusing with one another may be a more gradual process. In this case compared to the C_{12}BT, the particles seem to be approximately twice as large as the aggregates detected via DLS. Attempts were made to capture images of smaller molecules; however, this was not possible due to electron charging and the effect of the focused electron beam on the sample.

The SEM images show that the general shape of all the aggregates is spherical. This would suggest that liposomes or micelles may be forming, however this is purely speculative. The micrographs confirmed that aggregates are being formed by both the aliphatic- and phenylene-linked BTs in the micromolar range. The capability of the BTs to aggregate continues to coincide with biological activity against bacteria observed in the MIC studies. C_{12}BT, *m*-PhBT and *p*-PhBT formed aggregates and all three compounds have shown some level of activity against bacteria in these studies. The size of the aggregates forming in the PBS solution does not appear to be a determining factor in the efficacy of the amphiphiles against the bacteria. The *p*-PhBT appears to form some of the largest aggregates, however, is the least potent (MIC = 128 µM) against *E. coli* (K-12) of the three compounds in this SEM study. The C_{12}BT showed the most potency in these MIC studies (MIC = 12 µM), yet it forms the smallest aggregates of these three amphiphiles.

4.5 Conclusion

Earlier work in the Gokel lab demonstrated that certain *bis*(tryptophan) (BT) derivatives showed antimicrobial activity against a range of bacteria. The genesis of this effort was the hypothesis that tryptophan would function as a head group in the amphiphilic sense. If the molecules were amphiphiles, they were likely to have an affinity for other membranes. It was well established that a range of amphiphiles previously studied could insert into synthetic bilayers and create ion channels. [5] [6] [19] This was documented by planar bilayer voltage clamp experiments. Many of these compounds were found to function as antibacterial agents. Of course, their potency and efficacy were dependent on compound structure and organism. [20]

It was surmised that the effective amphiphiles inserted in the boundary layers of bacteria, enhanced membrane permeability, which led to ion leakage. These non-rectifying amphiphiles disrupted ion homeostasis, which in turn affected the function of any enzyme that is ion regulated. Studies on other amphiphiles developed in the lab showed that they disrupted the function of efflux pumps. [6] To the extent that ejection of the antimicrobial amphiphile was retained in the bacterium, it could have an additional deleterious effect.

At the outset of this project, several BTs had been prepared and surveyed for biological activity. [7] [21] The present effort was to augment the series, to determine if any additional biological activity was apparent, and to characterize some of the physical properties of the BT amphiphiles. It was well understood that what might be learned about membrane formation or membrane interactions

by the BTs would not be directly applicable to the complex bacterial boundary layers. However, correlations were sought between the physical and biological findings that have proved to be revealing. In addition, the Gokel lab had previously conducted a study in which the tryptophan was replaced with other common amino acids. [7] None of these compounds showed any antimicrobial activity. This further encouraged the present study.

The bacterial study for the BTs shows that all three of the newly synthesized compounds were active against Gram-positive and Gram-negative bacteria, at concentrations of 128 μM or lower. **Fig. 4.24** shows a graph of the biological data over the series of BTs having alkylene spacers. These compounds are $Cl^{-}{}^{+}H_3N$-Trp-$(CH_2)_n$-Trp-$NH_3{}^{+}Cl^{-}$ in which the number of methylene groups is 3, 4, 6, 8, 10, 12, and 14. What is clear from the graph is that *E. coli* (K-12) and methicillin resistant *S. aureus* (MRSA) respond to the BTs in a similar way, which multidrug resistant *E. coli* does not. There are two key findings here. First, extension of the alkylene spacer from dodecylene to tetradecylene further enhanced the antimicrobial potencies against *E. coli* (K-12) and MRSA. This is a positive finding. Second, the behavior of MDR *E. coli* is significantly different and it is clear that none of the BTs would be useful against it. Note that the highest values for each organism are artificially limited to 128 μM, a value that indicates no significant activity. In some cases, the values measured were much higher, but their inclusion in the graph would make the trends less discernable.

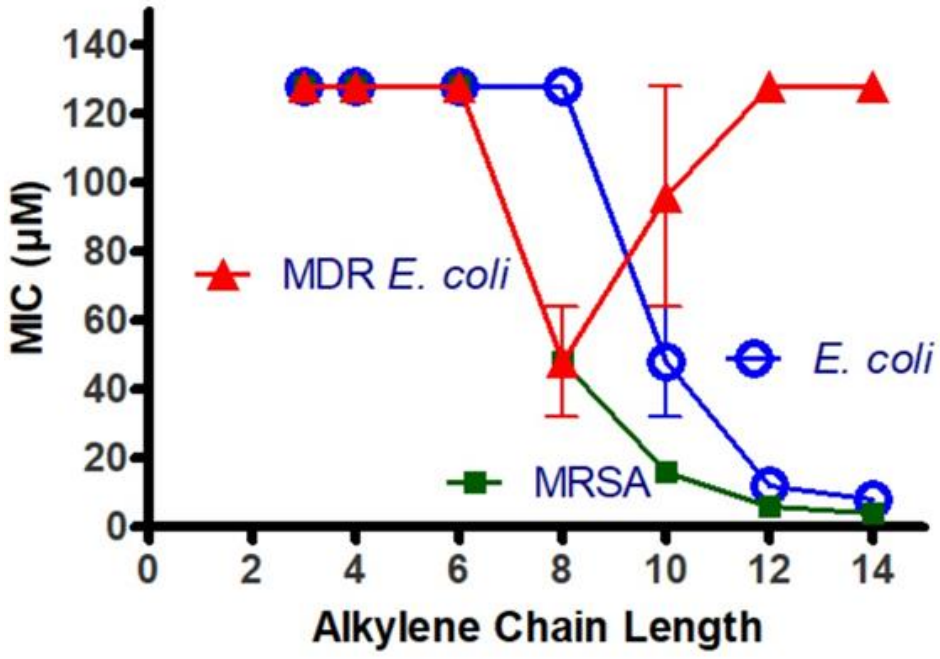

Figure 4.24 Graph comparing the change in MIC of the aliphatic BTs against *E. coli* (K-12), MRSA and MDR *E. coli* as the alkylene chain length is increased.

The biological data from which the graph of **Fig. 4.24** are included in **Table 4.1.** Note that the table actually includes two classes of BTs: those having alkylene spacers and those having arylene linkers. These two groups are not thought necessarily to be directly comparable. More is known about the latter, so they are included as controls.

Table 4.1 Summary of the biological activity and aggregation of BTs

Compound	MIC (μM)			Aggregation	Max Z-diameter	clog*P*
	E. coli **(K-12)**	**MRSA**	**MDR *E. Coli***	**1st Observed (μM)**	**@ 128 μM**	
C_3BT	>128	>128	>128	N/A	N/A	1.07
C_4BT	>128	>128	>128	N/A	N/A	1.59
C_6BT	>128	>128	>128	N/A	N/A	2.48
C_8BT	128	32-64	32-64	32	2700 nm	3.37
C_{10}BT	32-64	16	64-128	8	1500 nm	4.26
C_{12}BT	8-16	4-8	>128	8	1300 nm	5.15
C_{14}BT	8	≤4	>128	8	1600 nm	6.04
m-PhBT	64	--	--	≤128	1300 nm	3.25
p-PhBT	128	--	--	≤128	800 nm	3.25

Several apparent correlations stand out. First, no biological activity is observed against the three organisms listed for C_3BT, C_4BT, and C_6BT. In all cases, no biological activity was observed up to 128 μM. Because the linker chains are short, it might be expected that amphiphilic behavior is unlikely. Indeed, dynamic light scattering (DLS) shows that no aggregates form from this group of compounds. The inference that we draw from this is that amphiphilic character is required for the compounds to interact with either the Gram-positive or Gram-negative boundary layers of the bacteria.

The scanning electron microscopy (SEM) studies confirmed that organized assemblies are formed by the C_{12}BT and arylene-linked BTs. They

confirm that the aggregates are spherical, presumably liposomal, and of a size comparable to those detected by DLS. Neither the DLS nor the SEM studies provide further information in regard to the complex membrane structure of bacterial cells.

An additional correlation is found in the hydrophobicity index clog*P*. The calculated distribution constants for C_3BT, C_4BT, and C_6BT are all below 3. C_8BT and the phenylene compounds have clog*P* values close to, but above, 3 and show biological activity. However, the phenylene compounds bear a structural resemblance to the well-known tris(arene) structures prepared by Crabtree and coworkers. [22] In a previous study conducted in the Gokel lab, it was shown that the Crabtree compound was a chloride complexing agent. [23] Complexation of chloride could disrupt ion homeostasis. Rather than functioning as an amphiphile, the arenyl BTs could be functioning as ion complexing carriers in the bacterial membranes. A comparison of the Crabtree structure and *m*-PhBT are shown in the figure below (**Fig. 4.25**).

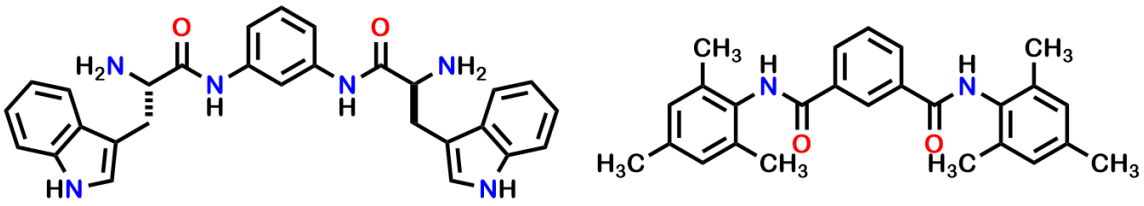

Figure 4.25 Structures of the Gokel lab compound *m*-PhBT (left) and the Crabtree *tris*(arene) compound (right)

The longer chain BTs (C_{10}BT – C_{14}BT) have clog*P* values above 4. The values represent the increased hydrophobic character due to the longer aliphatic chains. The added hydrophobicity and resulting amphiphilic character of the BTs is thought to be important for aggregation and activity with the Gram-positive and Gram-negative boundary layers.

Notwithstanding the differences in membrane structure found in Gram-negative or Gram-positive bacteria, amphiphiles comprise part of either's boundary layer. The ability of BTs to form aggregates was expected to give an indication of their affinity for other amphiphilic membrane systems. To the extent a bacterial membrane interaction with BTs is suggested by the aggregation data, the inference is that some structural influence on the membrane would occur. Any disorganization or disruption of a bacterial membrane is likely to enhance the penetration of the BT or other exogenous material.

4.6 Experimental Details

4.6.1 Dynamic Light Scattering (DLS). Measurements were performed on a Brookhaven Instruments Corp. ZetaPALS instrument at 25 °C using a 660 nm laser and correlating scattering at 90°. Samples were prepared by dissolving *bis*(tryptophan) amphiphile in DMSO and adding a 15 µL aliquot to 2985 µL of solvent (PBS solution, 18.2 MΩ H_2O or MHII media) to maintain a 0.5% (v/v) DMSO concentration. The sample was added to a clean quartz cuvette and equilibrated in the instrument for 5 min at 25 °C. Ten measurements were made on each sample at equal time intervals, depending on the total time of the experiment (24 mins for 4-hour experiments, 6 minutes for 1-hour experiments). The average effective diameter (Z-diameter) was calculated and reported. Cleaning of cuvettes included initial overnight soaking in 2 M HNO_3, wash with 95% ethanol (x 3), deionized water (x 3) and rinse with appropriate solvent (e.g., PBS solution). Solutions are prepared and used immediately or stored in a clean vial and capped to avoid contamination and dust particles. The dust-filter option on the instrument is also applied for all experiments as the instrument is sensitive to dust particles.

4.6.2 *Scanning Electron Microscopy (SEM).* Measurements were performed on a Thermo Fisher Scientific Apreo 2 C SEM instrument at 25 °C using the Trinity Detection System. Samples prepared for DLS were also used for SEM imaging. The samples were adhered to conductive carbon fiber adhesive tape and allowed to dry. Samples were mounted on the Eucentric

goniometer stage before being placed under vacuum in the instrument for analysis to proceed. The voltage range of the electron beam was 200 V – 30 kV and the current range was 1 pA – 50 nA.

4.7 References

[1] C. F. Le, C. M. Fang and S. D. Sekaran, "Intracellular Targeting Mechanisms by Antimicrobial Peptides," *Antimicrobial Agents and Chemotherapy,* vol. 61, no. 4, 2017.

[2] D. I. Chan, E. J. Prenner and H. J. Vogel, "Tryptophan- and Arginine-rich Antimicrobial Peptides: Structure and Mechanisms of Action," *Biochemica et Biophysica Acta,* vol. 1758, no. 9, pp. 1184-1202, 2006.

[3] S. U. Gorr, J. B. Sotsky, A. P. Shelar and D. R. Demuth, "Design of Bacteria-agglutinating Peptides derived from Parotid Secretory Protein, a Member of the Bactericidal/Permeability Increasing-like Protein Family," *Peptides,* vol. 29, no. 12, pp. 2118-2127, 2008.

[4] J. L. Atkins, M. B. Patel, Z. Cusumano and G. W. Gokel, "Enhancement of Antimicrobial Activity by Synthetic Ion Channel Synergy," *Chemical Communications,* vol. 46, pp. 8166-8167, 2010.

[5] S. Negin, B. A. Smith, A. Unger, W. M. Leevy and G. W. Gokel, "Hydraphiles: A Rigorously Studied Class of Synthetic Channel Compounds with In Vivo Activity," *International Journal of Biomedical Imaging,* pp. 1-11, 2013.

[6] S. Negin, M. B. Patel, M. R. Gokel, J. W. Meisel and G. W. Gokel, "Antibiotic Potency against E. coliis Enhanced by Channel-Forming Alkyl Lariat Ethers," *ChemBioChem,* vol. 17, pp. 2153-2161, 2016.

[7] M. Patel, S. Negin, J. Meisel, S. Yin, M. Gokel, H. Gill and G. Gokel, "Bis(Tryptophan) Amphiphiles Form Ion Conducting Pores and Enhance Antimicrobial Activity against Resistant Bacteria," *Antibiotics,* vol. 10, no. 1391, pp. 1-18, 2021.

[8] J. Stetefeld, S. A. McKenna and T. R. Patel, "Dynamic Light Scattering: A Practical Guide and Applications in Biomedical Sciences," *Biophysical Reviews,* vol. 8, no. 4, pp. 409-427, 2016.

[9] G. Reshes, S. Vanounou, I. Fishov and M. Feingold, "Cell Shape Dynamics in Escherichia coli," *Biophysical Journal,* vol. 94, pp. 251-264, 2008.

[10] L. Nicoud, M. Lattuada, A. Yates and M. Morbidelli, "Impact of Aggregate Formation on the Viscosity of Protein Solutions," *Soft Matter,* vol. 11, pp. 5513-5522, 2015.

[11] K. A. Brogden, "Antimicrobial Peptides: Pore Formers or Metabolic Inhibitors in Bacteria?," *Nature Reviews,* vol. 3, pp. 238-250, 2005.

[12] S. L. Keller, S. M. Bezrukov, S. M. Gruner, M. W. Tate, I. Vodyanoy and V. A. Parsegian, "Probability of Alamethicin Conductance States Varies with Nonlamellar Tendency of Bilayer Phospholipids," *Biophysical Journal,* vol. 65, pp. 23-27, 1993.

[13] A. Pokorny and P. F. F. Almeida, "Permeabilization of Raft-Containing Lipid Vesicles by delta-Lysin: A Mechanism for Cell Sensitivity to Cytotoxic Peptides," *Biochemistry,* vol. 44, pp. 9538-9544, 2005.

[14] T. Chen and M. L. J. Li, "π-π Stacking Interaction: A Nondestructive and Facile Means in Material Engineering for Bioapplications," *Crystal Growth and Design,* vol. 18, pp. 2765-2783, 2018.

[15] J. M. Thornton, J. Singh, S. Campbell and T. L. Blundell, "Protein-protein Recognition via Side-chain Interactions," *Biochemical Society Transactions,* vol. 16, no. 6, pp. 927-930, 1988.

[16] U. Samanta, D. Pal and P. Chakrabarti, "Packing or Aromatic Rings against Tryptophan Residues in Proteins," *Biological Crystallography,* vol. 55, pp. 1421-1427, 1999.

[17] SciMed, "A Brief Introduction to SEM (Scanning Electron Microscopy)," 2022. [Online]. Available: https://www.scimed.co.uk/education/sem-scanning-electron-microscopy/. [Accessed 18 March 2022].

[18] M. Martin-Hidalgo, K. Camacho-Soto, V. Gubala and J. R. Rivera, "Self-assembled Cation Transporters made from Lipophilic 8-Phenyl-2'-deoxyguanosine Derivatives," *Supramolecular Chemistry,* vol. 22, pp. 862-869, 2010.

[19] M. R. Gokel, M. McKeever, J. W. Meisel, S. Negin, M. B. Patel, S. Yin and G. W. Gokel, "Crown Ethers having Side Arms: A Diverse and Versatile Supramolecular Chemistry," *Journal of Coordination Chemistry,* vol. 74, no. 1-3, pp. 14-39, 2021.

[20] M. B. Patel, J. W. Meisel, S. Negin, M. R. Gokel and G. W. Gokel, "Resensitization of Resistant Bacteria to Antimicrobials," *Annals of Pharmacology and Pharmaceutics,* vol. 2, no. 10, pp. 1-5, 2017.

[21] J. W. Meisel, M. B. Patel, E. Garrad, R. A. Stanton and G. W. Gokel, "Reversal of Teracycline Resistance in Escherichia coli by Noncytotoxic bis(Tryptophan)s," *Journal of the American Chemical Society,* vol. 138, pp. 10571-10577, 2016.

[22] K. Kavallieratos, C. M. Berato and R. H. Crabtree, "Hydrogen Bonding in Anion Recognition: A Family of Versatile, Nonpreorganizd Neutral and Acyclic Receptors," *Journal of Organic Chemistry,* vol. 64, pp. 1675-1683, 1999.

[23] R. Pajewski, R. Ferdani, P. H. Schlesinger and G. W. Gokel, "Chloride Complexation by Heptapeptides: Influence of C- and N-terminal Sidechains and Counterion," *Chemical Communications,* pp. 160-161, 2004.

[24] C. A. Lipinski, F. Lombardo, B. W. Dominy and P. J. Feeney, "Experimental and Computational Approaches to Estimate Solubility and Permeability in Drug Discovery and Development Settings," *Advanced Drug Delivery Reviews,* vol. 46, no. 1-3, pp. 3-26, 2001.

[25] L. Z. Benet, C. M. Hosey, O. Ursu and T. I. Opera, "BDDCS, the Rule of 5 and Drugability," *Advanced Drug Delivery Reviews,* vol. 101, pp. 89-98, 2016.

[26] C. Wu and L. Z. Benet, "Predicting Drug Disposition via Application of BCS: Transport/Absorption/Elimination Interplay and Development of a Biopharmaceutics Drug Disposition Classification System," *Pharmaceutical Research,* vol. 22, no. 1, pp. 11-23, 2005.